Sebastian D. Eastham
Research Scientist,
Laboratory for Aviation and the Environment
Department of Aeronautics and Astronautics

Massachusetts Institute of Technology
77 Massachusetts Avenue, Building 33-322A
Cambridge, Massachusetts 02139–4307, USA
http://lae.mit.edu

Atmospheric Chemistry and Physics Editorial Office

23rd February 2020

Dear Editor,

Re: Revisions for "The role of plume-scale processes in long-term impacts of aircraft emissions" after submission to *Atmospheric Chemistry and Physics*

Thank you for considering our submission and for arranging the detailed and careful reviews. We appreciate the time and effort taken to provide feedback on this manuscript. We are grateful for the detailed comments received which have guided us to make significant improvements to the paper.

Please find below our responses (in **bold**) to each of the reviewers' comments (in *italics*). We have attached two copies of the manuscript: one "clean" version incorporating all changes, and a "markup" version in which all changes are highlighted. Line numbers below correspond to the "markup" version.

All simulations were re-run to account for changes suggested by the reviewers. The inclusion of a constant aggregation efficiency changed the total number of particles in bins with radii greater than 30 μm by at most 0.3%, as our previous estimate of aggregation efficiencies was close to the constant value prescribed in Sölch and Kärcher (2010). Furthermore, based on review of Kärcher et al. (2009), we have updated our contrail simulations to use a more realistic background condition. We now use the background meteorological conditions described in Unterstrasser et al. (2010), in which a background 50% relative humidity and a single supersaturated band (1 km in thickness) are prescribed. This change also enabled us to perform direct comparison of our results to those from Unterstrasser et al. (2010) in Appendix D of the manuscript. Neither modification has changed the qualitative conclusions of the paper.

References:

Kärcher, Bernd et al. "Factors controlling contrail cirrus optical depth". *Atmospheric Chemistry and Physics* 9 (2009): 6229-6254.

Sölch, Ingo, and Bernd Kärcher. "A large-eddy model for cirrus clouds with explicit aerosol and ice microphysics and Lagrangian ice particle tracking." *Quarterly Journal of the Royal Meteorological Society* 136.653 (2010): 2074-2093.

Unterstrasser, Simon, and Klaus Gierens. "Numerical simulations of contrail-to-cirrus transition – Part 1: An extensive parametric study." *Atmospheric Chemistry and Physics* 10.4 (2010): 2017-2036.

Referee: 1

Received and published: 13 August 2019

This is an interesting and important analysis that emphasizes the potential impacts of plume processing of aircraft emissions prior to their incorporation into climate models at their grid scales. This is an important point that has been made previously on a number of occasions but is often ignored and not included in analyses.

I find some parts of the modeling results to be useful, and worthy of publication. However, there are a number of issues that should be addressed before this manuscript be accepted for publication, in my opinion. The gaseous chemistry regarding ozone formation is compelling, useful, and is quoted as agreeing with prior analyses. This is useful confirmation of the importance of plume processing for ozone impacts. The contrail impacts are also of interest in how particle properties are affected by plume processing. However, the details of the way the contrail modeling has been done need to be qualified to a greater degree, due to assumptions that are made (mono-modal soot distribution) and implied (dependence, or lack thereof of, of water uptake on particle surface composition).

We thank the reviewer for their interest in our manuscript and are grateful for their detailed comments and in-depth analysis. We have modified the paper substantially in order to give more detail regarding the approach, and the justification of said approach. Please find our responses to each individual comment below.

1) The approach shown for volatile PM (nucleation and growth of new particles, and uptake on soot particle coatings), seems incomplete and thus potentially flawed. No specific results are shown in plots nor discussed, and it is not clear that such results impact the chemistry nor contrails results that ARE shown. This perspective will be discussed further below, where I suggest removing or discussing in a much different way. 2) The contrail modeling has made some simplifications that may impact the results that the authors claim to be important. They need to discuss in more detail how the assumptions might qualify their results and the claimed quantification of the effects that they observe. 3) There are a number of more minor wording or presentation issues that I will identify below, along with some suggestions for how they might be addressed.

1. In section 2.2.3, page 6, line 15, "Soot and ice particles can also grow by condensation of water vapor, sulfuric acid, and nitric acid...". Experimental results show that the growth of particle mass in aircraft exhaust plumes is dominated by organic species (and nitric acid is not usually observed in the initial plume regions). Leaving out organic species is leaving out a primary contributor to the mass of these newly formed particles (prior to water deposition in contrail formation) as well as the coatings on soot particles.Thus, the presented microphysical approach is missing the major contribution to mass. (Yet the authors do note that volatile organics are in the exhaust, section 3.1, page 10, line18.)

We share the reviewer's concerns regarding the role played by organic species in the initial plume phase. We agree that organic species may alter the freezing behavior of aerosols, as has been shown in previous studies (Cziczo et al. (2004); Kärcher et al., (2005); Murray et al., (2010)). Kärcher et al. (2015) in particular describes the role of organics in great detail and has been a valuable source of knowledge. However, the theory behind particle growth enhanced by organic species or nucleation is still limited and it is not clear how best to incorporate this information. In addition, a large number of soluble organic species involved are typically involved and the processes by which the organic compounds contribute to the aerosol growth are complex and poorly understood. As a consequence, we do not explicitly consider the effects of organic species in these calculations.

However, we have now performed additional sensitivity calculations to try and bound the possible roles of organic aerosol. Specifically, we consider two possibilities: that organic aerosol could act like sulfate aerosol (i.e. as a coating material on soot), and that organic aerosol might act as additional ice nuclei. In the

first case, we simulate additional cases in which the soot coating fraction is assumed to be increased from the baseline value (0%) to between 0 and 25% due to the role of organic matter prior to water deposition. This is presented as a sensitivity analysis in Section 3.1.1. This shows that the inclusion of organic species leads to a faster growth rate through the deposition of gaseous water. However, the particle radius after ~1 second was unchanged in all cases (whether the background was subsaturated or supersaturated). Similarly, the gaseous chemical composition is unaffected by the condensation of organic compounds onto soot particles, even under supersaturated conditions. This suggests that the contrail evolution and chemical consequences of an aircraft exhaust plume are not sensitive to this assumption (page 10, lines 90-92). We also simulate the effect of changing the black carbon emissions index in Section 3.1.3. If organic aerosol acts as a nucleus rather than as a coating, then the result of doubling the black carbon emissions index can be considered as an analog for the effect of including organic aerosols. We now make this comparison explicit (page 13, lines 11-15) but recognize that this is, at best, only a crude approximation of the role of organic aerosol.

We have added a paragraph discussing this limitation in Section 2.2.3, reviewing the literature discussed above (page 5, lines 64-88). We have also added as "future work" the goal of explicitly modeling condensation of organic species to enable a more robust investigation of the potential effect of organic aerosols with respect to contrail formation and plume chemistry (page 22, lines 36-38).

However, there are no results presented in the paper that show the importance of this microphysical processing. Neither results showing newly nucleated sulfate aerosol nor the coatings on the soot particles (and their composition) are presented in the paper. It is not clear from the material presented how the eventual uptake of water is dependent on the condensed matter due to these species. Is the later water uptake affected by the surface composition? If not, there seems to be no impact of this analysis on the contrail results presented later in the paper. No size distribution results are shown, so it is not clear how the soot distribution and newly nucleated particles make up the input to the downstream mature plume modeling, and how they affect the subsequent analysis.

The later water uptake is influenced by the soot coating fraction as the bare soot particles are assumed to be hydrophobic. In our current modeling approach, this coating is made up of sulfuric acid and water. We now include an analysis in Section 3.1 which demonstrates the microphysical evolution of the plume, including the partitioning between gaseous and liquid sulfur, including the aerosol distribution, and how this changes over the first 15 minutes (section 3.1).

After formation, the sulfate aerosol distribution and ice particle mean radius are used to initialize the mature plume module. The contrail ice particles are initialized with a log-normal distribution. We have added the following in Section 2.3.3 to clarify how the results from the early plume module propagate to the later simulation stages: "The aerosol distributions in the mature plume phase are initialized based on the output from the early-plume module. The distribution of sulfate aerosols is unchanged while ice particles are distributed assuming a log-normal distribution, using the mean ice particle radius and a geometric standard deviation of 1.6 (Goodman et al., 1998; Jensen et al., 1998a). The use of a log-normal distribution is based on *in situ* measurements (Schröder et al., 2018) and this assumption has been used in previous work to initialize the contrail ice particle size distribution (Jensen et al., 1998b; Picot et al., 2015)." (page 7, lines 59-62).

It is worth noting that many other modeling studies suggest that the "nucleation mode" is not important for contrail processes when the soot mode is present, due to the larger size of the soot mode. Thus, there is a basis for questioning the importance of this smaller mode. The question of the compositional changes of the soot surface due to condensation seems open, but unaddressed by the present study.

Our results support the finding that the nucleation mode plays a negligible role compared to the soot mode, due to its larger size. We include a nucleation mode to enable the model to capture the behavior of contrails for engines with very low soot emissions indices. Under these circumstances, it has been hypothesized that liquid plume and ambient particles could play a significant role in contrail formation. Kärcher et al. (2009) describes three regimes for the origin of ice crystals based on the soot number emission index:

- **In a soot-rich regime ($EI_N > 10^{15}$ particles / kg fuel), contrail ice is formed when water freezes onto soot (black carbon) particles.**
- **In a soot-poor regime ($EI_N < 10^{13}$ particles / kg fuel), contrail ice is formed when water freezes onto/with liquid particles.**
- **In the intermediate regime, ice can form on both soot particles and liquid particles. The crossover point varies as a function of ambient parameters, but is consistently estimated to be below soot particle number emissions indices (EI_N) of 10^{14} particles / kg fuel.**

***In situ* observations showed that, for current engines, the soot number emission indices vary between 3.5×10^{14} and 1.7×10^{15} particles / kg fuel (Petzold et al., 1999). Those measurements suggest that ice particles currently form by freezing of water around soot cores. However, it is possible that alternative fuels or new combustor technologies may reduce the emissions index to the point that this nucleation mode is significant. We have included a sentence in Section 2.2.3 which clarifies this (page 5, lines 15-20).**

Unless more information is provided, it seems that this is an incomplete analysis that has limited bearing on the problem at hand, and it does not appear that the model has a means to include the effects of this analysis on the key results presented. I suggest this part of the analysis be removed or completely re-described.

We have made the changes above in an effort to make clearer the strengths of our approach, and to clarify where there are limitations or opportunities for further research (Sections 2.2, 3.1, 4).

2. In a related issue, the modeling assumes (section 2.2.3, page 6, line 5) that the soot distribution is a mono-modal distribution ("a single representative particle"). While that may make sense to define a more computationally tractable problem, the microphysical modeling discussed in 1. above seems to require a binned size distribution approach (page 7 line 3), so why is it necessary to force the soot to be mono-modal? But if the response to issue 1. above is to remove the volatile particle modeling, then perhaps the mono-modal soot distribution may be justifiable to simplify the computations.

However, if the approach is to accept a more limited modeling approach, based on a mono-modal soot distribution as has been done before (as referenced by the authors), then another separate question arises. The results show important differences due to differences in the fate of large particles versus small particles in the later plume processing (section 3.5.1, line 12 et seq.). If the initial soot distribution is mono-modal, the contrail particles will also be mono-modal for those particles that have had the same history (i.e., in the same ring). There needs to be more discussion of how the history of particles might generate a size distribution that differs from the initial mono-modal soot size distribution, if this is, indeed, what generates a polydisperse contrail particle size distribution.

The soot particles are represented as a monodisperse distribution, with the assumption that (if a contrail forms) they will act as "seeds" for ice crystals. At this point, the contrail ice particles are initialized with a log-normal distribution whose median radius is computed using the initial box model and with a geometric standard deviation of 1.6 (as now described in Section 2.3.3, page 7, lines 53-62). Even without the application of a log-normal distribution to initialize the model, a polydisperse distribution would arise due to coagulation. This results in different settling velocities, such that the larger particles are exposed to "fresher" air, further changing the overall particle size distribution. Shear of the plume also results in particles in different parts of the plume being exposed to different conditions. The soot distribution is only

used to make the problem more computationally tractable initially. The above description is now included in Section 2.3.3 (page 7, line 65 - page 8, line 3).

Regarding the ring-shaped mesh, this is only used to reduce the computational cost associated with the chemistry. Both transport and microphysical processes are performed on the fine cartesian grid as described in Section 2.3 (page 6, lines 68-70).

3. Presentation issues and typos:

a. In the introduction (page 2, line 29 - 30), "aviation is . . . the only direct, significant source . . .", what about rockets? May not be as large,but rockets may still be significant.

We agree that the rocket industry is an expanding sector and the number of launches is growing each year. However, there were a total of 90 rocket launches in 2017, while ICAO registered 37 million flights for the same year. In terms of fuel burn, the first stage of the Falcon Heavy (which burns for the first 70 km or so of altitude gain) has a tank capacity of 123 tonnes of kerosene, meaning that the total kerosene burn below 70 km would be ~11 Gg if we use the Falcon Heavy first stage as a generic proxy. In 2015 there was, for comparison, approximately 240 Tg of fuel burn from commercial aviation (from FAA's AEDT). Rocket launches thus correspond to at most 0.005% of the total aviation fuel burn.

We replaced the sentence with: "aviation is a unique sector in terms of its environmental challenges as it is the most significant anthropogenic source of pollution at high altitude (8-12 km). In 2015, an estimated 240 Tg of jet fuel were burned for commercial aviation according to the global inventory from the FAA Aviation Environmental Design Tool (AEDT). For comparison, even under a very conservative assumption - that every rocket launch in 2015 was performed with the high-capacity, kerosene-burning "Falcon Heavy" - we estimate that rockets burned at most 11 Gg of fuel below the stratopause in that year." (page 1, line 61 - page 2, line 3).

b. Also, in the introduction: this is not meant to be a review article, but it might be worth mentioning that the importance of plume processing has a history that goes back to CIAP (CIAP monograph 3, 1975, DOT-TST-75-53, chapter 2 and references therein) and, {especially since the manuscript is a NASA sponsored study}, to NASA (Atmospheric Effect of Aviation: First Report of the Subsonic Assessment Project, 1996, NASA Ref. Pub. 1385, chapter 4 and references therein).

We have added the following sentence "The impact of plume-scale modeling of aircraft wakes has been investigated over the past few decades mostly for its relevance to the environmental impact of aviation." and we cite the CIAP Monograph 3 and NASA report (page 2, lines 29-36).

c. Figure 1. As a schematic, this figure seems to address only the 2.3 mature plume modeling part. There is an inset box that discusses the plume box model processing, but there is no schematic representation of the box model in the artwork. And there is no equivalent inset box that describes the discretized rings in the figure.

If the box model inset box were removed from the existing figure, I would suggest this figure would sit better in section 2.3, where the mature plume modeling is discussed. It has little schematic value for the box model as drawn so doesn't provide much benefit as placed in section 1. If, on the other hand, the figure was adjusted so that there were schematic aspects and inset boxes for both parts of the model, then perhaps a redrawn version might have reason to remain in section 1.

We agree, Figure 1 only represents the evolution of the plume in the mature phase. We have moved Figure 1 accordingly to Section 2.3.

d. Section 2.1, page 4, line 13. "The output of this box model..." This sentence is confusing. The antecedent to "this box model" doesn't exist, since the model hasn't been mentioned yet, and is described in the subsequent section.

The preceding paragraph describes the physical phenomena to be addressed, but there is no mention of the box model that will be used. One solution would be to briefly mention how a box model (to be described in detail later) will be formulated to capture the elements described.

Another solution would be to drop that sentence and pick it up later after the two models are discussed. If this approach is taken, then the material in these two paragraphs (last two paragraphs of section 2.1) would just be discussing the physical phenomena in the two regimes and leave the box and ring models' discussion for the later sections. (If this approach is taken, the title of 2.1 might need to be adjusted.)

As written, the sentence is confusing, referencing models that haven't been introduced yet.

Thank you for catching this oversight. As suggested, we now provide a brief description of the box model at first mention (page 3, lines 36-39).

e. Section 2.2.2, page 5, line 22, Tremmel, (and by Lukachko et al., 1998 JGR 103, and in 2008, J. Eng. Gas Turbines and Power, 130, 2008) found that the conversion of S(IV)to S(VI) occurred primarily in the engine's turbine, and not in the plume to a significant degree. Later processing in the atmosphere happens also, but at time-scales much longer than the initial plume being addressed by this study.

The studies from Lukachko et al. (1998) and Tremmel et al. indicate that a significant fraction of S(VI) production occurs between the combustor and the nozzle of the engine. We model this by prescribing a fraction of S(IV) that gets converted to S(VI) at the exit plane of the engine. Brown et al. (1996) also describes that the gas phase oxidation is a much slower process and thus acts as a weaker source of S(VI) than the initial conversion in the aircraft engine. Thus, a large fraction of the sulfur present in the plume 24 hours after emission was already present in the plume at the engine exit plane. To make this clearer to the reader we now state that "Oxidation of S(IV) to gaseous S(VI) is not simulated during this period. This process mostly occurs in the engine's turbines and only a negligible fraction is converted in the young aircraft plume." in Section 2.2.2 (page 4, lines 81-85).

f. Section 2.4.1, page 9, line 21. "equipped with GEnx engines". In what sense is this engine represented in the model? In section 3.5.3, page 19, line 8, a soot emission index (EI) is given as 0.06 g/gfuel. (I assume this is a typo, and it is meant to be 0.06 g/kgfuel, or 60 mg/kgfuel).

The use of "g/g fuel" was a typo. This has been fixed and changed to mg/kg fuel (page 21, lines 30-31). We answer the broader question of representation of the GEnx engine below.

This seems very high for the GEnx engine, especially at cruise at altitude. This (even after correcting for the typo!) is 1.5 times the {high} value used in the 1999 IPCC report of 0.04 g/ kgfuel. And where was the EI soot data obtained? In addition, is the NOx EI chosen to be representative of the GEnx from the ICAO Databank?

The representation of the GEnx engines in APCEMM at cruise altitude uses the equations of the Boeing Fuel Flow Method 2 (Dubois et al., 2006) to compute a cruise NO_x emission index from the ones provided by the ICAO Engine Emissions Databank.

The value of 60 mg soot/kg fuel is not intended to specifically characterize the GEnx, but is rather part of a sensitivity analysis for that section only. In all other areas, we use the SN-C_{BC} method described in Stettler et al. (2013), equation (5) to estimate the mass soot emission index. As a consequence, the soot emissions

index used (unless otherwise specified) is 10 - 14 mg/kg fuel (depending on local conditions based on the SN-C_{BC} method). We now describe this approach on page 9, lines 17-38, and specify the calculated soot and NO_x EIs where relevant (e.g. page 14, lines 11-12).

In Sections 3.5.2 and 3.5.3, we explicitly varied the soot emission index from 10 mg/kg fuel to 60 mg/kg fuel to estimate the sensitivity of our results to this parameter. Stettler et al (2013) estimate that the fleet-wide average soot emissions index is 28 mg/kg fuel. Previous estimates have found that different engines in the fleet can have emissions indices which vary by an order of magnitude (e.g. 11 - 100 mg/kg fuel as estimated by Petzold et al., 1999). This clarification has been included in page 19, lines 50-60.

By varying the soot emission index, we do not intend to model variation in the GEnx engine but rather to focus on the impact of different soot emission indices on contrail and chemical properties. We thus keep everything unchanged from the GEnx emission characteristics except from the soot emissions. To clarify, we added the following to the manuscript (changes underlined):
"We next model how changes in soot emissions affect the properties of the contrail. We simulate an aircraft plume <u>in which the</u> soot mass emission indices <u>are varied between</u> 10 and 60 mg/kg fuel<u>, compared to 10 to 14 mg/kg estimated using the SN-C_{BC} method for the GEnx engine</u>. <u>All other aircraft and engine emissions parameters are fixed for this sensitivity analysis.</u>" (page 19, line 50-60).

g. Section 3.5.1, page 16, line 1. Supersaturations of 102% to 108% are quoted, but is this respect to water or ice? (And is 108% observed in the natural atmosphere?)

The saturations quoted in the paper are expressed with respect to the ice saturation pressure. Gierens et al. (1999) estimate that, in supersaturated regions of the upper troposphere, the mean supersaturation is 15% (corresponding to a relative humidity with respect to ice of 115%). This clarification is now given in the main text on page 18, line 22-25.

<u>References:</u>

Brown, R. C., et al. "Aircraft exhaust sulfur emissions." *Geophysical research letters* 23.24 (1996): 3603-3606.

DuBois, Doug, and Gerald C. Paynter. "" Fuel Flow Method2" for Estimating Aircraft Emissions." *SAE Transactions* (2006): 1-14.

Cziczo, D. J., et al. "Observations of organic species and atmospheric ice formation." *Geophysical research letters* 31.12 (2004).

Gierens, Klaus, et al. "A distribution law for relative humidity in the upper troposphere and lower stratosphere derived from three years of MOZAIC measurements." *Annales Geophysicae*. Vol. 17. No. 9. Springer-Verlag, 1999.

Goodman, J., et al. "Shape and size of contrails ice particles." *Geophysical research letters* 25.9 (1998): 1327-1330.

Jensen, E. J., et al. "Ice crystal nucleation and growth in contrails forming at low ambient temperatures." *Geophysical research letters* 25.9 (1998a): 1371-1374.

Jensen, Eric J., et al. "Spreading and growth of contrails in a sheared environment." *Journal of Geophysical Research: Atmospheres* 103.D24 (1998b): 31557-31567.

Kärcher, B., et al. "The microphysical pathway to contrail formation." ***Journal of Geophysical Research: Atmospheres*** **120.15 (2015): 7893-7927.**

Kärcher, B., and Thomas Koop. "The role of organic aerosols in homogeneous ice formation." ***Atmospheric Chemistry and Physics*** **5.3 (2005).**

Kärcher, B., and F. Yu. "Role of aircraft soot emissions in contrail formation." ***Geophysical Research Letters*** **36.1 (2009).**

Lukachko, S. P., et al. "Production of sulfate aerosol precursors in the turbine and exhaust nozzle of an aircraft engine." ***Journal of Geophysical Research: Atmospheres*** **103.D13 (1998): 16159-16174.**

Murray, Benjamin J., et al. "Heterogeneous nucleation of ice particles on glassy aerosols under cirrus conditions." ***Nature Geoscience*** **3.4 (2010): 233-237.**

Petzold, Andreas, et al. "In situ observations and model calculations of black carbon emission by aircraft at cruise altitude." ***Journal of Geophysical Research: Atmospheres*** **104.D18 (1999): 22171-22181.**

Picot, J., et al. "Large-eddy simulation of contrail evolution in the vortex phase and its interaction with atmospheric turbulence." ***Atmospheric Chemistry and Physics*** **15.13 (2015): 7369.**

Schröder, Franz, et al. "On the transition of contrails into cirrus clouds." ***Journal of the atmospheric sciences*** **75.2 (2018).**

Stettler, Marc EJ, et al. "Global civil aviation black carbon emissions." ***Environmental science & technology*** **47.18 (2013): 10397-10404.**

Tremmel, Hans Georg, and Ulrich Schumann. "Model simulations of fuel sulfur conversion efficiencies in an aircraft engine: Dependence on reaction rate constants and initial species mixing ratios." ***Aerospace Science and Technology*** **3 (1999): 417-430.**

Referee: 2

Received and published: 2 January 2020

The study introduces a new model called APCEMM, which is designed for simulating chemical processes in aircraft plumes and also considers the effect of contrails on plume chemistry. My impression is that authors do not have a strong background in atmospheric physics. This becomes apparent in quite a few passages of the manuscript. I recommend that the author team strengthens their expertise in atmospheric physics before revising the manuscript and redesigning the APCEMM. The manuscript could become publishable only after major revisions.

We thank the reviewer for their interest in our manuscript and we are grateful for their detailed comments and in-depth analysis. Please find our responses to each individual comment below.

General comments

As already stated in the summary above, I doubt that the implemention of the various atmospheric processes is done correctly. Moreover, sometimes processes or phenomena are included, that are irrelevant and only pretend to increase the level of detail in the model. Comments on the physical soundness of your apprach are listed in the section "Specific comments".

We have given specific responses below. However, we have also made a concerted effort to make both the details of implementation and the rationale (with regards to level of detail) of our modeling choices clearer throughout the entire methods section.

Here, only several general comments on terminology and language are made.

> *• Even though often written and read, it is wrong: Temperature is not cold or warm. It is low or high and tells us if something is hot or warm. Please check the whole manuscript.*
>
> **Thank you for this correction. We have checked and corrected the entire manuscript accordingly.**
>
> *• E.g. formula (2), (4)*
> *I find it awkward to provide units for each quantity. This somehow pretends that the formulae are only valid in conjunction with exactly those units. This is certainly not the case. I understand that supplying units helps the reader to make a first check of the correctness of the formulae. But the way it is presented, it is misleading.*
>
> **We now clarify at relevant locations (e.g. page 4, line 39-42) that units are provided for the purpose of demonstration only, and are not fundamental to the formulae.**
>
> *• Aerosol is a gas with suspended particles. If you refer to the particles only, better use the term aerosol particle. Sometimes you use the term aerosol even for ice crystals (in particular, last paragraph of section 2.2.3). I would make a clear distinction between aerosol particles and ice crystals.*
> *http://glossary.ametsoc.org/wiki/Aerosol*
>
> **We now make an explicit statement regarding the distinction between aerosols and aerosol particles on page 6, line 47.**
>
> *• Please use the terms deposition, sublimation, condensation and evaporation consistently.*

We have modified the manuscript accordingly.

• p.4. l.31: those THAT were emitted
See https://www.wisegeek.com/what-is-the-difference-between-that-and-which.htm
Please check the whole manuscript.

We have modified the manuscript accordingly.

• Concerning statements in the abstract like "evaporate ~9% faster and are 14% optically thinner"
Given the accuracy of the (still) simplified treatment, I would prefer to leave out such precise numbers (in the abstract). How much are they worth? If you use another definition of optical thickness or define the time of evaporation slightly differently, I am sure you can get anything between 5% and 20%.

We agree that the original wording was too precise and may have overstated the achievable accuracy. As such, we have reworded the relevant phrases in the abstract to highlight the qualitative rather than quantitative outcome, and provide the full range of simulated outcomes as an example rather than as a definitive consequence of the use of biofuels. The section in question now reads (page 1, lines 34-37):

"Our results suggest that a 50% reduction in black carbon emissions, as may be possible through blending with certain biofuels, may lead to thinner, shorter-lived contrails. For the cases which were modeled, these contrails evaporate ~5 to 15% sooner and are 10 to 22% optically thinner"

Table 7 and 8
Given the uncertainties, it is not meaningful to provide numbers like −5.35% with two decimal places. Please round them to a reasonable precision. Similarly the value 1.2581 in Table 4 it "too" precise. Please go through the whole manuscript.

Given the achievable accuracy of the method, all numbers in the paper have been rounded to two significant figures.

Specific comments

p.2, l.39:
what are "local aerosol clouds"?

The sentence has been replaced with:
"This approach does not explicitly capture the high initial species concentrations within the plume, including the effects of non-linear chemistry in the early stages or the formation (and chemical effects) of aerosols and ice crystals (i.e. contrails) in the exhaust plumes. " (page 2, lines 20-21)

p.4, l.5:
The ambient temperature at cruise altitude is not 280K. Climate change is not that fast:-)

This typo has now been corrected to the less alarming temperature of 220K.

p.4, l.14:
Your statement implies that the coherent vortex flow field is just turbulence which is not the case. Please better describe how the vortices break up. Paoli and Shariff (2016) is a good source of information for contrail-specific processes and phenomena.

We agree with the reviewer and we realize that the vortex flow field is not purely turbulence. We have used Paoli and Shariff (2016) as a reference to extend our discussion of the flow field, our simplified treatment of it in this model, and possible future extensions of the work.

We realize that "viscous dissipation of turbulent energy causes the vortices to break apart" is imprecise and do not mean to claim that the coherent vortex flow field is purely turbulence. As such, we have also added a discussion of relevant vortex dynamics in the first 10 minutes in Section 2.1 (page 3, lines 9-17).

In our model, the vortex flow field is not explicitly represented. We assume that the vortex breakup occurs over 5 to 10 minutes. During that period of time, we use the simplifying assumption that the chemical species and ice particles are well-mixed. We acknowledge that this is a limitation of this study, however, and have added a statement to this effect in Section 2.2.1 (page 4, lines 56-61).
We also realize that enhancing diffusion in the beginning of the mature plume phase is a simplistic assumption and does not allow us to model the aircraft-induced wake dynamics accurately. We added the following sentence is Section 2.3.1: "Although computationally efficient, our current representation of the aircraft-induced turbulence is simplistic and does not allow us to model the spatial heterogeneity that would arise after the dissipation of the vortex pair."

p.4., l.16:
Schumann, 2012 is a long paper. Which formula do you use? Do assume that the vertical motion is constant over time during the vortex phase? Note that in a stably stratified atmosphere, large parts of the vertically displaced plume rise back to the original emission altitude after vortex breakup due to buoyancy. As some portion of the ice crystals (or some other tracer) remains at lower levels, the vortex sinking causes a strong and fast vertical plume expansion (compared to timescales of natural processes). It seems that this effect is not considered in your model.

We compute the sinking depth according to Equation (13) from Schumann (2012). We do assume in the current model that the sinking velocity is constant over time during the vortex phase.

We are also aware that the plume can rise back to its original emissions due to buoyancy. We model this phenomenon as an upward motion applied over the first hour of the plume. We indeed notice that the vortex sinking followed by the updraft leads to a considerable stretching of the contrail, much more than is expected due to vertical diffusion alone. We now note this effect on page 3, lines 49-58. We now also state explicitly that the treatment of vertical motions used in this study is simplified, and an area for potential future improvement (page 7, lines 36-39).

p.7, l.45:
Who is the user in this case and is supposed to choose a value for Dh?

The text has been clarified and now specifies that APCEMM requires the horizontal diffusion coefficient as an input (page 7, line 8). Table S1 in the Supplementary Information lists all the inputs required by APCEMM

p.8, first paragraph:
The way you include the effect of radiation is not correct. Contrail parts with the highest IWC are usually heated the most. This heating causes an uplift of those contrail parts during which the air cools adiabatically (again proportional to Γd). Assuming the atmosphere is stably stratified, the local uplift is sustained as long the ambient temperature is below the temperature of the contrail patch. So for typical stratification values, the initial heating actually translates in a cooling of the contrail! As the heating in the contrailfall streak is usually not that strong, radiation leads to a contrail vertical stretching.

See introductory textbooks on lifting condensation level for the general physics (unlike to warm clouds however, the latent heating effects are not that important in ice clouds and the moist-adiabatic lapse rate Γm is roughly the same as Γd).

We are aware of the fact that contrails experience a non-uniform uplift due to heterogeneity in the local ice water content. The current configuration partly reflects the physics described above. Contrail radiative imbalance is modeled as a transient updraft, which results in the contrail cooling (due to the presence of a vertical temperature gradient). We have clarified this in Section 2.3.1 and we have added a sentence in Section 4, discussing the limitations of the current approach (page 22, lines 29-38).

p.8, l.11:
Could you describe in a few words what KPP is.

KPP stands for the Kinetic Pre-Processor. KPP is a software tool which from a set of chemical reactions and rate coefficients generates code to integrate the differential equations and compute the time evolution of chemical species with a suitable numerical integration scheme. This explanation has been added on page 7, lines 48-51.

p.8:
The inclusion of ice aggregation seems very sophisticated (iterative determination of coalescene efficiency) compared to the treatment of other processes in the model. But more aggravating is the fact that the cited Beard & Ochs paper deals with precipitation drops and not ice crystals. Please refer to literature refering to aggregation, not coalescene of liquid cloud droplets. Section 4 of Sölch and Kärcher (2010) could be a good starting point to dive into the physics behind the aggregation efficiency.

We agree with the reviewer. Additional literature review confirmed that Beard & Ochs (1995) refers indeed to liquid cloud droplets. We now adopt the methodology described in Sölch and Kärcher (2010) by setting a constant aggregation efficiency.

The appropriate paragraph has been removed from the manuscript and replaced by:
"Following the approach from Sölch and Kärcher (2010), we assume a constant aggregation efficiency for ice particles." (page 8, lines 21-23). All analyses in the manuscript have been repeated using the updated methodology. Changes in outcomes due to this modification are included in the summary provided at the start of the reviewer responses, but overall this did not affect the conclusions of the paper. The inclusion of a constant aggregation efficiency for ice particles (equal to 1 as in Sölch and Kärcher (2010)) lead to minor changes as our previous aggregation efficiencies converged towards unity for particles smaller than 50 µm. As an estimate, in a typical experiment (similar to the setup described in Unterstrasser et al. (2010a)), the integrated number of particles larger than 30 µm changed by less than 0.3% after 6 hours.

p.9., l.21:
What specifications of the chosen aircraft and engine type appear in the model, and which ones matter in the end? Are your results only valid for this specific aircraft/engine combination or can your findings be generalised?

A number of aircraft parameters come into the model. These vary from emission characteristics (NO_x, H_2O and soot emission indices, fuel flow), aircraft properties (aircraft mass, wingspan) and flight conditions (flight level, background meteorological and chemical conditions).

The main factors influencing our metrics are the NO_x emission index, and the flight-level conditions, as demonstrated in Sections 3.2, 3.3 and 3.4. Microphysical characteristics are more sensitive to the soot emission index, aircraft properties and meteorological conditions as well.

To make these dependencies clearer, we now include a table in the SI which lists all of the input parameters used by the model; which are specific to the aircraft type; which are engine parameters; and so on. We also list the sources used for the examples in the paper (Table S1).

Only results from a B747-800 equipped with GEnx engines are presented, but all relevant parameters can be modified through the input structure provided to APCEMM. Comparison of results using other aircraft/engine combinations is a future research opportunity and this is now mentioned on page 9, lines 43-45.

p.9:
Why is it important to evaluate the error X after 24 hours, hence at the same time of the day as the initialisation was done? Wouldn't it be better to evaluate the error at a time where the spatial dimensions of the APCEMM-modelled plume and the BOX-modelled plume are similar? Refering to Figure 2, you state in the text that 1.2 kg or 0.2 kg ozone is produced, giving a fatcor 6 difference between the two modelling approaches. A variation of the evaluation time would dramatically change this factor. Using an earlier point in time (e.g. 2 hours earlier at time 6:00) the factor would be much higher. Could you make clearer the strategy behind your evaluation effort.

We use the 24 hour timescale as a convenient approximation, and recognize that it could be further refined. We chose 24 hours for two reasons:

1. **After 24 hours, the sunlight conditions are identical to the ones after emissions. This is necessary to compare the concentrations of photochemically active species, like NO or O_3. Comparing O_3 under different photochemical states would not be a fair comparison for this study.**
2. **The plume model allows us to model fine-scale chemical phenomena, like HO_x depletion, early on in the plume. This process cannot be captured with a single box model. After 24 hours, we assume that the plume is sufficiently diluted to conclude that the fine-scale representation is no longer needed, and thus, that the box model and the plume model behave similarly. The plume's dimensions could still be much smaller than that of the box model. Indeed, in most cases we calculate that the "characteristic width" of the plume, based on the extent in which 95% of an emitted tracer is contained, is still only 50 km, compared to the box width (typical of modern global atmospheric simulations) of 100 km.**

As such, we consider 24 hours to be a convenient stopping point, rather than being necessarily the optimal point at which the plume could be considered "ready" for hand-off to a lower-resolution model. We clarified this in the manuscript by adding the underlined text in Section 2.4.2 (page 9, lines 84-92): "Evaluation after 24 hours ensures that the domain is in the same photochemical state as at initialization. <u>This ensures that we make a fair comparison for photochemically-active species. However, the plume may still be sufficiently concentrated that adding it to a grid cell in a larger simulation may still result in misrepresentation of plume chemistry. Additional work will be needed to quantify the magnitude of this error if plume processing is embedded into a global-scale model.</u> "

Remarks on section 3.5.1:

> *• Several choices of the background conditions are not reasonable at all. Section 2.2 of Kärcher et al. (2009) may help to choose more realistic cases.*
>
> **Based on review of Kärcher et al. (2009), we have updated our contrail simulations to use a more realistic background condition. Specifically, we use the approach described in Unterstrasser et al. (2010a), in which a background 50% relative humidity and a single supersaturated band (1 km in thickness) are prescribed. The description in Section 3.5 has been updated to reflect this (page 18,**

lines 18-19), and all results have been updated accordingly. This change also enabled us to perform direct comparison of our results to Unterstrasser's (see later comment).

• A 10 cm/s cooling over 24 hours translates into a lifting by 8 km and an adiabatic cooling by 80K. This is not realistic. Compared to this, the 0.1 K diurnal temperature variation can be safely neglected.

The simulated updraft is used to model buoyancy and the effect of radiative imbalance, and is only applied during the first hour. As such it results in a lifting of only ~150 m, and a cooling of ~1 K. This is described in Section 2.3.1. (page 7, lines 34-35).

• Persistent contrail formation is likely to occur in a RHi-range of 100%−−140% (above the upper limit, natural cirrus formation could not be neglected)

We agree. We have restricted our analysis to meteorological conditions with a relative humidity below 140%.

• Does the depth of supersatured layer remain constant over time? Given the prescribed uplift, the initially subsaturated layer above/below the supersaturedlayer would eventually become supersatured as well and the supersaturated layer would grow in size. If you used a time-constant 200m thick layer and included the radiation effect correctly, the contrail would move out of supersaturated layer into the drier air above. This leads to entrainment of dry air into the contrail which would then start to vanish.

We have assumed in our study that the depth of the supersaturated layer remains constant over time. However, the contrail is able to move relative to the layer, and does so during the first hour ("updraft"). In our current cases, we use a thicker (1 km) layer, consistent with Unterstrasser et al (2010a). Depending on the updraft velocity, the contrail can therefore rise out of the supersaturated band (page 19, lines 27-32).

• Given the quite thin supersaturated layer, the simulated contrail lifetimes of >10h appear to be too large (in particular for vUP= 0).

Following the implementation of more realistic background conditions, the predicted lifetimes have reduced. We now find lifetimes between 6 and 10 hours, consistent with Lewellen et al (2014a).

• You first make a link between in-situ loss and aggregation and few lines later you say in-situ loss is due to Ostwald ripening.

This is a mistake in the original manuscript. *In situ* losses are not linked to aggregation of particles. In situ losses correspond to the sublimation of small crystals at a relative humidity close to 100% in favor of larger crystals, as described by Lewellen et al. (2014a). The corresponding clause ("represented in the coagulation kernel applied during the diffusion regime") has been deleted and this has been clarified (page 19, lines 10-16).

• line 21: Yes, it is usually warmer further down, but this is irrelevant here. Or do really want to say the ice crystal melt and become water droplets? What matters is that it is dry and the ice crystals sublimate and are lost eventually.

We agree that this was worded incorrectly. What was meant is that the ice crystals enter a drier region and sublimate. The manuscript has been updated accordingly (page 19, line 41).

• If your contrail model produces reasonable results, could be checked by a comparison with the higher resolution model used in Unterstrasser & Gierens, 2010 a,b. This comparion should be feasible to achieve with small extra effort as you anyway use mainly their definitions of contrail properties. It would only require to specify the same background conditions. This could show if your modeled contrail lifetimes and response to variations of RHi or EIsoot are reasonable.

We thank the review for this suggestion. We performed a number of validation tests and now compare our results directly to those presented by Unterstrasser & Gierens (2010a). The inter-comparison is shown in Figure R1 of this document, and a discussion of this comparison (along with the figure itself, in two parts) has been added to the manuscript as Appendix D. The upper 12 panels show results from Unterstrasser & Gierens (2010a), while the lower 12 panels show results from APCEMM.

We show total ice particle number concentration, ice water content, extinction and RH_i at three time instances for the same meteorological conditions and emissions as Unterstrasser & Gierens (2010a). Based on visual inspection, we estimate that the integrated ice particle number and ice mass agree to within ~10%. The spatial distributions of ice crystal number and mass densities at t = 2,000 s are in agreement, with a maximum horizontal discrepancy less than 500 m. At later times, APCEMM fails to capture the large horizontal extent observed in the results from Unterstrasser & Gierens (2010a), caused by the fallstreak. This discrepancy is clearly visible on the ice water content row where APCEMM predicts a contrail spreading of 6 and 12 km at t = 8,000 s and t = 17,000 s respectively. By comparison, the LES simulation predicts extents of 10 and 22 km. However, vertical extents appear to be well represented.

Overall, APCEMM seems to predict a longer contrail lifetime with greater contrail ice mass, particle number and extinction. This could be explained by the inherent turbulent motions around supersaturation as described in Gierens et al. (2009) and Unterstrasser et al. (2010a). Such local fluctuations in an overall supersaturated region would induce changes in the total ice mass and cause the local sublimation of ice crystals which would tend to reduce the contrail lifetime. Efforts to parameterize this effect, if it is indeed the cause, are now suggested as future work in Sections 3.6 and 4.

In spite of this, we believe that the bulk features of the simulated contrails are in good agreement, with a maximum error on the integrated ice mass of less than 10%. The largest discrepancy lies in the horizontal spreading of the profiles but we think that APCEMM produces useful results given the simplicity of the approach taken to model contrail dynamics.

Table 8:
Wouldn't it be interesting and more insightful to compare all four simulations to the non-contrail simulation?

We now present the results of the contrail-induced chemical impact against the baseline case where no contrail is present (assuming the same background meteorological conditions). This comparison is shown and discussed in Section 3.6.3, which has been reframed accordingly (page 21, line 12).

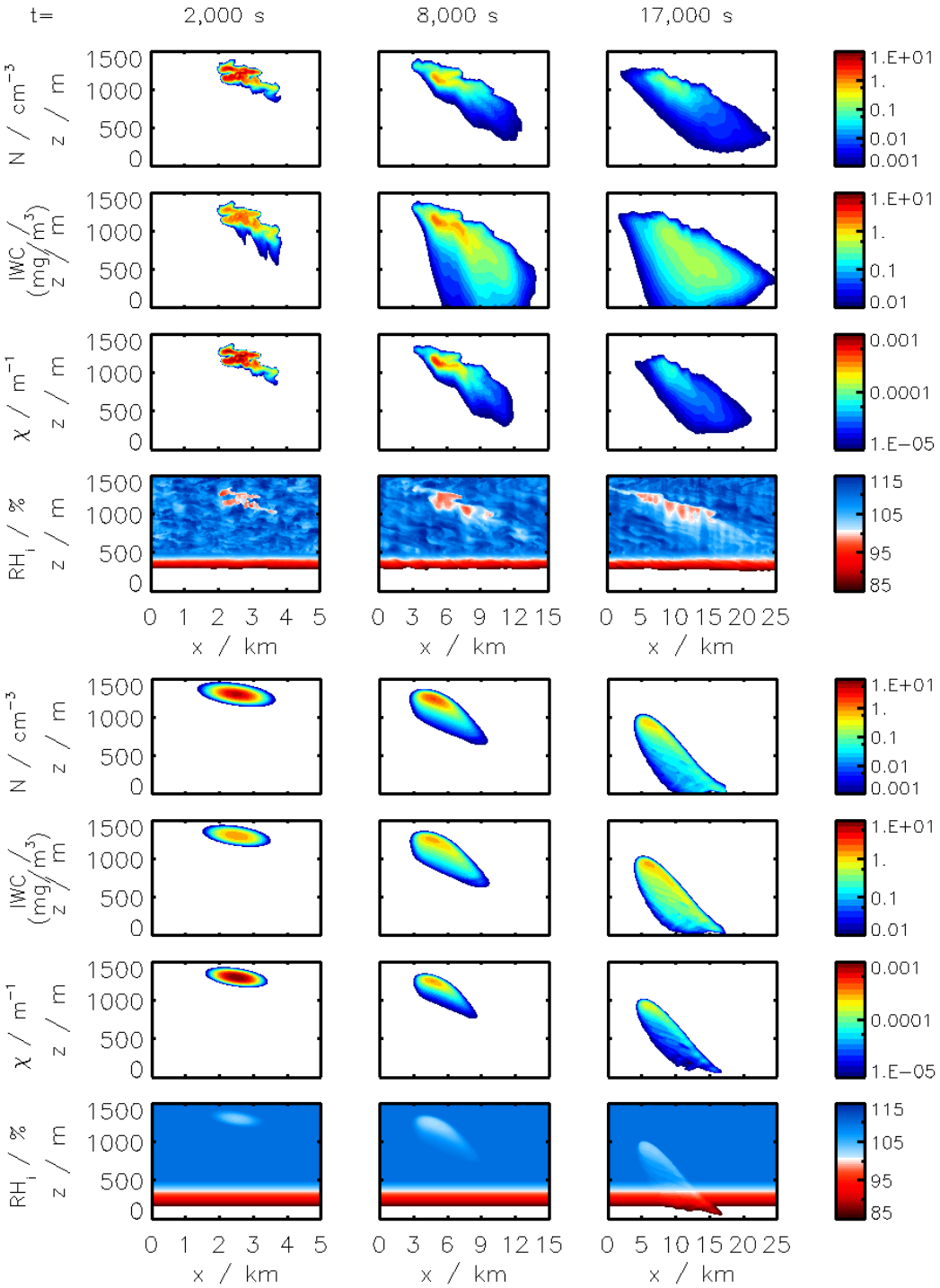

Figure R1. **Comparison of results from Unterstrasser & Gierens (2010a) (top) to a simulation in APCEMM (bottom) which attempted to reproduce the same input conditions. Data for the upper plot was kindly provided by the authors of the original paper.**

Technical corrections

p.3, l.14: the effects OF these

The changes have been made.

p.7, l.21/22: No complete sentence.

The sentence has been removed.

p.7, l.42: repetition of "a measure of local .."

The second instance has been removed.

p.11, l.24: please reformulate the sentence.

We have reformulated the paragraph:
"The instant dilution approach overestimates ozone production for any emission time, with emission conversion factors in the box model which are up to three times their respective values in the plume model. These discrepancies are greatest in summertime due to the larger ozone production term. The size of the ozone perturbation is sensitive to background concentrations of NO_x in both models.

During summertime, increasing the background concentration of NO_x from 100 to 200 pptv reduces the net (positive) ozone perturbation by 30-45% in both models. During wintertime, the same change in background NO_x has a negligible effect in the plume model, as shown in Figure 8. However, the instant dilution approach is still sensitive to this change. It produces a larger (more negative) ozone perturbation when the background NO_x is increased during wintertime. This pattern is explained by a less efficient conversion of NO_x to reservoir species at night. The transition between net positive and net negative ozone also changes as a function of the background NO_x. At 50 pptv of background NO_x, the plume model simulates net ozone production for 10 months, compared to 8 months in the instant dilution model. At 200 pptv, net production is simulated for 6 and 5 months by the two models respectively. This inconsistency in the magnitude and sign of the error between the two models means that the true impact of aviation emissions will be inconsistently modeled by an instant dilution approach." (pages 15, lines 6-31)

References:

Beard, Kenneth V., and Harry T. Ochs III. "Collisions between small precipitation drops. Part II: Formulas for coalescence, temporary coalescence, and satellites." ***Journal of the atmospheric sciences*** **52.22 (1995): 3977-3996.**

Gierens, Klaus, and Sebastian Bretl. "Analytical treatment of ice sublimation and test of sublimation parameterisations in two-moment ice microphysics models." ***Atmospheric Chemistry and Physics*** **9 (2009): 7481-7490.**

Kärcher, B., et al. "Factors controlling contrail cirrus optical depth." ***Atmos. Chem. Phys*** **9.16 (2009): 6229-6254.**

Lewellen, D. C., O. Meza, and W. W. Huebsch. "Persistent contrails and contrail cirrus. Part I: Large-eddy simulations from inception to demise." ***Journal of the Atmospheric Sciences*** **71.12 (2014a): 4399-4419.**

Lewellen, D. C. "Persistent contrails and contrail cirrus. Part II: Full lifetime behavior." ***Journal of the Atmospheric Sciences*** **71.12 (2014b): 4420-4438.**

Paoli, Roberto, and Karim Shariff. "Contrail modeling and simulation." ***Annual Review of Fluid Mechanics*** **48 (2016).**

Schumann, Ulrich. "A contrail cirrus prediction model." ***Geoscientific Model Development*** **5 (2012): 543-580.**

Sölch, Ingo, and Bernd Kärcher. "A large-eddy model for cirrus clouds with explicit aerosol and ice microphysics and Lagrangian ice particle tracking." ***Quarterly Journal of the Royal Meteorological Society*** **136.653 (2010): 2074-2093.**

Unterstrasser, Simon, and Klaus Gierens. "Numerical simulations of contrail-to-cirrus transition – Part 1: An extensive parametric study." ***Atmospheric Chemistry and Physics*** **10.4 (2010a): 2017-2036.**

Referee: 3

Received and published: 12 January 2020

This paper describes a detailed chemical and microphysical model that calculates the composition of aircraft plumes and its interaction with the atmosphere. This is certainly one of the most comprehensive studies that accounts for many chemical reactions and interactions between chemistry and microphysics of particles. The results obtained confirm previous studies, like for example the overestimation of ozone production due to NOx emissions when instantaneous dilution is adopted in CTMs and the role of heterogeneous processes that convert part of the emitted NOx into HNO3. All those results are interesting but in my opinion there are several issues that should be further discussed. Follows my major points.

We thank the reviewer for their interest in our manuscript and we are grateful for their detailed comments and in-depth analysis. Please find our responses to each individual comment below.

1/ In the introduction it is claimed that almost all the CTM use the instantaneous dilution (ID) approximation to account for aircraft emissions. The authors seem to ignore the many attempts of modelers to introduce plume processing in their large-scale model. The authors should refer to the review paper by Paoli et al. (2011) that gives a comprehensive review of the different approaches that have been followed to account for plume effects: Effective Emission Indexes, Emission Conversion Factors or Emission Reaction Rates. In the same paper are listed the CTM that use those parameterizations and the limitations of each approach.

Paoli et al. (2011) gives an in-depth overview of the methods used to account for a plume-scale processing of emissions and should have been included as a reference in the current paper. We have added a discussion of this previous work on page 2, lines 29-36.

2/ In contrast to the detailed chemistry and microphysics introduced in their model the authors have chosen a very simplified representation of the contrail and plume dynamics based on a simple diffusion model. This is a very crude approach that for instance ignores the details of contrail dynamics with the role of the crow instability, the formation of secondary vortices that maintain a significant fraction of the emissions at flight level with often persisting ice particles, and the complex nature of atmospheric turbulence and its interaction with radiation (e.g. Paoli et al., 2017). For instance wind shear and diffusion are considered as separate processes, although depending on the scale considered wind shear and diffusions are both the results of turbulence in a stratified atmosphere. Thus, it is very difficult to evaluate how the approximations made can influence the results of the model. Is it a balanced approach to introduce a detailed chemical and microphysics schemes with such a simplified dynamical scheme?

We agree that our approach to model the mixing between the plume and the background air is simplistic and does not account for the Crow instability and other plume-scale dynamical phenomena. We prioritized chemistry and microphysics on the expectation of being able to make significant new insights into the chemical behavior of the plume. However we agree that a more complex representation of plume dynamics could result in changes in the results, in particular with regards to contrail formation and persistence. This is reflected in the comparison now performed against the large eddy simulation results of Unterstrasser and Geirens (2010), in Appendix D.

We have added several paragraphs discussing the vortex dynamics in the early plume (Section 2.1) and the simplified representation used in APCEMM. As discussed in the response to Reviewer #2, we now mention in Section 2.2.1 that the current parameterization for plume mixing is not able to capture the spatial heterogeneity that could arise from vortex dynamics. We also added discussion in Section 2.3.1 which clarifies that the enhanced diffusion in the mature plume representation is a simplification, and that a

higher-fidelity approach would be needed to capture the effects of vortex structures on the optical and chemical properties of the plume (page 7, lines 17-19).

3/ Little is said on the validation of the model. Do we have measurements to confront to the model outputs? Can we constraint ozone formation rates and the conversion fraction of the emitted NOx to nitrogen reservoirs?

We agree that validating the model is a crucial step when developing software. We have compared as best as we can with previous papers dealing with the same topic and the results presented in this paper are in good agreement with previous publications (Petry et al., 1998; Meijer et al, 2000; Kraabøl et al, 2000). Although observational data is sparse, we also note in the discussion that direct comparison to *in-situ* measurements of both plume chemistry and ice would be a valuable future step (page 24, lines 52-54).

4/ In the conclusion it is concluded that plume effects are important and should be included in CTM. This is not new (see all the articles referenced by Paoli et al. 2011) and leaves open the difficulty to do that in a consistent manner with the chemistry and microphysics in place in those CTMs or GCMs. It is often because this consistency is difficult to preserve that the CTM and MCG modelers keep the ID approach despite its limitation.

We agree that maintaining the current capabilities of the chemical and microphysical processes of the CTMs and GCMs while adding a new capability - with an online treatment of aircraft emissions - could prove to be tricky. We now state explicitly on page 22, lines 46-48 that finding and maintaining an efficient implementation in a global simulation is a non-trivial challenge which we intend to confront in a future study.

References :

Paoli, R., O. Thouron, D. Cariolle, M. Garcia and J. Escobar. Three-dimensional large-eddy simulations of the early phase of contrail-to-cirrus transition: effects of atmo-spheric turbulence and radiative transfert. Meteorologische Zeitschrift, Vol. 26, 6, 597-620, 2017.

Paoli, R., D. Cariolle, R. Sausen. Review of effective emissions modeling and computation. Geosci. Mod. Dev., 4, 643-667, 2011.

Unterstrasser, Simon, and Klaus Gierens. "Numerical simulations of contrail-to-cirrus transition – Part 1: An extensive parametric study." *Atmospheric Chemistry and Physics* 10.4 (2010a): 2017-2036.

Thank you again for arranging this review. We look forward to your response.

Sincerely,

Sebastian Eastham

The role of plume-scale processes in long-term impacts of aircraft emissions

Thibaud M. Fritz, Sebastian D. Eastham, Raymond L. Speth, and Steven R.H. Barrett

Laboratory for Aviation and the Environment, Department of Aeronautics and Astronautics, Massachusetts Institute of Technology, Cambridge, MA 02139, USA

Correspondence to: S.D. Eastham (seastham@mit.edu)

Abstract. Emissions from aircraft engines contribute to atmospheric NO_x, driving changes in both the climate and in surface air quality. Existing atmospheric models typically assume instant dilution of emissions into large-scale grid cells, neglecting non-linear, small-scale processes occurring in aircraft wakes. They also do not explicitly simulate the formation of ice crystals, which could drive local chemical processing. This assumption may lead to errors in estimates of aircraft-attributable ozone production, and in turn to biased estimates of aviation's current impacts on the atmosphere and the effect of future changes in emissions. This includes black carbon emissions, on which contrail ice forms. These emissions are expected to reduce as biofuel usage increases, but their chemical effects are not well captured by existing models.

To address this problem, we develop a Lagrangian model which explicitly models the chemical and microphysical evolution of an aircraft plume. It includes a unified tropospheric-stratospheric chemical mechanism that incorporates heterogeneous chemistry on background and aircraft-induced aerosols. Microphysical processes are also simulated, including the formation, persistence, and chemical influence of contrails. The plume model is used to quantify how the long-term (24-hour) atmospheric chemical response to an aircraft plume varies in response to different environmental conditions, engine characteristics, and fuel properties. We find that an instant dilution model consistently overestimates ozone production compared to the plume model, up to a maximum error of ~200% at cruise altitudes. Instant dilution of emissions also underestimates the fraction of remaining NO_x, although the magnitude and sign of the error vary with season, altitude, and latitude. We also quantify how changes in black carbon emissions affect plume behavior. Our results suggest that a 50% reduction in black carbon emissions, as may be possible through blending with certain biofuels, may lead to thinner, shorter-lived contrails. For the cases that we modeled, these contrails sublimate ~5 to 15% sooner and are 10 to 22% optically thinner. The conversion of emitted NO_x to HNO_3 and N_2O_5 falls by 16% and 33% respectively, resulting in chemical feedbacks which are not resolved by instant-dilution approaches. The persistent discrepancies between results from the instant dilution approach and from the aircraft plume model demonstrate that a parametrization of effective emission indices should be incorporated into 3-D atmospheric chemistry transport models.

1 Introduction

Worldwide air passenger traffic is projected to grow at an annual rate of 5% over the next two decades (Airbus, 2017; Boeing, 2017). Commercial aviation fuel usage has continuously increased (Mazraati, 2010) as demand for air transport has outpaced improvements in efficiency (Lee et al., 2001). Combined with difficulties in reducing emissions of pollutants such as nitrogen oxides (NO_x) from aircraft engines, aviation has a unique and growing influence on the chemical composition of the atmosphere.

The release of chemically reactive substances from aircraft exhausts induces perturbations in the environmental chemical balance that can persist for days (Meijer, 2001). Additionally, aviation is a unique sector in terms of its environmental challenges as it is the most significant anthropogenic source of pollution at high altitude (8-12 km). In 2015, an estimated 240 Tg of jet fuel were burned for commercial aviation according to the global inventory from the FAA Aviation Environmental Design Tool (AEDT). For comparison, even under a very conservative assumption - that every rocket launch

in 2015 was performed with the high-capacity, kerosene-burning "Falcon Heavy" - we estimate that rockets burned at most 11 Gg of fuel below the stratopause in that year. Nitrogen oxides ($NO_x = NO + NO_2$) released from aircraft engines have been estimated to increase ozone concentrations in the Northern hemisphere by 2 to 9% (Penner, 1999; Schumann, 1997; Brasseur et al., 1996), while the ice clouds that form in aircraft exhausts ("contrails") have been estimated as having climate impacts of the same order of magnitude as the carbon-dioxide released in the plume (Kärcher, 2018).

The chemical effects of these emissions are typically simulated using global, Eulerian, 3-D atmospheric chemistry transport models. These models simulate aircraft exhaust as being released instantaneously into homogeneously-mixed grid cells which are orders of magnitude larger than the aircraft plume (Brasseur et al., 1998; Meijer et al., 2000; Eyring et al., 2007). This approach does not explicitly capture the high initial species concentrations within the plume, including the effects of non-linear chemistry in the early stages or the formation (and chemical effects) of aerosols and ice crystals (i.e. contrails) in the exhaust plumes. Shortly after release into the atmosphere, species concentrations in the aircraft plume can be several orders of magnitude larger than their background levels. NO_x concentrations at cruise altitude can exceed values up to 20 ppbv in the early stages of the plume, whereas background NO_x levels are typically between 0.007 ppbv and 0.15 ppbv in flight corridor such as the North Atlantic Flight Corridor (NAFC) (Schumann et al., 1998).

The impact of plume-scale modeling of aircraft wakes has been investigated over the past few decades mostly for its relevance to the environmental impact of aviation (Hidalgo, 1974; Thompson et al., 1996). Paoli et al. (2011) extensively covers the different approaches adopted to account for plume scale effects. They also list previous efforts to incorporate plume-scale processing of aircraft emissions into global chemistry-transport models. Prior studies have explicitly modeled the gas-phase components of the plume and have shown that the "instant dilution" approach results in inaccurate estimation of the plume's chemical effects on the environment (Petry et al., 1998; Kraabøl et al., 2000; Cariolle et al., 2009; Huszar et al., 2013). Furthermore, the effects of interactions between contrail ice and the plume chemistry - including as a surface for rapid heterogeneous chemistry - have not yet been quantified.

Field measurements over the past decades, such as the SUCCESS (Toon and Miake-Lye, 1998), POLINAT (Schumann et al., 2000) and SULFUR experiments (Schumann et al., 2002), have measured the microphysical characteristics of both liquid aerosol and ice particles (contrails) in aircraft plumes. Contrail modeling efforts based on these measurements have shown that these aerosols are sensitive to ambient relative humidity, fuel sulfur content, and the amount of emitted solid particles (Kärcher, 1998; Wong and Miake-Lye, 2010). In the early stages, non-volatile aerosols take up a significant amount of the emitted water vapor through condensation and heterogeneous freezing, potentially leading to the formation of liquid aerosols and ice crystals. During the plume expansion regime, gas species react and diffuse, potentially reacting with one another through heterogeneous chemistry on their surface. This suggests that the formation of ice in aircraft exhausts may result in additional chemical processing which is not captured in either global atmospheric models or gas-phase aircraft plume models.

This gap also affects assessment of new fuels for aviation. Biofuels have been identified as an option to reduce aviation's climate impacts by reducing the net contribution of aviation to atmospheric CO_2. However, several of these alternative fuels are also expected to produce less black carbon (Speth et al., 2015) and to have a lower sulfur content (Gupta et al., 2010; Rojo et al., 2015). The effect that these changes will have on aircraft plume chemistry and contrail evolution - and therefore on the total environmental impact of aircraft emissions - depend on the microphysical response of the plume. As such, the atmospheric effects of changing from conventional jet fuel to alternative fuels are not yet fully understood. In the following, soot emissions are identified as black carbon emissions.

To address these issues we develop the Aircraft Plume Chemistry, Emissions, and Microphysics Model (APCEMM). APCEMM is applied under a variety of conditions to simulate the influence of changes in environment, aircraft characteristics, and fuel properties on in-plume chemistry and aerosol size distribution. Finally, the effects of these changes are presented in terms of their impact on large-scale properties such as net 24-hour ozone production, end-of-lifetime NO_x partitioning, and contrail optical thickness.

2 Methods

We first describe the overall modeling approach used by APCEMM to simulate the chemistry and physics of an aircraft plume (Sections 2.1). Sections 2.2 and 2.3 describe the details of the different models used for the initial and mature plume evolution phases, respectively. Finally, Section 2.4 describes the experimental design used to determine the overall impact of plume-scale processes on long-term aircraft emissions impacts.

2.1 Model overview

APCEMM models the growth and chemical evolution of a single aircraft plume. Chemical concentrations and aerosol characteristics are calculated for a 2-D cross-section of the plume, perpendicular to the flight path. Dynamics, chemistry, and microphysics are explicitly modelled within the plume, using two different approaches depending on the age of the plume.

Observations and high-resolution modeling of aircraft wakes has shown three dynamical regimes in the first few

Table 1. Plume timescales and dilution ratios (Kärcher, 1995). Dilution ratios are the ratio of the initial plume air mass to the air mass at the target time.

	Early-plume model			Long-term plume model
Phases	Early Jet Regime	Jet Regime	Vortex Regime	Diffusion Regime
Timescale	0.1 s	10 s	100 s	Few hours up to a day
Dilution ratio at end of phase [-]	5.5×10^{-1}	2.6×10^{-3}	9.9×10^{-4}	$< 1.0 \times 10^{-4}$

minutes after emission, before the wake develops into a "mature" plume. Typical timescales and dilution ratios for an aircraft plume are shown in Table 1.

During the initial "early jet"and "jet" regimes, compressibility effects arise from the momentum-driven jet that last for a short amount of time of the order of a few seconds (Kärcher, 1995). After ~10 seconds the wing-tip vortices have formed and begin to affect the emissions plume. During this "vortex regime", the counter-rotating vortex pair causes the plume to descend by distances of the order of several hundred meters (Kärcher, 1995; Schumann, 2012). The wake is prone to instabilities triggered by atmospheric or aircraft-induced turbulence. Crow instability can occur in aircraft plumes and cause small sinusoidal distortions in the vortex shape to be amplified (Paoli and Shariff, 2016). These enhanced oscillations cause the vortex system to collapse (Naiman et al., 2011). We do not explicitly simulate these processes, instead treating the early-plume as well-mixed.

Over the period of these three initial regimes, the plume cools rapidly to ambient temperatures (~220 K) from an initial temperature of 500-600 K, leading to a spike in ice and liquid water saturations approximately 100 ms after emission and triggering a range of microphysical processes (Kärcher et al., 2015). During this period, formation of sulfate aerosols, freezing on solid nuclei, condensation, heterogeneous nucleation, and coagulation also occur. Homogeneous freezing is not included. Previous studies have suggested that homogeneous freezing is unlikely in aircraft plumes given the number of pre-existing nuclei (Wong and Miake-Lye, 2010). This is because combustion particles can acquire an ice coating at temperatures much higher than cruise temperatures, implying that ice crystals formed in the vicinity of the engines freeze by virtue of heterogeneous nucleation. In APCEMM, the plume is assumed to be well mixed during these first three regimes - the "early plume phase" (Section 2.2). We model this early plume as a uniform, well-mixed air mass evolving through time. In the following, we refer to this early-plume representation as a "box model".

The output of this box model is then provided as the initial condition for the model of the long term diffusion regime (Section 2.3). This regime begins when the aircraft-induced vortices break apart. In this regime, the plume expands in ambient air. The rate of diffusion is controlled by the vertical stratification of the atmosphere and by the vertical gradient of the wind speed (wind shear). Unlike the early plume phase, spatial heterogeneity of the plume is explicitly accounted for in APCEMM during the diffusion regime, allowing for cross-plume concentration gradients. For the first hour of this regime, we simulate an upward motion of the plume. This is because the vortex sinking which occurred during the early plume phase, modeled as a simple vertical displacement, results in adiabatic compression of the plume. In a stably-stratified atmosphere, this causes the plume to be warmer than its surroundings. The resulting buoyancy and radiative imbalance causes the plume to rise back to its original emission altitude, which we simulate as taking place over a one-hour timescale (Heymsfield et al., 1998).

2.2 Modeling of the early plume

During the early plume phase, the plume is treated as a single, well-mixed air mass. The air mass grows, dilutes, and cools through turbulent mixing with ambient air (entrainment). It also sinks and heats up due to the effect of the aircraft wing-tip vortices (vortex sinking). Throughout this phase we simulate rapid chemical changes, including the formation of liquid and solid aerosols.

2.2.1 Dilution and temperature evolution of the early plume

In the jet and vortex regimes, we adopt a formulation similar to the box model used in Kärcher (1995). The rate of change of chemical concentrations within the plume is dominated in this regime by dilution due to turbulent mixing. The contribution of wake mixing is approximated as a first-order decay term proportional to a time-dependent entrainment rate, i.e. $\omega_C(t)$.

$$\left(\frac{DC_k}{Dt}\right)\Big|_{\text{mix}} = -\omega_{C_k}(t)(C_k - C_{\text{Amb},k}), \quad (1)$$

where C_k is the molecular concentration of species k.

This entrainment rate agrees with the experimental data and curve fit provided in Schumann et al. (1998) for times greater than 1 s. $C_{\text{Amb},k}$ is the ambient molecular concentration of species k and is assumed to be constant during the jet and vortex regimes considering that the timescale associated with gas-phase chemistry is much greater than the time taken to reach the diffusion regime. We assume that, during this time, gas-phase chemistry does not influence the concentrations of most species within the plume. The only exceptions are conversion of S(IV) to S(VI) and NO_x to HONO and HNO_3 as described in Section 2.2.2, which evolve on similar timescales due to high initial concentrations (Kärcher et al., 1996).

The temperature of the plume during this initial phase is controlled by two processes. Firstly, prior experiments have shown that typical Lewis numbers are close to unity in coaxial jets, such as aircraft plumes (Forstall and Shapiro, 1950). Mixing of cold air with the hot exhaust stream (cooling the plume) is therefore assumed to occur at the same rate as entrainment of ambient chemical species. Secondly, the downward motion induced by the wing tip vortices also causes the air to heat up adiabatically, independently of the local lapse rate (Unterstrasser et al., 2008). The plume temperature evolution is therefore expressed as the sum of a positive heating due to vortex sinking and a first-order decay term representing entrainment, i.e.

$$\frac{dT_p}{dt} = \Gamma_d v_z - \omega_T(t)(T_p - T_{\text{Amb}}(z)), \quad (2)$$

In the present section, units are provided for the purpose of demonstration only, and are not fundamental to the formulae. In Equation 2, T_p is the plume temperature in K, Γ_d the adiabatic lapse rate expressed in K/m, v_z the vertical velocity in m/s of the plume and T_{Amb} the ambient temperature in K evaluated as a function of the ambient lapse rate, which has been obtained as a function of latitude and altitude from monthly-averaged meteorological data obtained from the Modern-Era Retrospective analysis for Research and Applications, Version 2 (MERRA-2). The plume acquires a vertical motion during the vortex regime such that v_z is assumed to be non-zero only between the time at which the vortices start inducing a vertical displacement of the plume and the vortex break-up time. The wake vortex sinking is computed according to a parametric formulation described in Schumann (2012) from which we evaluate the mean downward displacement as a function of aircraft and ambient atmospheric characteristics. This parameterization of the aircraft-induced mixing does not allow us to accurately capture the vortex dynamics and neglects the spatial heterogeneity that could arise. The inclusion of a more accurate representation of the early-plume dynamics in APCEMM is an area for future development.

Table 2. Assumed conversion efficiencies of NO_x and SO_2 to secondary species

NO	→	HONO	1.5%
NO_2	→	HNO_3	4.0%
SO_2	→	H_2SO_4	0.5%
OH	→	H_2O_2	2.0%

2.2.2 Chemical conversions in the early plume

In the early stages of the plume, oxidation of NO and NO_2 results in the formation of HONO and HNO_3. As described in Kärcher (1999), conversion efficiencies of NO, NO_2 and SO_2 depend on the exit plane hydroxyl radical concentration. Tremmel et al. (1998) inferred initial OH concentrations at the combustor and engine exit through measurements of NO, HONO, HNO_3 as well as CO_2 to account for plume dilution. Their results indicate that the OH emission index ranges between 0.32 and 0.39 g/kg_{fuel} for the JT9D-7A, which corresponds to an engine exit mixing ratio lying between 9.0 and 14.4 ppmv. Conversion efficiencies used in APCEMM are depicted in Table 2. Even though the conversion efficiencies remain of the order of a few percent, they increase monotonically with the OH engine exit mixing ratio, as more radicals are available for the following reactions (Kärcher et al., 1996).

$$\begin{aligned} \text{NO} + \text{OH} &\rightarrow \text{HONO} \\ \text{NO}_2 + \text{OH} &\rightarrow \text{HNO}_3 \\ \text{OH} + \text{OH} &\rightarrow \text{H}_2\text{O}_2 \end{aligned}$$

Oxidation of S(IV) to gaseous S(VI) is not simulated during this period. This process mostly occurs in the engine's turbines and only a negligible fraction is converted in the young aircraft plume (Lukachko et al. (1998); Tremmel and Schumann (1999)).

2.2.3 Microphysical representation of the early plume

As the plume cools down and mixes with ambient air, aerosols begin to form, supplementing those that were emitted directly from the engine (e.g. black carbon particles). This both modifies the local chemical concentrations and changes the initial aerosol size distribution during the second phase of the plume. Four microphysical processes are explicitly considered: freezing of liquid particles into solid ones, condensation of gas onto liquid particles, nucleation of new liquid particles, and coagulation of both solid and liquid particles.

We first consider growth of an existing particle population. The mathematical formulation is given in detail in Appendix A, but is covered briefly here. The microphysical model for growth of ice particles is adapted from Kärcher (1998). According to Kärcher and Yu (2009) and *in situ* measurements of black carbon number emissions at cruise altitude from Petzold et al. (1999), the plume is in a "soot-rich" regime, favoring freezing of water around black carbon cores rather than freezing of liquid and ambient particles. We thus assume that solid particles (black carbon and metal) emitted by the aircraft serve as condensation nuclei for water vapor. Under supersatured conditions, deposition induces ice crystal growth, depleting gaseous water vapor. During this initial phase, ice crystals are treated as mono-disperse (single size) and are considered spherical. Under these assumptions, we need only consider the growth of a single "representative" particle, rather than analyzing the population as a whole. Because of the low ambient temperatures, water that condenses is assumed to freeze instantaneously, such that ice crystals grow by deposition of water molecules onto their surface. The rate of change in the ice mass of a particle, m_p, is then given by

$$\frac{dm_p}{dt} = H_p^{\text{act}}(m_p) \times 4\pi C_p D_{\text{v,eff}} \left(P_{\text{H}_2\text{O}} - P_{\text{H}_2\text{O}}^{\text{sat}}\right), \quad (3)$$

where $H_{\text{p}}^{\text{act}}$ is a function accounting for nucleus activation (equation A3), C_p is the ice crystal capacitance (equal to the particle radius r_p for spherical nuclei), $D_{\text{v,eff}}$ is the effective water vapor diffusion coefficient in air (equation A4), and $P_{\text{H}_2\text{O}}$ the water partial pressure. Assuming that each ice particle is nucleated on a black carbon particle with a dry radius of 20 nm, and using a fixed mass density for ice of 916.7 kg/m^3, this calculation also gives the rate of change of radius of solid particles in the plume. Calculation of each of the terms in equation 3 is described in Appendix A1.

Black carbon and ice particles can also grow by condensation of water vapor, sulfuric acid, and nitric acid into a partial liquid surface layer. The growth of this layer is related to the condensation (or evaporation) rate of H_2O, H_2SO_4 and HNO_3, calculated as

$$\frac{dN_{k,p}}{dt} = 4\pi r_p D_k \beta(r_p) \left(\frac{P_k - P_k^{\text{sat}}}{k_B T}\right) \times \theta \quad (4)$$

where $N_{k,p}$ is the number of molecules of type k on a particle of type p, D_k is the gas diffusivity in m^2/s, and P_k and P_k^{sat} are the partial and saturation pressures of species k, respectively, expressed in Pa. The function β accounts for changes in uptake in different gas regimes, and is described in equation A5. Experimentally-derived deposition coefficients for heteromolecular condensation, used in the calculation of β, are taken from Kärcher (1998). On black carbon particles, θ describes the fractional surface coverage of the particle liquid coating and is calculated according to Kärcher (1998). For all other particles, this limitation is ignored and θ is set to 1. Gas diffusivities for H_2SO_4 and HNO_3 are taken from Tang et al. (2014).

Similar to sulfur, organic compounds in the upper troposphere have been found to alter the freezing behavior of aerosols and the black carbon coating fraction, θ, even in natural conditions (Cziczo et al., 2004; Kärcher and Koop, 2005; Murray et al., 2010). In aircraft plumes, the formation of condensable organic species originates in the production of electrically charged clusters (chemi-ions) (Kärcher et al., 2015). These organic compounds have been found to be either aqueous aerosols or soluble in aqueous H_2SO_4 solutions (Yu et al., 1999; Kärcher et al., 2015). Their high solubility makes organic matter a prime contributor to the mass of ultrafine plume particles and could also enhance the black carbon particle coating (Rojo et al., 2015). Previous studies estimated the mass of particulate organic matter in aqueous form to be approximately 20 $\text{mg}/\text{kg}_{\text{fuel}}$ (Kärcher et al., 2000). The theory behind the role of organics on particle growth and their chemical speciation is still limited. In most of the experiments described in this paper we neglect the role of organic aerosol. However, as a sensitivity study, we estimate the effect of organic matter on the fractional coating by prescribing an initial fraction of coated black carbon (Section 3.1). We also perform simulations in which we calculate the effect of changes in black carbon emissions, which can be considered as a proxy for the effect of organic aerosol if the aerosols are capable of acting as ice nuclei (Section 3.1.3).

In addition to growth of existing particles, new liquid particles can form through binary homogeneous and heterogeneous nucleation. Several nucleation parameterizations have been established to simulate binary homogeneous nucleation in a sulfur-rich environment (Jaecker-Voirol and Mirabel, 1989; Napari et al., 2002; Vehkamäki et al., 2002). Jung et al. (2008) have computed different sensitivities using these models and provided further validation of the models cited previously, comparing the results to field measurements. Given the range of ambient conditions relevant to an aircraft plume, we calculate cluster size, composition, and nucleation rate using the parameterization from Vehkamäki et al. (2002). While this model is only considered valid between 230.15 K and 305.15 K, we expect that most nucleation of fresh sulfate aerosol will occur while the plume is still cooling down, within this temperature range. Liquid aerosols are assumed to remain liquid throughout the plume lifetime. Previous stud-

ies (e.g. Kärcher, 1998; Tabazadeh et al., 1997) have quantified the freezing behavior of sulfate aerosols and liquid sulfur coating at low temperatures and found that freezing of sulfate aerosols requires an ice supersaturation of about 1.5 at 210 K. Additionally, Kärcher et al. (1998) conclude that heterogeneous freezing on coated black carbon particles drives the contrail formation phase. We thus neglect the freezing of sulfate aerosols similarly to Wong and Miake-Lye (2010).

The number concentration of aerosol particles in the plume can also change through coagulation, as emitted and entrained particles collide and coalesce. During the early plume phase, we consider only the coagulation of liquid aerosols, and the scavenging of liquid aerosols by ice and black carbon particles. Self-aggregation of ice and black carbon particles on the time scale of the early plume is assumed to be negligible. Since all aerosols during this phase are likely to be small, all collisions are assumed to result in coagulation (a coalescence efficiency of 1) (Jacobson, 2011). Particle breakup and shattering is neglected for the same reason (Beard and Ochs III, 1995; Jacobson, 2011). The effect of coagulation on the number concentration of aerosols in size bin k, covering the size interval $[r_k, r_{k+1}]$, is modeled as

$$\frac{dn_k}{dt} = \frac{1}{2}\sum_{j=1}^{k-1} \mathrm{K}_{j,k-j} n_j n_{k-j} - \sum_{j=1}^{+\infty} \mathrm{K}_{k,j} n_k n_j, \tag{5}$$

where n_k is the number density of particles in bin k and $\mathrm{K}_{i,j}$ is the coagulation kernel appropriate to collisions between size bins i and j, which represents the physics of the problem. A full description of the coagulation kernel and its calculation is given in Appendix B. Equation (5) states that the rate of change in the number density in bin k corresponds to the rate at which smaller particles of size $k-j$ coagulate with particles of size j minus the rate at which the particles of size k are lost due to coagulation with particle of all sizes.

During the early plume phase, liquid aerosols are modeled using 64 size bins, from a minimum radius of 0.1 nm to a maximum of 0.5 µm. Ice and black carbon aerosols are considered to have a single size, as estimated based on equations (3) and (4). Instead of solving equation (5) directly for every size bin, aerosol coagulation is computed using a semi-implicit, non-iterative, volume-conserving and unconditionally stable numerical scheme described in Jacobson et al. (1994). This model has been used extensively in aerosol modeling and aircraft plume simulations (Paoli et al., 2008). The rate of particle coagulation peaks shortly after emission and then significantly reduces as entrainment of ambient air into the plume decreases the number of aerosol particles present per unit volume of air.

The number and size of the aerosol particles present at the end of the early phase is used to provide the initial conditions for the mature plume phase, with one adjustment. The downward movement induced by the aircraft wake vortices (Unterstrasser et al., 2008) increases the depth of the contrail, while adiabatic heating and turbulent temperature fluctuations result in crystal losses through sublimation. These losses are represented using a survival fraction, which we compute using a parameterization based on large-eddy simulations (Unterstrasser, 2016). This survival fraction is typically of the order of 0.5, such that the initial aerosol population for the mature plume phase includes roughly half the number of aerosol particles as were present at the end of the early phase.

2.3 Modeling of the mature plume

Following breakdown of the wingtip vortices, the plume is considered to enter the "diffusion regime". In this regime, the plume is no longer considered to be well mixed, and diffusion of chemical constituents becomes important.

In APCEMM, we use an operator splitting method which allows us to treat the chemical kinetics terms separately from the turbulent diffusion terms, and to apply optimized solution methods for these different processes. For chemistry calculations, the domain is represented using a set of fixed concentric elliptical rings (Figure 1). The central ring (semi-major and semi-minor axis of ~75 m and ~30 m respectively) is initialized using chemical concentrations and aerosol properties as calculated at the end of the "early plume" stage (Section 2.2), and after accounting for losses due to vortex sinking. All other rings are initialized with ambient air. Each ring is further discretized into a lower and upper half-ring to allow for vertical variations in temperature, and to account for sedimentation of aerosols.

Diffusion and advection of pollutants relative to the plume centerline (due to wind shear), in addition to sedimentation of aerosols and buoyant motion, are simulated on a regular, rectilinear grid with a horizontal and vertical grid spacing of ~100 m horizontally and ~5 m vertically. Prior to these "transport" processes, concentrations of constituents in the rings are mapped to the rectilinear grid. Diffusion, advection, and settling of the constituents is then simulated using a spectral scheme (Gottlieb and Orszag, 1977). This scheme is also used to allow shear to distort the chemical rings. Following transport, the constituents are mapped back to the ring discretization.

Diffusion of pollutants, chemistry, and aerosol microphysics are all explicitly accounted for using a time stepping scheme. All processes are simulated using a variable timestep. During the first 10 minutes, and within 10 minutes of local sunrise or sunset, the time step is restricted to 30 seconds to ensure that rapid chemical changes are captured. At all other times, a time step of 5 minutes is used.

2.3.1 Diffusion and shear in the mature plume

The rate of diffusion of the plume's constituents is modeled using directional diffusion coefficients. The degree of diffusion anisotropy is dictated by the Richardson number, a measure of local atmospheric stability (Dürbeck and Gerz, 1996; Schumann et al., 1998). In APCEMM, the vertical diffusion

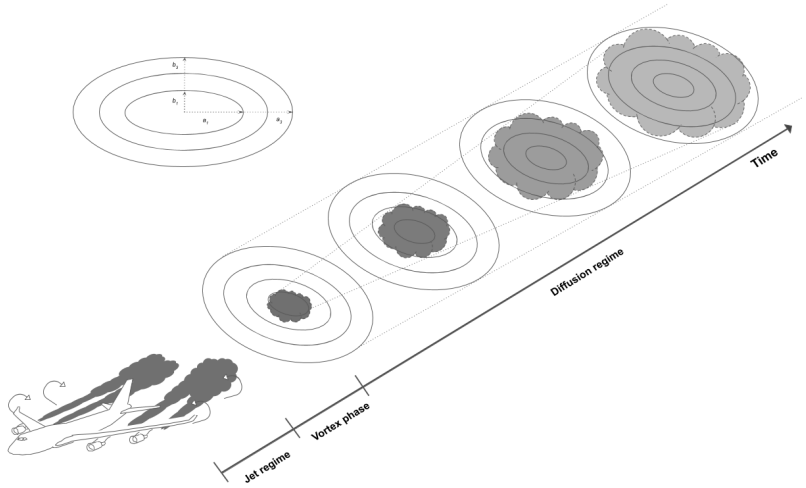

Figure 1. Schematic of the discretized ring approach used in APCEMM. The rings' major and minor axis are denoted by a_i and b_i respectively.

coefficient D_v is estimated using the approach from Schumann et al. (1995) using the local Brunt-Väisäla frequency and Richardson number, which is in turn computed from the local wind shear. To account for initial turbulence, D_v is increased to 1.1 m^2/s, after which it is reduced exponentially to its background value with an e-folding time of 13 minutes (Kraabøl et al., 2000). The horizontal diffusion coefficient is required as an input to APCEMM. Dürbeck and Gerz (1996) found that, for Richardson numbers above unity, the horizontal and vertical diffusion coefficients lie in the range $15\ m^2/s \leq D_h \leq 23\ m^2/s$ and $0.15\ m^2/s \leq D_v \leq 0.18\ m^2/s$ respectively, which agree with measurements from Schumann et al. (1995). Although computationally efficient, our current representation of the aircraft-induced turbulence is idealized and does not allow us to model the spatial heterogeneity that would arise after the dissipation of the vortex pair. A higher-fidelity approach would be needed to capture the effects of vortex structures on the optical and chemical properties of the plume.

In addition to diffusion across the domain, advection due to wind shear is explicitly accounted for using the same spectral scheme as is applied to simulate diffusion. The horizontal wind speed relative to the plume center line is calculated assuming a constant vertical wind shear across the domain.

We also simulate bulk vertical motions of the air mass. Heymsfield et al. (1998) reported through *in situ* measurements the existence of large-scale vertical motion in an aircraft wake. This upward motion is predominantly due to absorption of upwelling infrared radiation, resulting in a radiative imbalance (Jensen et al., 1998b). The contrail net heating drives a local updraft with speeds of up to 10 $cm\ s^{-1}$ during the first hour (Heymsfield et al., 1998), consistent with estimates that the contrail core can rise over the first hour after its formation (Jensen et al., 1998b). In this study, we adopt an exponentially-decaying velocity profile with a time scale of one hour. This is a simplified representation of contrail dynamics and its coupling with radiation. The inclusion of a radiative imbalance module in APCEMM is an area for future development.

2.3.2 Chemistry in the mature plume

The gas-phase chemistry mechanism is taken from GEOS-Chem v11 (Eastham et al., 2014). Heterogeneous halogen, N_2O_5 and HO_x chemistry, as well as formation and evaporation of stratospheric aerosols are considered. Due to their long lifetimes, reactions involving CFCs and HCFCs are neglected. The set of chemical reactions is solved numerically with the Kinetic Pre-Processor (KPP) (Damian et al., 2002). KPP is a software tool which from a set of chemical reactions and rate coefficients generates code to integrate the differential equations and compute the time evolution of chemical species with a suitable numerical integration scheme.

2.3.3 Aerosol modelling in the mature plume

The aerosol distributions in the mature plume phase are initialized based on the output from the early-plume module. The distribution of sulfate aerosols is unchanged while ice particles are distributed assuming a log-normal distribution, using the mean ice particle radius and a geometric standard deviation of 1.6 (Goodman et al., 1998; Jensen et al., 1998a). The use of a log-normal distribution is based on *in situ* measurements (Schröder et al., 2018) and this assumption has been used in previous work to initialize the contrail ice particle size distribution (Jensen et al., 1998b; Picot et al., 2015).

As the plume expands, the ice crystal size distribution changes due to growth, sublimation, gravitational settling and coagulation. Even without the application of a log-

normal distribution, a polydisperse distribution would arise due to coagulation and the different meteorological conditions throughout the plume. Particle growth is treated using a moving-center size structure (Jacobson, 1997). Ice crystal growth is characterized by the "advection" of the particle density distribution across diameter space (Jacobson, 2003).

Ice crystal growth modifies the particle volume but leaves the number of particles constant. Sublimation mechanisms lead to a loss of ice crystals and act as a source of water vapor, modifying the cell's relative humidity and release a dry particle core which is then considered "deactivated" and unable to take up water vapor as ice. The extent of sublimation is moderated by the size of the droplet cores, as larger hydrometeors can persist in subsaturated air. Evaporation and sublimation are both endothermic processes that cool down the surface of an ice crystal. The equilibrium surface temperature is obtained through an iterative process that allows us to compute the particle sublimation rate (Jacobson, 2003).

Aggregation of ice particles uses the same algorithm and the same coagulation kernel described previously for sulfate aerosols. Following the approach from Sölch and Kärcher (2010), we assume a constant aggregation efficiency for ice particles.

Gravitational settling causes the ice particles to fall vertically, thus entering warmer regions. Ice particle terminal velocities are computed according to Stokes law, accounting for the slip correction, as in Pruppacher et al. (1998). The settling velocity of an ice crystal depends on its size, with larger particles falling faster. Different parts of a contrail have different crystal sizes, meaning that they settle at different speeds (Unterstrasser et al., 2016). This differential settling effect is often neglected in reduced-order contrail models.

Finally, liquid (sulfate) aerosols are modeled using the same 64-bin approach as in the early plume phase. In the mature plume phase, the distribution of sulfate aerosols is affected only by coagulation, using the same coagulation kernel as before.

2.4 Experimental description

We first present the chemical and microphysical evolution of the plume in the first 15 minutes after emissions (Section 3.1), including the effect of changes in fuel sulfur content (FSC) and the potential role of condensable organic species. These factors are likely to be important for the formation and growth of ultrafine volatile particles and ice crystals in the aircraft wake. In addition, the theory behind the role of organic compounds is still poorly understood but Kärcher et al. (2000) estimate that particulate organic matter is a primary contributor to the mass of volatile particles. In this study, the impact of organic matter on the early evolution of black carbon particles and ice crystal growth is quantified by prescribing an initial fraction of coated black carbon. We also perform simulations to assess the role of the fuel sulfur content and the black carbon number emission index on the surface coating of black carbon particles and the formation of liquid sulfate particles. FSC varies from an average of ~2 to 600 ppm, depending on fuel type (Rojo et al., 2015). A range of black carbon emissions has been measured in a number of different aircraft wakes and has been found to vary by an order of magnitude (11 - 100 mg/kg_{fuel} as estimated by Petzold et al. (1999)). Results for different black carbon emission rates may also provide insight into the effect of organic aerosol, if said aerosol is acting as a nucleation site rather than as a coating for existing black carbon.

We then simulate the chemical evolution of a plume from a single flight using both approaches and compare the results to the literature (Section 3.2). We compute the impact of changes in background conditions (Section 3.3), engine emissions (Section 3.4), and flight location (Section 3.5). These simulations are intended to both validate the ability of APCEMM to accurately model non-linear plume chemistry and to quantify the extent to which the output of an instant dilution approach differs from that of a fully resolved plume model,

We also perform a set of dedicated experiments to quantify the relationship between different parameters and the behavior of a contrail forming in the plume. This includes the role of relative humidity and updraft velocity (Section 3.6.1), and the effect of changes in black carbon emissions (Section 3.6.2). Finally, we combine these assessments to determine how accounting for contrail ice could directly affect the chemistry of the plume, and how this effect is modified by changes in black carbon emissions (Section 3.6.3). Most global models do not include contrail simulation, so only APCEMM results are provided in these sections.

All plumes are simulated for 24 hours. For typical diffusion parameters of D_h = 15 m^2/s and D_v = 0.15 m^2/s, this results in 0.03% of emitted material reaching the edge of the computational domain by the end of the simulation.

2.4.1 Model setup

Both models, APCEMM and the instant-dilution approach, are initialized with background mixing ratios obtained from a year-long GEOS-Chem simulation. Noontime photolysis rates are retrieved from that same run. Atmospheric background conditions are obtained from a spin-up run over 5 days. Meteorological data for each altitude, latitude, longitude, and time are taken from the Modern-Era Retrospective analysis for Research and Applications, Version 2 (MERRA-2) for 2013. This includes the vertical wind shear and (longitudinally-averaged) Brunt-Väisäla frequency, used for calculation of the vertical diffusion coefficient. This approach provides an upper bound on vertical diffusion, as it overpredicts the diffusion parameter at large Richardson numbers. The probability distribution of the Brunt-Väisäla frequency, Richardson number, and resulting vertical diffusion parameter are given in the SI for different pressure levels. As shown in Dürbeck and Gerz (1996), the Brunt-

Väisäla distribution is unimodal in the troposphere and peaks around $N = 0.01\ s^{-1}$. A second mode appears in the stratosphere at approximately $N = 0.02\ s^{-1}$. Some further analysis shows that 90% of the distribution lies at Richardson numbers greater than 5, indicating weak and/or fast decaying turbulence. The distribution and its support agree with the values in Schumann et al. (1995) and the mean values lie in the range given by Dürbeck and Gerz (1996). A horizontal diffusion parameter D_h of 20 m^2/s is assumed for all simulations. Unless otherwise specified, we assume zero wind shear, although the effects of this assumption are investigated. A list of all the input parameters expected by APCEMM is provided in Table S1 of the Supplementary Information.

All the cases in this analysis consider emissions from a B747-8 equipped with GEnx engines, which are released in the innermost ring, with a cross-sectional area of 6,000 m^2. The representation of the GEnx engines in APCEMM at cruise altitude uses the equations of the Boeing Fuel Flow Method 2 (DuBois and Paynter, 2006) to compute a cruise NO_x emission index from the ones provided by the ICAO Engine Emissions Databank. For black carbon emissions, we use the "$SN - C_{BC}$" method described in Stettler et al. (2013), equation (5) in their paper. The black carbon mass emission index varied from 10 to 14 mg/kg_{fuel} for this particular engine except in Sections 3.1.3 and in 3.6.2, 3.6.3 and 3.6.4 where we prescribe different black carbon emission indices representing the heterogeneity in current cruise soot emissions. The emission rates for black carbon particles or "number emissions indices", $EI_{\#}$, are derived from the mass indices EI_m as

$$EI_{\#} = \frac{3EI_m}{4\pi\rho_{BC}r_{BC}^3}\exp(-\frac{9}{2}\ln^2(\sigma_{BC})), \tag{6}$$

where ρ_{BC}, r_{BC} and σ_{BC} are the black carbon mass density, median radius and geometric standard deviation. For all the cases described in this paper, we use a black carbon median radius of 20 nm and a geometric standard deviation equal to 1.6. This means that changes in the overall mass of black carbon emitted are modelled as a change in the number of particles.

The fuel sulfur content is kept constant at 500 ppm throughout all cases, except in Section 3.1.2 where we quantify the effect of changes in fuel sulfur content on the early-plume black carbon fractional coating and liquid sulfate aerosol formation and evolution. Analysis of results using other aircraft/engine combinations is a future research opportunity.

2.4.2 Metrics of the chemical response

To evaluate the error resulting from neglecting non-linear plume chemistry, we compare results generated using the instant dilution approach and using APCEMM. The discrepancies between both models are first compared in terms of total ozone mass per unit length in flight direction (kg/km). In addition, the conversion of short-lived nitrogen oxides to reservoir species affects long-term ozone production, heterogeneous chemistry, particle formation and/or growth, with known long-term impacts on air quality (Eastham and Barrett, 2016). The evolution of nitrogen partitioning is therefore computed for both models.

The total emitted NO_y (E_{NO_y}) is a conserved quantity throughout the plume lifetime and is equal to the plume-integrated NO_y perturbation $\left(E_{NO_y} = \Delta\left(NO_y\right) = \iint_A \left(\left[NO_y\right] - \left[NO_y\right]^{Amb}\right) dA\right)$, where the notation $[\cdot]^{Amb}$ refers to ambient conditions. At any given instant $\Delta\left(NO_y\right)(t) = \Delta\left(NO_x\right)(t = 0)$, which is proportional to the NO_x emission index. Averaging the perturbation due to aircraft emissions allows us to compute the time-dependent chemical conversions from one species to another. The emission conversion factor of species X, ECF_X, is then defined as:

$$ECF_X(t) = \frac{1}{E_{NO_y}} \iint_A \left([X](t) - [X]^{Amb}(t)\right) dA. \tag{7}$$

The emission conversion factor quantifies how many moles of species X are obtained for one mole of emitted NO_y. For ozone, this is similar to the ozone production efficiency (OPE), although the ECF is time-dependent and does not include ozone which has been produced and later destroyed. Given that nitrogen oxides are converted to reservoir species over the plume lifetime, ECF_{NO_x} decreases with time.

We use the ECF to quantify the discrepancy between the two approaches. For a species X, we define the error as the difference in ECF after 24 hours:

$$\varepsilon_X = ECF_X^{Box}(t = 24\ \text{hrs}) - ECF_X^{APCEMM}(t = 24\ \text{hrs}). \tag{8}$$

A positive error means that instant dilution of aircraft emissions overestimates the chemical production of species X compared to the aircraft plume model.

Evaluation after 24 hours ensures that the domain is in the same photochemical state as at initialization. This guarantees that we make a fair comparison for photochemically-active species. However, the plume may still be sufficiently concentrated that adding it to a grid cell in a larger simulation may still result in misrepresentation of plume chemistry. Additional work will be needed to quantify the magnitude of this error if plume processing is embedded into a global-scale model.

3 Results

3.1 Results of the early-plume phase

In this section, we model the evolution of the plume in the first 15 minutes after initial emission. In addition to chemical

effects, we quantify the role that organic matter, fuel sulfur content, and black carbon emissions have on the early size distribution of aerosols in the plume.

In these simulations, the background air is initially subsaturated with respect to water at a temperature of 215 K. As described in Section 2.2.3, organic matter influences the total mass of aqueous aerosols and the coating on black carbon particles, thus indirectly modifying the water deposition rate. Section 3.1.1 describes the early-plume microphysical evolution and quantifies the role of organic matter on particle growth. The formation of ultrafine volatile plume particles (composed of dissolved H_2SO_4 and organic compounds) modifies the gaseous composition of the plume and thus the condensation of soluble species on black carbon particles. Section 3.1.2 quantifies the sensitivity of the black carbon coating fraction to fuel sulfur content, and examines the partitioning between liquid and gaseous H_2SO_4. An analogy is then used to identify the impact of organic aqueous aerosols on the black carbon surface composition. Section 3.1.3 then considers how changes in black carbon emissions affect its surface coating. The simulations carried out in this last section could also be used to provide some insight into a potential role for ultrafine organic particles at low temperatures. We consider these simulations and outcomes because of their relevance to the aged plume in terms of ice uptake, aerosol surface area, and contrail lifetime.

3.1.1 Early-plume evolution and role of organic matter

This section first describes the evolution of the aerosol size distribution during the early plume phase, from the engine exit plane to approximately 15 minutes after initial emission. We then quantify one potential effect of organic species on plume chemistry and aerosol size distribution through their effect on black carbon surface composition, by varying the initial fractional coating between 0 and 25%.

Figure 2 displays the evolution of the early plume over different timescales. The air at the exit plane of the engine is assumed to be at a temperature of ~550 K. The plume undergoes rapid cooling in the jet phase and fresh ambient air is entrained into the warm plume. As the temperature decreases, the plume reaches saturation and remains saturated for ~2 seconds. During this time, rapid deposition of water increases the particle radius of ice nuclei (as shown in the upper-right plot). As plume mixing continues, fresh, dry air enters the plume. As the relative humidity with respect to ice falls below saturation, the particles start to melt. The loss of ice mass serves to maintain the plume's relative humidity at 100% with respect to ice. This continues until all ice mass has melted, after which point mixing drives the plume relative humidity to the background humidity.

The history of the plume can be displayed as a "mixing line" (on the bottom-right plot in Figure 2) on which the water partial pressure is plotted against plume temperature. The line starts in warm and moist conditions at the engine exit. The dilution of the plume, acting similarly on temperature and water mixing ratio, leads to a straight mixing line until the plume becomes supersaturated. Uptake of gaseous water onto aerosol then reduces the gaseous water partial pressure. Further mixing brings the plume to background state.

Some fraction of the fuel sulfur which is released in the engine combustor is converted to gaseoues H_2SO_4, which quickly condenses. This results in both liquid sulfate aerosol particles, but also coats already-existing particles (including engine-emitted black carbon particles). The bottom-left plot in Figure 2 shows the coating fraction of black carbon particles over time. This fraction is the result of both adsorption (gas-phase H_2SO_4 condensing onto black carbon directly) and scavenging (collision with existing liquid droplets) as described in Kärcher (1998). In the absence of organic matter, the fractional coating is dominated by sulfuric acid. Adsorption of sulfur particles is initially the prevailing pathway to the formation of a black carbon coating. The coating fraction attributed to adsorption plateaus after ~0.1 seconds as the gaseous molecular concentration of sulfuric acid becomes negligible. The remaining growth in the coating fraction is attributed to the scavenging of liquid sulfur aerosols onto black carbon particles.

As described in Section 2.2.3, organic matter can influence the black carbon fractional coating. Given the short timescales associated with formation of particulate organic matter, we assume that the black carbon particles are partially coated with condensable organic compounds in the first few milliseconds. As a sensitivity test, we vary the coating fraction attributable to organic species between 0 and 25%. The bottom-left plot of Figure 2 shows the effect on total fractional coating. Our simplified treatment of organic species shows that the inclusion of organic compounds results in faster particle growth, affecting the transient regime in the first second after emission, but does not have any effect on particle radius (upper-right) after approximately one second. Similarly, the gaseous chemical composition is unaffected by the condensation of organic compounds onto black carbon particles, even under supersaturated conditions.

3.1.2 Effects of fuel sulfur content

We next quantify the role of sulfur emissions on the plume gaseous composition and microphysical evolution. Ultrafine volatile particles are generated early-on in the plume by gas-to-particle conversion, containing both sulfuric acid and organic compounds. As already discussed, these highly-soluble species can condense onto the surface of black carbon particles, thus enhancing the coating fraction.

Figure 3 shows the effect of the fuel sulfur content on the black carbon fractional coverage and the partitioning between gaseous and liquid H_2SO_4. In this set of simulations, we vary the FSC between 50 and 5000 ppm. The results from our early-plume representation are in good agreement with the results from Kärcher (1998). The total sulfur concentra-

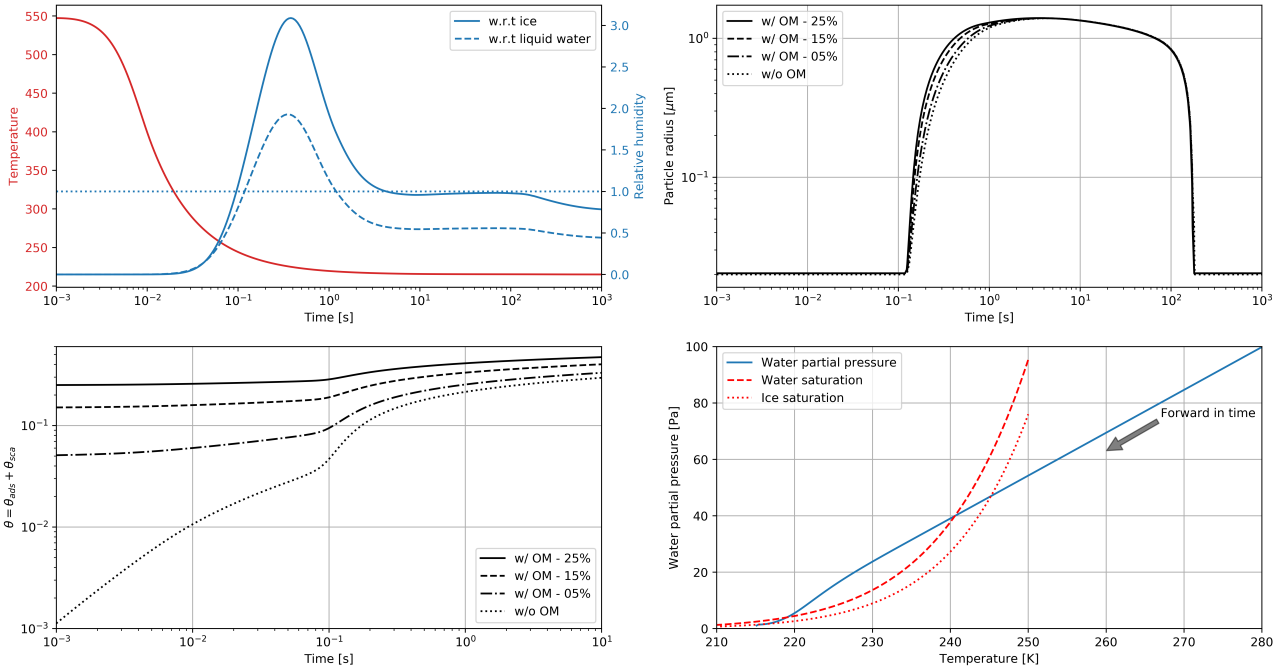

Figure 2. Clockwise, from top left: Simulated plume temperature and relative humidities (the saturation threshold is plotted as a dotted line), particle radius (different line styles represent the effect of organic compounds, a mass emission index of 15 mg/kg_{fuel} is prescribed), water mixing line and black carbon fraction coverage. We here consider subsaturated conditions with a background temperature of 215 K. We assume that organic species coat black carbon early-on in the plume (in the first few milliseconds). "OM" refers to the percentage coating by organic matter.

tion is the sum of gaseous H_2SO_4 and liquid sulfate and only decreases over time because of plume dilution.

In the low sulfur case, the black carbon particles are only coated on less than 5% of their surface after 100 seconds. This value compares to ~70% in the high FSC case. Our median scenario, assuming a typical fuel sulfur content of 500 ppm by weight, reaches 35%, with 30% originating from the scavenging contribution. These median values are comparable with other studies of the early-plume microphysics (Wong and Miake-Lye, 2010; Kärcher, 1998).

As the plume cools down, H_2SO_4 undergoes conversion from gaseous phase to liquid. A large fraction of the emitted sulfur is consumed to form liquid particles and coat the aircraft-emitted particles over the first 100 milliseconds after emissions (see Figure 3).

Figure 3 indicates that increasing FSC enhances the particle coatings and the number of liquid plume particles. In addition, a smaller activated fraction on black carbon particles reduces the initial water condensation rate. However, when particles grow in diameter (of the order of ~0.1 µm or more), the coating fraction becomes unimportant because of the much larger ice surface area. We observe no significant difference in the peak particle radius when varying the fuel sulfur content. This is in agreement with Busen and Schumann (1995) where no visual impact on contrail properties is detected after drastically reducing the FSC to 2 ppm.

Figure 4 describes the sensitivity of the sulfate aerosol distribution to the fuel sulfur content and its evolution throughout the first few minutes. In three experiments, we set the FSC to 50, 500 and 5000 ppm. Two regimes appear. In the low sulfur emission case, very few liquid particles are formed at the nucleation mode (~0.5 nm). In this regime, coagulation is slow and the shape of the aerosol distribution is dictated by the dilution and the entrainment of background aerosols (whose mode is not represented in Figure 4, given their larger size and smaller concentrations). In the high sulfur emission scenario, coagulation is more efficient and leads to the apparition of a second mode (~3 nm). After 100 seconds, the two modes have approximately the same number of particles. At later times, the rate particle formation is reduced, thus promoting the coarser mode. At intermediate FSC values, the two modes still coexist but the larger mode contains more particles.

Similarly to liquid sulfate aerosols, particulate organic matter in aqueous aerosols is a primary contributor to the mass of ultrafine volatile particles. Previous studies have estimated its emission index at ~20 mg/kg_{fuel}, comparable to the sulfuric acid mass emission index, assuming an average fuel composition and conversion fraction from S(IV) to S(VI). Their similar emission indices and high solubility allow us to treat organic matter in an analogous way as sulfate aerosols and to draw conclusions that only differ quantitatively.

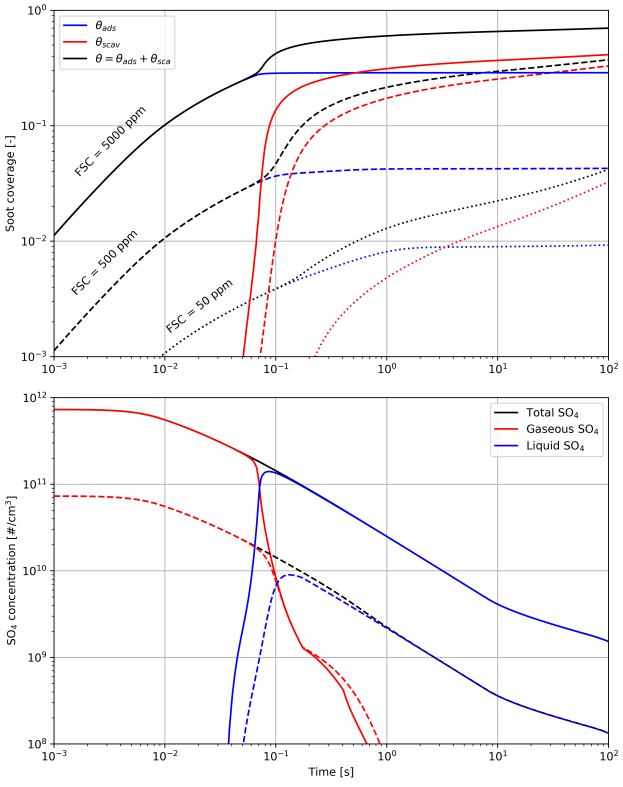

Figure 3. Black carbon fractional coverage (top) and number density of H_2SO_4 molecules (bottom), in gas and liquid form, as a function of time after emission. The total black carbon fraction coverage θ is the sum of the adsorption and scavenging contributions. Different line styles correspond to different fuel sulfur content (50, 500 and 5000 ppm).

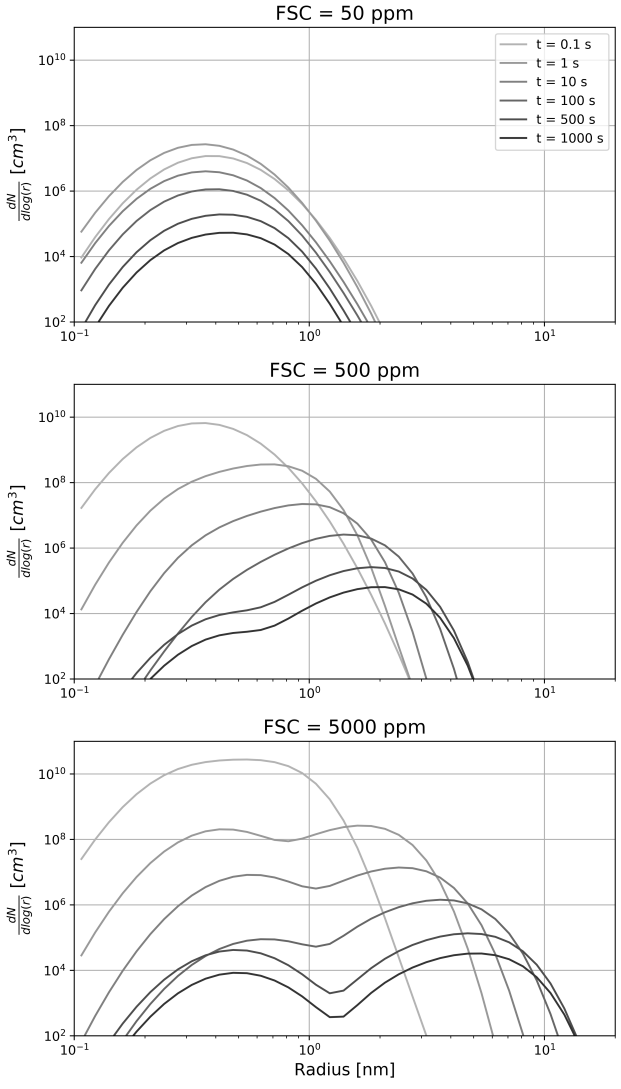

Figure 4. Time evolution of the sulfate aerosol distribution as a function of the fuel sulfur content. From top to bottom, the FSC is set to 50, 500 and 5000 ppm on a mass basis. The color shading depicts the time evolution, with lighter shading corresponding to a younger plume.

3.1.3 Role of black carbon emissions

In this section, we investigate the role of the black carbon emission index on the early plume aerosol size distribution. We perform simulations in which the black carbon mass emission index is varied between 0.01 mg/kg$_{fuel}$ and 50 mg/kg$_{fuel}$, to cover the potential range of current and future engine emission characteristics. We first focus on the impact of the emitted black carbon mass on its surface coating and then consider the effect on the particle radius over time, as both components could ice uptake and contrail lifetime.

Figure 5 indicates that we find no significant difference on the fractional coverage when varying the black carbon emissions by three orders of magnitude. In all cases, the contribution of sulfur adsorption to the black carbon area coverage is identical, and the contribution from liquid particle scavenging differs by a negligible amount.

Based on the results from Figure 5, all cases studied in this section have similar coating fractions, independent of the black carbon emission index. However, Figure 6 shows the in-plume relative humidity and particle radius when the black carbon emission index is varied. When the plume reaches saturation with respect to ice, the particle growth rate is the same regardless of the number of particles. In all simulations, the particles are competing for the same quantity of water. As a result, increasing the black carbon particle number density leads to smaller crystals, which in turn reduces the length of the supersaturated period for exhaust plumes in an initially subsaturated air mass. However, the same mechanism would be expected to result in longer contrail lifetimes for higher emissions indices if the air was initially saturated or supersaturated, due to the lower settling velocities of smaller particles.

Further reductions in the black carbon emission index could change the contrail formation pathway. The studies

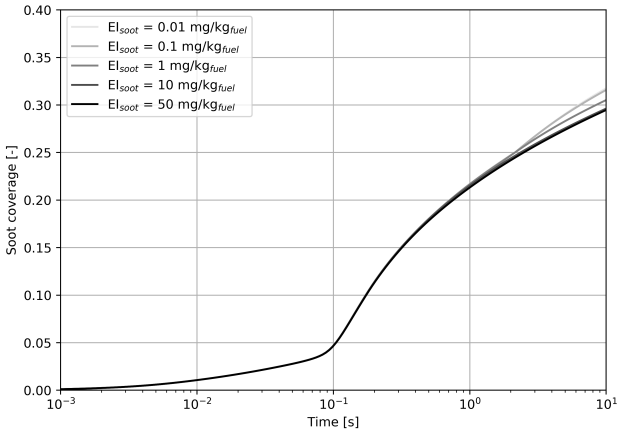

Figure 5. Simulated black carbon fraction coverage as a function of the black carbon mass emission index, varied from 0.01 to 50 mg/kg$_{fuel}$.

from Kärcher and Yu (2009) demonstrate that liquid plume particles (containing dissolved H_2SO_4 and organic compounds) could play a role in contrail ice formation at low black carbon number emissions and low temperatures. Ambient liquid particles are characterized by low number concentrations compared to an aircraft plume and thus cannot by themselves explain contrail formation. However, recent numerical simulations from Rojo et al. (2015) suggest that volatile particles could influence contrail formation, especially for alternative fuels in which the fuel sulfur content and black carbon emissions may be lower. Although we do not explicitly model the freezing of liquid plume particles, our simulations with increased black carbon number emissions provide some insight into the possible effect of organic and sulfate aerosols if they are capable of acting as ice nuclei.

3.2 Limitations of instant dilution

We first simulate the evolution of an aircraft plume as simulated using APCEMM. Figure 7 shows the time series of the ozone and NO_x perturbations over the first 24 hours after emission. The results as calculated under an instant dilution assumption (single, well-mixed box) are also shown.

The chemical evolution of the plume can be split into three regimes, distinct from the dynamical regimes described in Section 2.1 (Song et al., 2003; Vinken et al., 2011). The first regime is characterized by very high NO_x mixing ratios (>1 ppmv), causing ozone titration. In this period, typically lasting 10 minutes, high mixing ratios of nitric oxide (NO) rapidly deplete local ozone concentrations, resulting in a burst of NO_2 production through reaction [A1] (see Table 3). In this regime, HO_x ($= OH + HO_2$) production is suppressed by the lack of ozone (reactions [A5-A6]).

As the plume dilutes and NO_x mixing ratios fall below 1 ppmv, it enters the second regime. With little ozone remaining, HO_2 reacts with the remaining NO (reaction [A4]), producing OH and NO_2 without depleting ozone. This leads to increased OH levels and enhanced ozone production. Meanwhile, photolysis of NO_2 through reaction [A2] results in the recovery of ozone which had been depleted during the first regime. Between one and two hours after emission, ozone has been restored to its background value. Reactions [A7] through [A10] lead to conversion of emitted NO_x to nitrogen reservoir species.

A few hours after emission, the third regime begins, characterized by NO_x mixing ratios below 1 ppbv. Reaction [A4] and reactions including organic peroxides (such as [A12]) cause increasing levels of ozone and additional conversion to reservoir species. Aircraft plumes, similarly to ship plumes, are characterized by a high NO_x to volatile organic compound (VOC) ratio, therefore favoring termination reactions (e.g. [A7]) over catalytic ozone formation (Song et al., 2003).

Differences between the model outputs are dominated by the behavior during the first two regimes. Explicitly modeling the plume allows the initial ozone destruction to be captured because the highly-concentrated plume is resolved. Although a recovery in ozone is later simulated once the plume diffuses, additional production which would have occurred during the early plume is prevented.

In the instant dilution model, this ozone destruction and production cut-off is not captured. Because ozone is not locally depleted, the instant dilution model instead simulates a prolonged period of net ozone production, as HO_x concen-

Table 3. Dominant $O_3/NO_y/HO_x$ reaction pathways in APCEMM.

Reaction #	Reaction
[A1]	$NO + O_3 \longrightarrow NO_2 + O_2$
[A2]	$NO_2 + h\nu \longrightarrow O(^3P) + NO$
[A3]	$O(^3P) + O_2 \longrightarrow O_3$
[A4]	$NO + HO_2 \longrightarrow NO_2 + OH$
[A5]	$O_3 + h\nu \longrightarrow O(^1D) + O_2$
[A6]	$O(^1D) + H_2O \longrightarrow 2OH$
[A7]	$NO_2 + OH + M \longrightarrow HNO_3 + M$
[A8]	$NO_2 + O_3 \longrightarrow NO_3 + O_2$
[A9]	$NO_3 + NO_2 \longrightarrow N_2O_5$
[A10]	$N_2O_5 + H_2O \xrightarrow{\text{Aerosol}} 2HNO_3$
[A11]	$CH_4 + OH \longrightarrow CH_3O_2 + H_2O$
[A12]	$CH_3O_2 + NO \longrightarrow HCHO + \ldots$
	$HO_2 + NO_2$
[A13]	$CO + OH \longrightarrow CO_2 + H$
[A14]	$H + O_2 + M \longrightarrow HO_2 + M$
[A15]	$RH + OH \xrightarrow{O_2} RO_2 + H_2O$
[A16]	$RO2 + NO \longrightarrow RO + NO_2$

R represents an organic compound. The RH notation is used to describe Volatile Organic Compounds (VOCs).

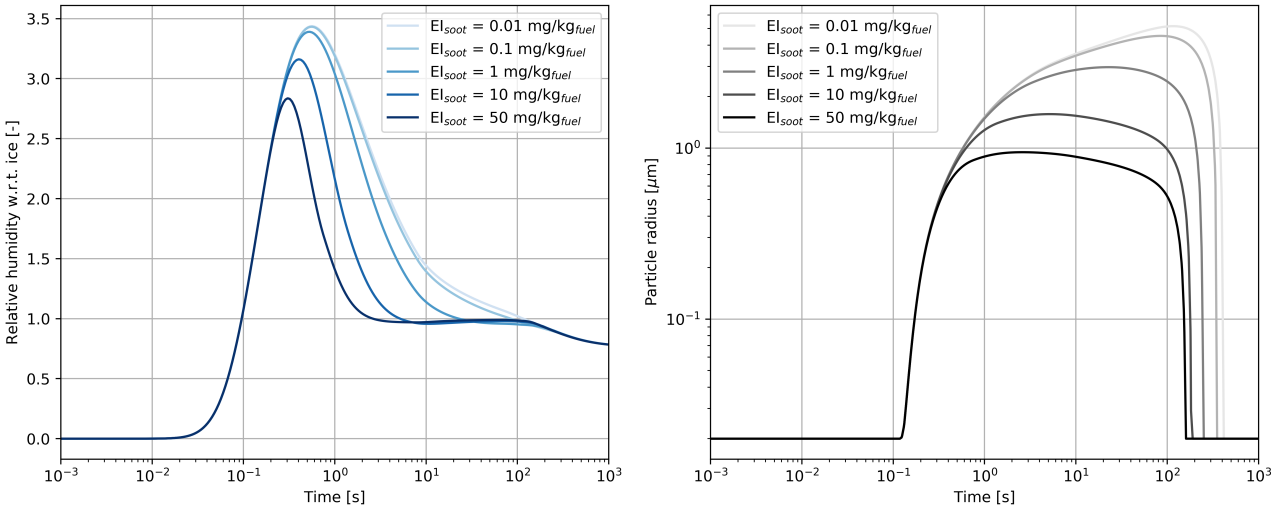

Figure 6. Relative humidity with respect to ice (left) and particle radius (right) for a black carbon mass emission index varying from 0.01 to 50 mg/kg$_{\text{fuel}}$.

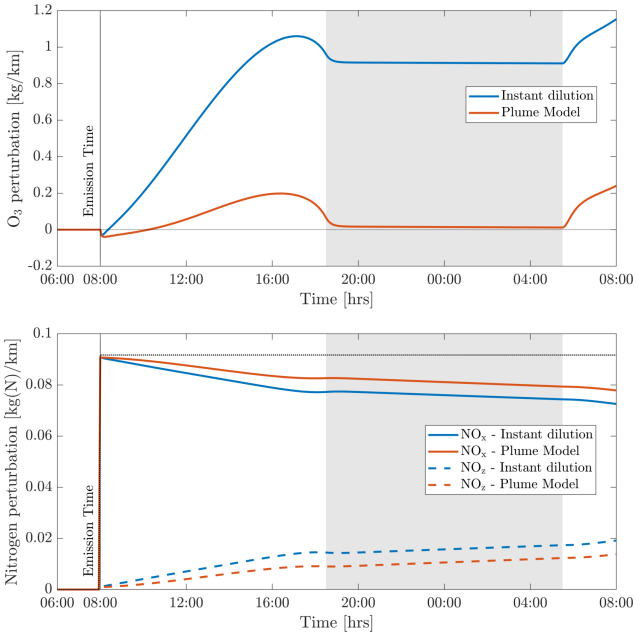

Figure 7. Perturbations in ozone (O_3), nitrogen oxides (NO_x) and the nitrogen reservoir species (NO_z) according to simulations using an instant dilution approach and the plume model. Emissions are released at 8:00 AM local time in a polluted environment. The black dotted line represents all nitrogen species (NO_y), which is a conserved quantity. The shaded areas correspond to nighttime.

trations remain close to background values. The instant dilution approach, unlike APCEMM, bypasses the first two HO_x-limited regimes and is therefore in a NO_x-rich, HO_x-rich environment, favoring daytime ozone production and conversion of NO_x to reservoir species. Additionally, instant dilution of aircraft emissions results in shorter NO_x lifetimes (see Appendix C for more details).

The net result is that, after 24 hours, the instant dilution approach estimates that the aircraft plume has produced ~1.2 kg of ozone per kilometer flown, compared to ~0.2 kg per kilometer estimated by APCEMM for a NO_x emission index of 11.5 g/kg$_{\text{fuel}}$. By this stage in the simulation both models show similar chemical behavior, as the plume has become sufficiently dilute to be well-represented by the instant dilution model. However, the erroneous simulation of ozone production in the initial phase leads to a persistent and significant error in the net ozone production of the plume.

This behavior, and the discrepancy between APCEMM and an instant dilution model, is strongly affected by local meteorology. Increased diffusion, or equivalently higher wind shear, dilutes the plume with a larger mass of air, minimizing ozone depletion. Therefore, total ozone production scales directly with mixing parameters. Table 4 shows the remaining NO_x and total mass of produced ozone after 24 hours as a function of the local diffusion coefficients. The results for instant dilution are shown in the last row. As diffusion rates increase and dilution becomes faster, the discrepancy between APCEMM and the instant dilution model decreases towards zero. Errors in global simulation of aircraft impacts will therefore be maximized in regions with low diffusion and/or wind shear.

3.3 Influence of background conditions

The in-plume ozone perturbation ($\Delta[O_3](t)$) and the conversion efficiency of NO_x to NO_y are influenced by parameters such as the emission time and background conditions. We first investigate the influence of changes in background NO_x. Figure 8 shows how the 24-hour ozone emission conversion

Table 4. Influence of diffusion parameters and wind shear on in-plume chemistry

	Diffusion coefficients [m^2/s]	Remain. NO_x [%]	O_3 perturbation [kg/km]
s = 0.000 s^{-1}	$D_h = 05, D_v = 0.05$	88	0.063
	$D_h = 10, D_v = 0.10$	86	0.17
	$D_h = 15, D_v = 0.15$	85	0.26
	$D_h = 20, D_v = 0.20$	84	0.34
	$D_h = 25, D_v = 0.25$	83	0.41
s = 0.003 s^{-1}	$D_h = 05, D_v = 0.05$	86	0.078
	$D_h = 10, D_v = 0.10$	84	0.21
	$D_h = 15, D_v = 0.15$	83	0.31
	$D_h = 20, D_v = 0.20$	82	0.42
	$D_h = 25, D_v = 0.25$	82	0.47
	Instant dilution:	79	1.3

Data obtained 24 hours after emission.

factor, ECF_{O_3}, varies as a function of NO_x background concentration and date of emission. Both simulations have been integrated over 24 hours. All simulations are conducted after a 5-day spin-up, and are simulated as occurring at 220 hPa altitude and 60° N.

The instant dilution approach overestimates ozone production for any emission time, with emission conversion factors in the box model which are up to three times their respective values in the plume model. These discrepancies are greatest in summertime due to the larger ozone production term. The size of the ozone perturbation is sensitive to background concentrations of NO_x in both models.

During summertime, increasing the background concentration of NO_x from 100 to 200 pptv reduces the net (positive) ozone perturbation by 30-45% in both models. During wintertime, the same change in background NO_x has a negligible effect in the plume model, as shown in Figure 8. However, the instant dilution approach is still sensitive to this change. It produces a larger (more negative) ozone perturbation when the background NO_x is increased during wintertime. This pattern is explained by a less efficient conversion of NO_x to reservoir species at night. The transition between net positive and net negative ozone also changes as a function of the background NO_x. At 50 pptv of background NO_x, the plume model simulates net ozone production for 10 months, compared to 8 months in the instant dilution model. At 200 pptv, net production is simulated for 6 and 5 months by the two models respectively. This inconsistency in the magnitude and sign of the error between the two models means that the true impact of aviation emissions will be inconsistently modeled by an instant dilution approach.

At a finer scale, we observe variations in emissions impacts depending on the time of day of the emission. Figure 9 shows contours of ozone and NO_x emission conversion factors for different times of day over the course of a year. For

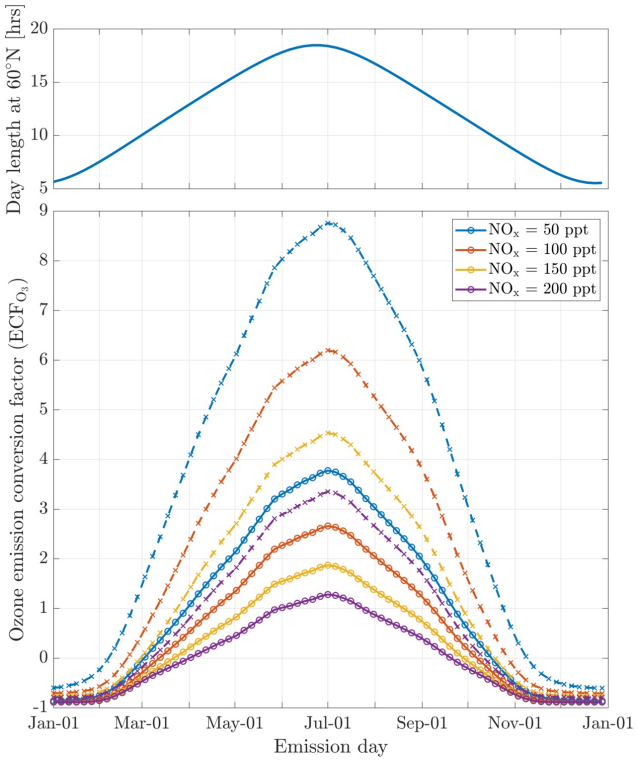

Figure 8. The bottom figure displays the 24-hour ozone emission conversion factor from the emission of a B747-8 equipped with GEnx engines at 08:00 local time, at 60° N, for an instant-dilution approach (dotted lines) and the plume model (continuous lines) as a function of day of the year. Different scenarios representing different background NO_x mixing ratios are displayed. The cases correspond to a background O_3 mixing ratio of 52 ppb. The figure on the top displays the amount of sunlight received at 60° N throughout the year, expressed in hours of daytime.

most of the year, the total production of ozone is relatively insensitive to the exact time of day of the emission. The exception is during summertime, when emissions immediately before local sunset (the upper dotted line) cause almost twice as much ozone to be produced as an emission during late morning. This is discussed in more detail in Appendix C.

3.4 Influence of NO_x emission index

In this section, we vary the NO_x emission index while keeping other emissions unchanged. The total NO_x emitted into the plume also affects chemical outcomes. Table 5 shows how a range of impact metrics are affected by changes in the NO_x emission index. The overall ozone ECF decreases as the NO_x emission index increases, falling from 3.2 for an EI of 8 g/kg_{fuel} to 1.5 for an EI of 20 g/kg_{fuel}. However, the product of these two factors - proportional to the total ozone present after 24 hours - still increase monotonically with the emission index of NO_x over the range of values considered.

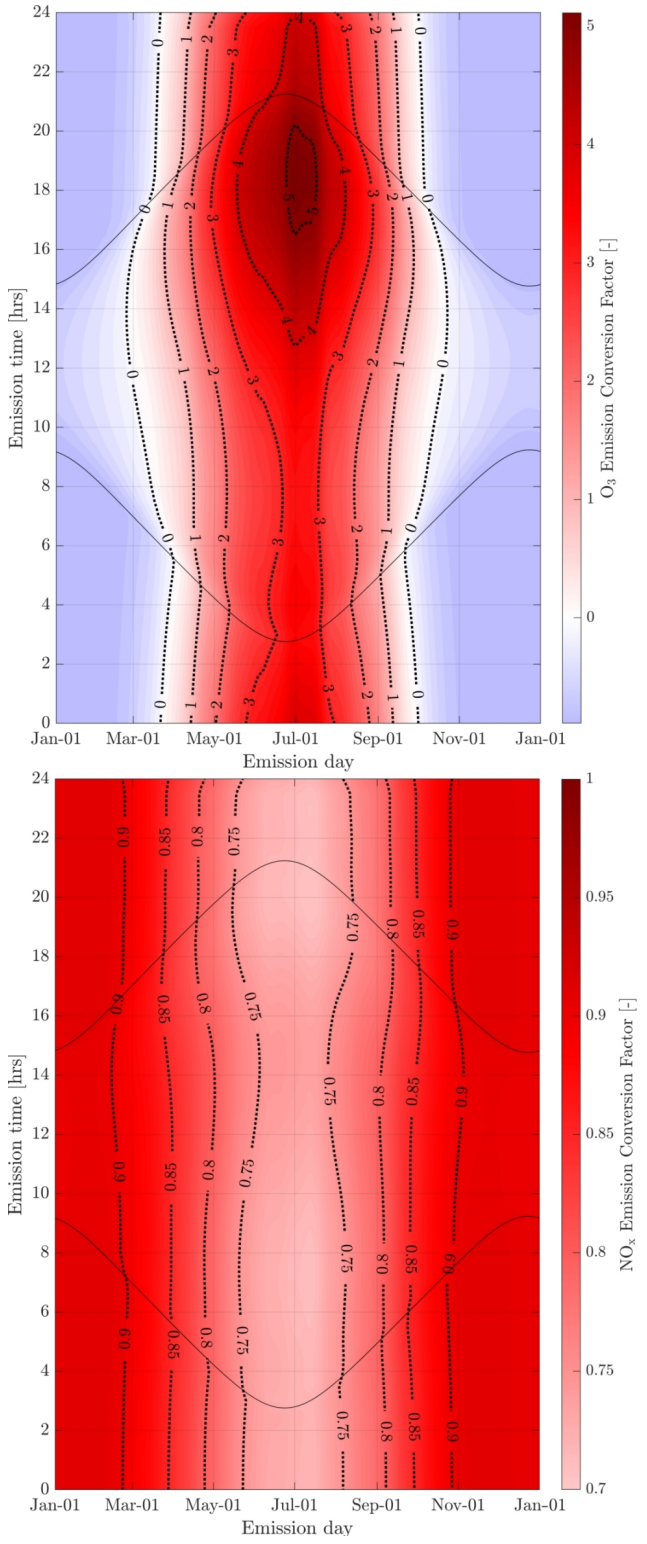

Figure 9. 24-hour O_3 (top) and NO_x (bottom) emission conversion factors from the emission of a B747-8 equipped with GEnx engines at 60° N. Dotted lines represent sunrise and sunset at the given latitude.

Table 5. Influence of NO_x emission index on emission conversion factors and in-plume ozone perturbation

EI_{NO_x} [g/kg_{fuel}]	ECF_{O_3} [-]	ECF_{NO_x} [-]	$\Delta[O_3]$ (24 h) [pptv]
EI_{NO_x} = 8.0	3.2	0.77	59
EI_{NO_x} = 12.0	2.4	0.79	67
EI_{NO_x} = 16.0	1.9	0.80	70
EI_{NO_x} = 20.0	1.5	0.82	70

Data obtained 24 hours after emission and for emission at 8:00 on June 16th.

This implies that decreasing the NO_x emission index provides non-linear benefits in terms of total ozone production. A one unit increase in the NO_x emission index (expressed in g/kg_{fuel}) leads to a reduction in ECF_{O_3} of 0.08 mol/mol under high EI_{NO_x} scenarios, but this increases to 0.2 mol/mol for the same absolute reduction in the NO_x under low EI_{NO_x} scenarios.

These results agree with the findings from Petry et al. (1998), Meijer (2001) and Vohralik et al. (2008). These simulations suggest that, relative to a plume-scale treatment of chemical processes, conventional instant-dilution approaches overestimate ozone production by up to a factor of three, and overestimate conversion of nitrogen oxides to reservoir species. We also find that decreasing aircraft emissions of NO_x emissions yields accelerating returns in terms of total in-plume ozone production, but that these results are sensitive to background NO_x concentrations.

3.5 Influence of pressure and latitude

The atmospheric response to aircraft emissions also varies as a function of the pressure and latitude of the emission. Although latitude is not a physical parameter of the model, it is equivalent to defining the amount of sunlight received, which affects photolysis rates and background conditions. We simulate pressures from 750 hPa to 150 hPa and latitudes from 0°N to 90°N. Temperature data is taken from monthly-averaged MERRA-2 meteorological data, for 2013. To capture variation of a single flight's emission conversion factors with geographic location and altitude, background conditions and photolysis rates are taken from GEOS-Chem. To also capture seasonal effects, simulations are carried out for emissions taking place on the winter and summer solstices as well as during the spring equinox, on March 21st. We perform simulations using both models. Results are presented in Figure 10 in terms of ozone and NO_x emission conversion factors. Isolines of the discrepancy between both models are plotted on Figure 10 for O_3 and NO_x (ε_{O_3} and ε_{NO_x}).

The results show a link between ozone production efficiency and latitude and pressure. Increasing pressure enhances the ozone emission conversion for the same amount of emitted NO_x, given sufficient sunlight. The amount of sunlight drives ozone production, as little ozone is generated

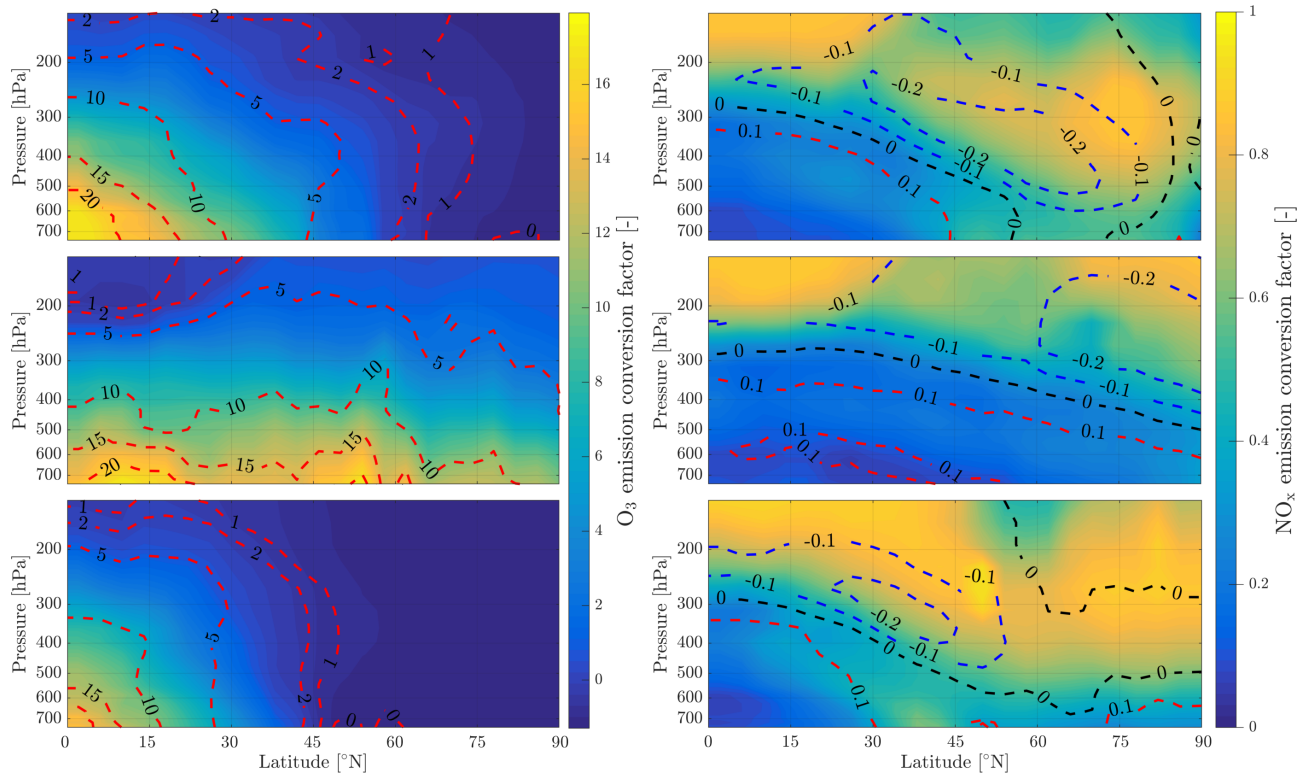

Figure 10. Contour plots of O_3 (left) and NO_x (right) conversion emission factor, 24 hours after emission from APCEMM. The isolines represent the discrepancy between the instant dilution approach and APCEMM. Blue isolines represent cases where the species ECF is underestimated, whereas the red isolines signify that the quantity is overestimated by instant dilution. Simulations have been carried out for emissions at 8:00 on March 21st, June 21st and December 21st (from top to bottom).

in the most northern latitudes during winter. At high flight altitudes or in cold regions, the daytime NO_x-driven ozone production is of the order of magnitude of the ozone loss at dusk and the early titration effect. This cancellation leads to a small in-plume ozone perturbation of varying sign as shown previously (Vohralik et al., 2008).

The instant dilution approach consistently overestimates the amount of ozone produced at cruise altitudes (~150 to ~240 hPa), as shown in Table 6. In absolute terms, the instant-dilution approach performs worst during summertime when ozone production is enhanced across the Northern hemisphere and the discrepancy in the ozone emission conversion factor (ε_{O_3}) is larger. The maximum ozone discrepancy (Table 6) reaches values around 5 in all seasons, corresponding to a relative error of approximately +200%.

NO_x conversion shows different sensitivities to location than the ozone ECF. As shown in the right panels of Figure 10, the NO_x ECF is positively correlated with ambient temperature but is insensitive to the amount of sunlight and season. As the temperature decreases with increasing altitude in the troposphere, the conversion of NO_x to NO_y is lowest at high altitude, going from an average value of 0.3 at 700 hPa to approximately 0.75 at 150 hPa. Greater conversion occurs in warmer air, around the equator and the tropics. Furthermore, the instant-dilution approach underestimates the amount of remaining NO_x at high altitudes but overestimates at lower levels. The crossover point varies significantly with season and latitude.

Table 6. Discrepancies between the instant-dilution approach and APCEMM at cruise altitudes. The left-most column shows the average ozone ECF as calculated in APCEMM, while the central column shows the average discrepancy in ECF between the instant dilution model and APCEMM. The right-most column shows the maximum calculated error. A positive error value means that the instant dilution model overestimates ozone production. All variables are evaluated and averaged over cruise altitudes only.

Date	$\overline{\mathrm{ECF}_{O_3}}$	$\overline{\varepsilon_{O_3}}$	$\max(\varepsilon_{O_3})$
03/21	+0.18	+2.6	+5.5
06/21	+0.98	+2.4	+4.4
12/21	-0.31	+2.0	+5.3

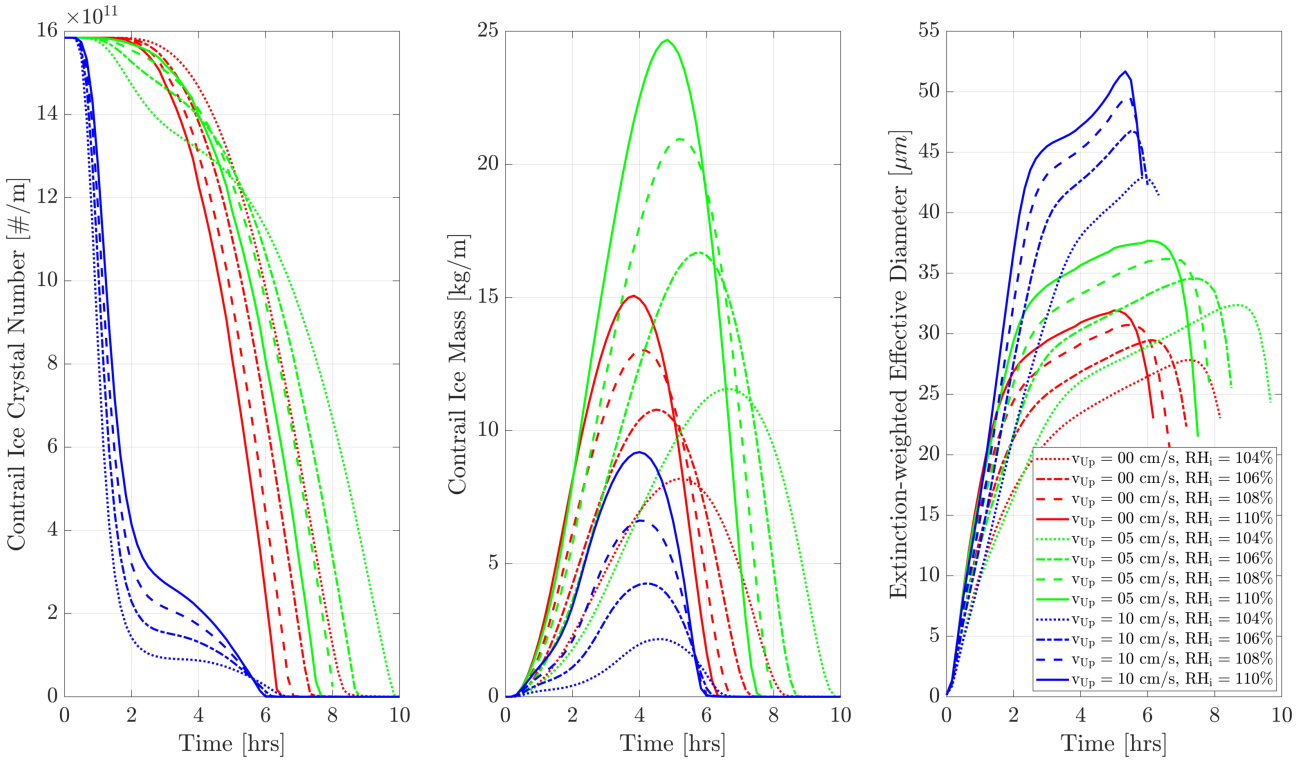

Figure 11. Contrail ice crystal number (left), ice crystal mass (middle) and extinction-weighted effective diameter (right) when varying background relative humidity and the updraft velocity magnitude.

3.6 Contrail microphysical, optical, and chemical properties

All analysis thus far has concerned conditions which are subsaturated with respect to ice. The simulated plumes have therefore been made up only of gas-phase constituents and non-ice aerosol particles. However, a second discrepancy between instant dilution models and real aircraft plumes is the lack of condensation trails in simulated aircraft exhaust, which can cause both climate and chemical impacts. This section assesses APCEMM's ability to simulate aircraft-induced condensation trails ("contrails"), quantifying how changes in background conditions affect the properties of the contrail. We then quantify the effect that these condensation trails have on the long-term atmospheric effects of aircraft emissions. This includes an investigation of differences in contrail lifetime and effects when forming in the stratosphere, as may result from supersonic flight.

In the following sections, we use similar background meteorological conditions to Unterstrasser and Gierens (2010a). We simulate a 1 km thick supersaturated layer, below which there is a linear decrease in relative humidity at a rate of 12% per hundred meters, to a background value of 50%. The average supersaturation in the upper troposphere has been estimated to be around 15% (Gierens et al., 1999), corresponding to a saturation of 115% with respect to ice. Atmospheric shear is set to 0.002 s^{-1}. The flight-level temperature is to 217 K. A diurnal temperature variation with a 0.1 K amplitude is applied, corresponding to daily temperature fluctuations in the upper-troposphere (Seidel et al., 2005). We also consider a range of updraft velocities, from 0 to 10 cm/s. This is based on previous studies which have shown that heating of contrail ice induces an upward convection motion with velocities in this range, such that the plume enters a colder environment (Unterstrasser and Gierens, 2010b; Unterstrasser et al., 2017). This updraft can cause the contrail to advect out of the supersaturated layer. An intercomparison between APCEMM and Unterstrasser and Gierens (2010a) is provided in Appendix D. As described in Appendix D2, the environment surrounding a contrail is characterized by local oscillations in the humidity field that arise from turbulent motion. This phenomenon is not explicitly in APCEMM and parameterization of these fluctuations is considered a future research priority.

3.6.1 Contrail simulations and the impact of relative humidity and initial updraft velocity

We first simulate the formation and evolution of a contrail in aircraft exhaust under a variety of conditions, to quantify the range of likely behaviors and verify behavior consistent with observations. For these purposes, we simulate an air-

craft plume in locally supersaturated air, with flight-level relative humidities ranging from 104% to 110%.

Figure 11 shows the temporal evolution of total contrail ice crystal number and mass for each combination of parameters, as well as the extinction-weighted effective diameter (Unterstrasser and Gierens, 2010a). In all cases, the contrail persists for at least 5 hours, but has sublimated after 10 hours. These lifetimes are consistent with observations, in spite of the idealized meteorological conditions considered here (Minnis et al., 1998; Iwabuchi et al., 2012). Most ice crystals are lost through sublimation and *in situ* losses. *In situ* losses correspond to the sublimation of small crystals in favor of larger crystals when the relative humidity approaches 100%. This phenomenon is attributed to Ostwald ripening through the Kelvin effect (Lewellen et al., 2014; Unterstrasser et al., 2017). Losses through Brownian coagulation are negligible as they account for less than 1% of particle losses. As the contrail expands, the contrail core is dehydrated through gravitational sedimentation of the largest particles, leaving behind a population of smaller ice crystals with little ice mass but a significant surface area. The formation and settling of large ice crystals (with a radius greater than 30 μm) lead to early variations in contrail ice mass. This means that growth in contrail ice mass slows earlier than would be captured by reduced order models which consider only the mean settling velocity.

The contrail ice crystal number is reduced when the updraft velocity is set to 10 cm/s. This is because the ice particles are advected out of the supersaturated region and thus sublimate quickly. The remaining crystals in the supersaturated region experience rapid growth, and their large settling velocity reduces the contrail lifetime. For updraft velocities of 0 and 5 cm/s, the contrail remains in the supersaturated layer, thus increasing the total ice mass over a larger number of particles, resulting in an increased contrail lifetime.

The contrail ice mass peaks between 4 and 5 hours after formation, with variations in timing affected by both the updraft velocity and background relative humidity. In both cases, moister air result in greater overall water uptake and therefore larger ice particles. These larger particles then fall to drier altitudes and melt, reducing the available number of particles. Higher relative humidity also increase the extinction-weighted effective diameter for the same reason. This results in a tradeoff between the "size" of the contrail, in terms of either the ice mass or effective diameter, and its lifetime, with more massive contrails having shorter lifetimes.

3.6.2 Influence of engine black carbon emission index on contrail properties

We next model how changes in black carbon emissions affect the properties of the contrail. We simulate an aircraft plume in which the black carbon mass emission indices are varied between 10 and 60 mg/kg_{fuel}, compared to 10 to 14 mg/kg_{fuel} estimated using the $SN - C_{BC}$ method for the GEnx engine. All other aircraft and engine emissions parameters are fixed for this sensitivity analysis. As a comparison, Stettler et al. (2013) estimate a fleet-wide average black carbon mass emission index of 28 mg/kg_{fuel} while *in situ* observations at cruise altitude have shown that different engines are estimated to have emission indices between 11 to 100 mg/kg fuel (Petzold et al., 1999). Each simulation assumes a flight-level temperature and relative humidity of 217 K and 110% respectively, and a post-vortex sinking updraft of 5 cm s^{-1}.

Figure 12 shows the evolution of the total ice particle number, total ice mass, and extinction-weighted effective diameter for each emissions scenario. Considering first the total ice mass, two distinct regimes are visible. The first regime occurs over the first three hours after formation. In this regime, all cases have identical ice masses. The contrail ice mass is controlled only by the ambient relative humidity, as all available water mass is taken up by whatever particles are available, with lower emission indices result in larger crystals.

After three hours, the simulations with the lowest emission indices start to lose ice mass. This is because of the discrepancy in ice crystal radius. Since the same ice mass is taken up on a smaller number of particles, they become larger and fall more rapidly to warmer altitudes. Lower emission indices result in smaller particles, extending the lifetime of the contrail. As the largest crystals are removed, only a core of small crystals remains.

These changes in contrail ice also affect the optical thickness of the plume. We calculate optical thickness by integrating the extinction χ, as defined in Ebert and Curry (1992). Figure 13 shows the temporal evolution of the optical thickness, integrated over the vertical and horizontal (perpendicular to the flight path) axes. As seen previously, the ice water content is identical in the first few hours for all simulations, meaning that a scenario with a large particle number has a larger total crystal surface area. This means that reducing the black carbon emission index decreases both the optical depth of the contrail and its lifetime. This is quantified in Table 7, which quantifies the "predominant" optical depth as

$$\tau_{\text{pre}}(t) = \frac{\int \tau^2(x,t)dx}{\int \tau(x,t)dx} \tag{9}$$

following the formulation of Unterstrasser and Gierens (2010a). Table 7 shows how this optical depth varies over time for each scenario. In all cases, the predominant optical depth increases with the black carbon emission index, with the relative difference between scenarios increasing over time until 4 hours after emissions. After this time, the cases with the lowest black carbon emission indices have almost fully sublimated. Scaling the emitted black carbon by a factor 2 with respect to the baseline case (set to 20 mg/kg_{fuel}) increases the 2-hour predominant optical depth by 14%. Fur-

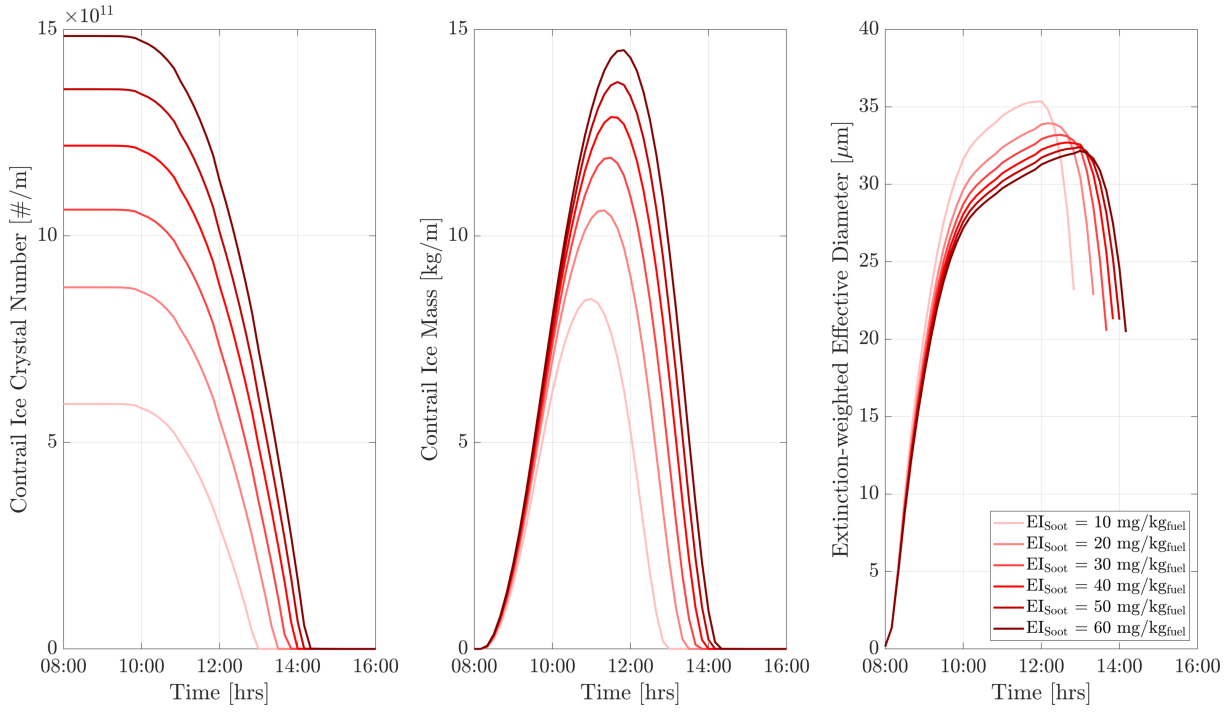

Figure 12. Total contrail ice crystal number (left), ice crystal mass (middle) and extinction-weighted effective diameter (right) for different black carbon emission indices. A background relative humidity of 110%, a temperature of 217 K at flight level are assumed.

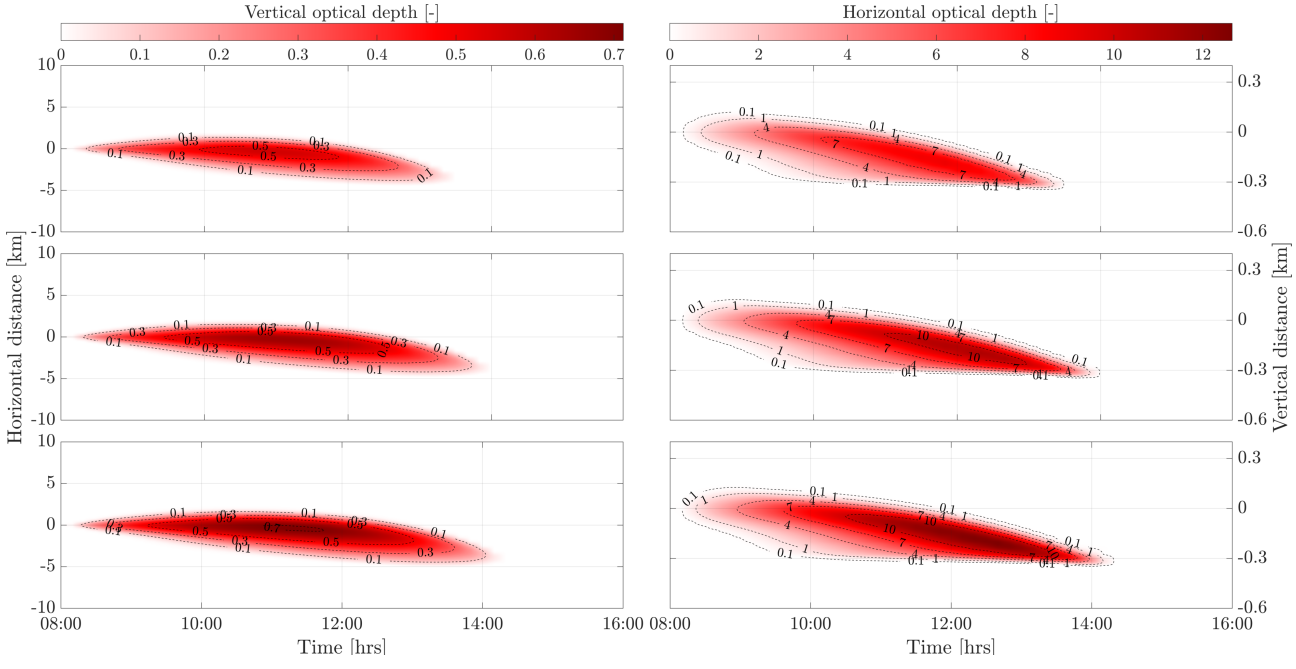

Figure 13. Contours of optical thickness along the vertical (left) and horizontal (right) direction for different black carbon mass emission indices: 20 (top), 40 (center), 60 mg/kg$_{\text{fuel}}$ (bottom) respectively. The horizontal axis is centered on the flight location. The vertical axis represents the distance with respect to the altitude after vortex sinking. The flight altitude before vortex sinking is at a pressure altitude of 10.6 km. Vortex sinking caused the plume to settle at a new altitude, 112 m lower, corresponding to the origin of the vertical axis. We apply a wind shear of 0.002 s^{-1}, causing the contrail to move left of the initial center line while sinking. An optical depth of 0.1-0.2 is usually given as a contrail detection threshold through satellite sensing (Kärcher et al., 2009).

Table 7. Predominant optical depth for different black carbon mass emission scenarios

EI_{BC} (mg/kg_{fuel})	30 min	1 hour	2 hours	5 hours
10	0.11 -20%*	0.22 -16%*	0.32 -15%*	0 -100%*
20	0.13 -	0.26 -	0.38 -	0.15 -
40	0.16 +20%*	0.30 +15%*	0.43 +14%*	0.30 +105%*
60	0.18 +32%*	0.32 +26%*	0.47 +24%*	0.39 +165%*

* Relative changes with respect to the baseline values corresponding to a black carbon mass emission index of 20 mg/kg_{fuel}

Table 8. Effect of changing the black carbon mass emission index on emission conversion factors in the upper troposphere

EI_{BC} (mg/kg_{fuel})	ECF_{O_3}	ECF_{NO_x}	ECF_{HNO_3}	$ECF_{N_2O_5}$
0[1]	0.68 -	0.78 -	0.12 -	0.041 -
10	0.62 -8.8%[2]	0.73 -6.4%[2]	0.32 +170%[2]	-0.042 -200%[2]
20	0.60 -12%[2]	0.72 -7.7%[2]	0.38 +220%[2]	-0.063 -250%[2]
40	0.58 -15%[2]	0.71 -9.0%[2]	0.45 +280%[2]	-0.093 -330%[2]
60	0.56 -17%[2]	0.70 -10%[2]	0.50 +320%[2]	-0.11 -370%[2]

Values are computed 24 hours after emissions. The emission time is set to 8:00 AM.
[1] A black carbon mass emission index of 0 mg/kg_{fuel} denotes a case in which no contrail forms.
[2] Relative changes with respect to the baseline case where no contrail forms.

ther enhancement of the black carbon emission index yields smaller increases in τ_{pre}, although we find no reversal in trend for EI_{BC} up to 3 times the baseline value.

Aggregating these results, we find that doubling the black carbon mass emission index from the baseline case increases the peak ice mass by approximately 24% and delays the time at which the peak occurs by up to 1 hour. This translates to a larger climate impact. Reducing the amount of released black carbon particles could instead cut down the contrail-cirrus radiative forcing; halving the black carbon emission index decreases the optical depth after two hours by ~15%.

3.6.3 Influence of engine black carbon emissions on chemical composition

In addition to changing the optical properties of the contrail, black carbon emissions affects the chemical impact of the plume. Table 8 shows how the 24-hour emissions conversion factors for ozone, NO_x, and NO_y reservoir species change between the scenarios described in Section 3.6.2. The comparison is here made with respect to a case where no contrail forms, thus yielding the contrail-related chemical perturbation.

Contrail-induced impacts on ozone production are small, with an overall difference of ~10% with respect to the pure gas-phase response. The NO_y partitioning is affected to a greater extent. The ice crystal surface area in the plume provides a surface for rapid, heterogeneous conversion of N_2O_5 to HNO_3. The descending, crystal-dense contrail therefore rapidly converts NO_x into reservoir forms, with the overall rate and extent of conversion increasing with black carbon emissions. At a black carbon mass emission index of 20 mg/kg_{fuel}, HNO_3 concentrations are 170% greater after 24 hours than for the baseline case. We also find that concentrations of NO_x, corresponding to the overall NO_x "survival fraction", are lower after 24 hours with higher black carbon emissions owing to the heterogeneous reactions on the surface of ice crystals.

Chemical species have an asymmetric profile across the contrail height. A greater aerosol surface area in the lower side of the plume leads to larger chemical rates through heterogeneous chemistry. The extent of the asymmetry depends on ice crystal microphysical parameters and therefore on meteorological conditions as well as aircraft parameters. Horizontally-integrated chemical perturbations of O_3, HNO_3 and N_2O_5 in the upper troposphere can be found in Figure S5 of the Supplementary Information.

3.6.4 Effects of stratospheric contrails

We carry out an additional simulation to quantify how the radiative and chemical impact of contrails is different when forming in the stratosphere. Although unlikely due to the dry conditions of the stratosphere, any contrails which survive the initial formation stage would be likely to persist for significant periods due to the low mixing rates in this region of the atmosphere.

The relative humidity profile is kept identical. We find that the lower temperature lapse rate in the stratosphere leads to a smaller contrail ice mass, with optically thinner contrails. This is explained by lower temperatures in the lower part of the contrail core and in the fallstreak. As explained in Unterstrasser and Gierens (2010a), a lower temperature reduces the effective crystal radius and optical thickness of the contrail. In the stratosphere, we find that contrails reach horizontal dimensions of 8 to 15 km compared to 5 to 10 km in the upper troposphere after 4 hours.

The nitric acid emission conversion factors are also greater compared to the tropospheric case. In some cases, the HNO_3 ECF reaches values above one as ambient, short-lived N_2O_5 is converted to long-lived HNO_3. At a pressure of 100 hPa, a black carbon mass emission index of 10 mg/kg_{fuel} leads to

greater absolute contrail-induced impacts compared to typical subsonic altitudes. The relative changes are however smaller, corresponding to a 73% and -69% change in the HNO_3 and N_2O_5 perturbations respectively compared to the baseline case. The same change in emission causes a decrease of the ozone perturbation per unit of NO_x emitted by 21% compared to 12% for the tropospheric case. Figure S6 of the Supplementary Information displays horizontally-integrated chemical perturbations of O_3, HNO_3 and N_2O_5 under stratospheric background conditions.

Aircraft-induced stratospheric cirrus clouds are found to have shorter lifetimes and lead to a smaller optical thickness compared to tropospheric altitudes assuming similar relative humidity profiles. Heterogeneous chemistry on ice crystals gains greater importance at lower pressures and shifts the N_2O_5-HNO_3 local equilibrium. Further work is needed to quantify how stratospheric contrails might differ from those that form in the troposphere.

4 Limitations and further work

Although our approach gives a significant improvement in terms of numerical fidelity compared to the instant dilution approach, additional work is needed to account for additional physical phenomena. For example, APCEMM accounts for mixing with ambient air and the effect of wind shear on the plume. However, it does not capture the enhanced diffusion from the small-scale vortices generated by the wind shear. We also consider a highly simplified approach to simulate the aircraft-induced vortex dynamics and the vertical motion of the plume due to radiative heating of the contrail. APCEMM does not explicitly model turbulence in the vicinity of the contrail, which induces fluctuations in the relative humidity field of the order of $\pm$5% around saturation (Unterstrasser and Gierens, 2010a; Gierens and Bretl, 2009). Contrail regions with greater ice water content experience more heating, thus leading to a non-uniform adiabatic uplift and a vertical stretching of the contrail. Additionally, we use a simplistic representation to model the role of organic species on the early-plume microphysics. Future work is planned to explicitly model these processes in APCEMM.

These results are also isolated to the 24-hour period immediately following passage of an aircraft. In order to translate these results into an assessment of the net global impact of aviation, we aim to implement the results of the plume-scale processing of aircraft emissions into a global atmospheric chemistry-transport model in a consistent manner with the chemistry and microphysical processes in place. However, doing so in a fashion which can be easily maintained will constitute a non-trivial software engineering challenge.

5 Conclusions

We develop a parameterized aircraft plume model to simulate chemistry in an aircraft wake. This study shows that neglecting the non-linear plume-scale processes leads to inaccuracies in the assessment of O_3 perturbations and of the conversion of NO_x to reservoir species.

We use APCEMM to quantify the 24-hour atmospheric chemical response to aircraft emissions, and how it differs from the results simulated under the "instant-dilution" approach typically used in global models. We also assess how this depends on ambient conditions, aircraft parameters and fuel properties. Based on a parameter sweep for typical cruise conditions, we find that the instant dilution assumption leads to greater ozone production compared to the plume model, with errors of up to ~200% at cruise altitude. This is due to plume-scale effects not resolved in the instant-dilution approach. In the plume model, the release of emissions into a small volume leads to O_3 depletion (through NO titration) and a HO_x-limited regime that last up to 5 hours after emissions. The lack of HO_x, which never occurs in the instant dilution approach, causes enhanced ozone production and a reduced fraction of NO_x remaining in the plume. We also quantify the role of wind shear and atmospheric diffusion.

Our approach also permits us to explicitly model the formation and effects of condensation trails. These affect the in-plume chemical response through heterogeneous reactions on the surface of ice crystals. Such plume-scale processes are not accounted for in almost all global-scale modeling approaches, but are needed in order to fully understand the role of aircraft particulate emissions in upper tropospheric chemistry. We find that a 50% reduction of the mass of emitted black carbon (assuming a baseline case of 20 mg/kg_{fuel}) leads to a decrease of 16% in the aircraft-attributable HNO_3 perturbation, while ozone and nitrogen oxides increase by ~3% and 1.5% respectively. This is accompanied by a 15% decrease in the 2-hour optical depth of the contrail, such changes would not be captured in models that lack explicit plume modeling.

Previous studies assessing the impacts of aviation emissions have released emissions at the grid-scale level. We recommend that atmospheric models include a plume-scale treatment (or parameterization thereof) of aircraft emissions to compensate for these errors. Parameters should include meteorological conditions, local atmospheric composition, flight properties as well as engine and fuel characteristics. This is expected to significantly affect the estimated contribution of aircraft emissions to atmospheric NO_x and ozone.

Appendix A: Growth during the early plume phase

A1 Growth of ice particles during the early phase

As previously stated, the rate of change in the ice mass of a particle, m_p, is given by

$$\frac{dm_p}{dt} = H_p^{\mathrm{act}}(m_p) \times 4\pi C_p D_{\mathrm{v,eff}} \left(P_{\mathrm{H_2O}} - P_{\mathrm{H_2O}}^{\mathrm{sat}}\right), \tag{A1}$$

where $H_{\mathrm{p}}^{\mathrm{act}}$ is a function accounting for nucleus activation (equation A3), C_p is the ice crystal capacitance (equal to the particle radius r_p for spherical nuclei), $D_{\mathrm{v,eff}}$ is the effective water vapor diffusion coefficient in air (equation A4), and $P_{\mathrm{H_2O}}$ the water partial pressure.

The saturation vapor pressure of water $P_{\mathrm{H_2O}}^{\mathrm{sat}}$ is calculated as

$$P_{\mathrm{H_2O}}^{\mathrm{sat}} = \exp\left(r_K/r_p\right) \times P_{\mathrm{H_2O}}^{\mathrm{flat}} \tag{A2}$$

where r_p is the particle radius (in nm), r_K is the Kelvin radius (set here to 2.3 nm), and $P_{\mathrm{H_2O}}^{\mathrm{flat}}$ is the saturation vapor pressure over a flat surface. The factor $\exp(r_K/r_p)$ represents the effect of particle curvature (the Kelvin effect), increasing the apparent vapor pressure over a convex surface relative to a flat surface (Lewellen et al., 2014). $p_{\mathrm{H_2O}}$ is calculated as a function of temperature only (Pruppacher et al., 1998).

Growth is only permitted if particles are activated, meaning that they either already have an ice coating or in air that is locally supersaturated. This is characterized through the variable H_p^{act}, as

$$H_p^{\mathrm{act}} = \begin{cases} 1 & \text{if } m_p > 0 \text{ or } \mathrm{RH}_{w,\mathrm{loc}} \geq 1 \\ 0 & \text{otherwise.} \end{cases} \tag{A3}$$

where $\mathrm{RH_{w,loc}}$ is the local relative humidity with respect to liquid water (Picot et al., 2015). $D_{\mathrm{v,eff}}$ accounts for latent heat effects, and is calculated as

$$D_{\mathrm{v,eff}} = \frac{D_{\mathrm{v}} \times \beta(r_p)}{\frac{D_{\mathrm{v}} L_s P_{\mathrm{H_2O}}^{\mathrm{sat}}}{\kappa_d T}\left(\frac{L_s}{R_{\mathrm{v}} T}\right) + R_{\mathrm{v}} T}, \tag{A4}$$

where L_s is the latent heat of sublimation and κ_d the thermal conductivity of air. The function β accounts for the transition in uptake behavior between the gas kinetic ($\mathrm{Kn} \gg 1$) to the diffusional regime ($\mathrm{Kn} \to 0$), and is calculated as

$$\beta(r_p) = \left(\frac{1}{1 + r_p/\lambda_v} + \frac{2 D_{\mathrm{v}} C_p}{\alpha v_{\mathrm{th,v}} r_p^2}\right)^{-1} \tag{A5}$$

with α being the deposition coefficient. For deposition of water molecules on ice particles, we take $\alpha = 0.5$ which is in agreement with laboratory and field studies from Haag et al. (2003). The mean free-path of vapor molecules λ_v and the diffusion coefficient of vapor in air $\mathrm{D_v}$ are functions of the local temperature and pressure and are computed according to relations from Pruppacher et al. (1998).

A2 Growth of liquid particles during the early phase

In the early plume phase, liquid particles form as the plume undergoes rapid cooling. As stated previously, we use the parameterization from Vehkamäki et al. (2002) to compute nucleation rates, cluster size and composition.

Throughout the plume lifetime, the growth of liquid particles is affected by coagulation, which dominates the early-plume phase because of the initially high aerosol particle concentrations. Coagulation is a volume-conserving process that decreases the aerosol number concentration.

Coagulation of newly-formed aerosols and scavenging by black carbon and ice particles take place on different timescales. The coagulation timescale of particles of radius r_1 can be evaluated from $t_{\mathrm{coa}} = 1/(\mathrm{K}(r_1, r_2) n_2)$, where n_2 and r_2 are the number density and the radius of the scavenging particles. As shown in the Supplementary Information, self-coagulation of liquid aerosols (r_1 = 0.5 - 10 nm) occurs on a timescale of a few seconds to minutes, assuming a typical number density between 10^6 and 10^{10} particles/cm^3. Similarly, scavenging by black carbon and ice particles happens over timescales that are of the same order of magnitude, assuming a radius of 50 nm (1 µm) for black carbon particles (for ice crystals, respectively) and a number density of 10^3 molecules/cm^3. On the other hand, self-aggregation of black carbon particles and ice crystals occur on timescales that are much longer, of the order of several hours.

Appendix B: Coagulation kernel

The coagulation kernel represents Brownian diffusion, convective Brownian diffusion enhancement, sedimentation-induced aggregation, and turbulent inertial motion, as well as enhancement due to turbulent shear. The kernel is described by the following equations, taken from Jacobson (2005). We here consider a particle of size i coagulating with particles of size j.

The Brownian collision kernel is described by:

$$\mathrm{K}_{i,j}^{\mathrm{B}} = \frac{4\pi(r_i + r_j)(D_{p,i} + D_{p,j})}{\frac{r_i + r_j}{r_i + r_j + \sqrt{\delta_i^2 + \delta_j^2}} + \frac{4(D_{p,i} + D_{p,j})}{\sqrt{\bar{v}_{p,i}^2 + \bar{v}_{p,j}^2}(r_i + r_j)}}, \tag{B1}$$

where r is the particle radius, D_p the particle diffusion coefficient, δ the mean distance from the center of a sphere reached by particles leaving the sphere's surface and traveling a distance equal to the particle mean free path and $\bar{v}_p$ the thermal speed of a particle in air.

The convective Brownian diffusion enhancement kernel is defined by:

$$\mathrm{K}_{i,j}^{\mathrm{DE}} = \begin{cases} \mathrm{K}_{i,j}^{\mathrm{B}} 0.45 \mathrm{Re}_j^{1/3} \mathrm{Sc}_{p,i}^{1/3} & \text{if } \mathrm{Re}_j \leq 1,\ r_j \geq r_i \\ \mathrm{K}_{i,j}^{\mathrm{B}} 0.45 \mathrm{Re}_j^{1/2} \mathrm{Sc}_{p,i}^{1/3} & \text{if } \mathrm{Re}_j > 1,\ r_j \geq r_i, \end{cases} \tag{B2}$$

where Re and Sc are the particle Reynolds and Schmidt numbers.

The sedimentation-induced aggregation kernel is described by:

$$K_{i,j}^{SI} = E_{agg}\pi(r_i + r_j)^2 \mid V_{f,i} - V_{f,j} \mid, \tag{B3}$$

where E_{agg} is a collision efficiency.

The turbulent inertial motion and turbulent shear kernel are defined by:

$$K_{i,j}^{TI} = \frac{\pi\varepsilon_d^{3/4}}{g\nu_a^{1/4}}(r_i + r_j)^2 \mid V_{f,i} - V_{f,j} \mid \tag{B4}$$

$$K_{i,j}^{TS} = \left(\frac{8\pi\varepsilon_d}{15\nu_a}\right)^{1/2}(r_i + r_j)^3, \tag{B5}$$

where ε_d is the rate of dissipation of turbulent kinetic energy, g the acceleration due to gravity and ν_a the kinematic viscosity.

The total coagulation kernel is equal to the sum of each individual kernel:

$$K_{i,j} = K_{i,j}^{B} + K_{i,j}^{DE} + K_{i,j}^{SI} + K_{i,j}^{TI} + K_{i,j}^{TS}. \tag{B6}$$

Appendix C: Plume-averaged NO_x chemical rate

We assume that the conversion of NO_x to reservoir species is dictated by the daytime conversion pathway through the following reactions:

$$NO_2 + OH \xrightarrow{M} HNO_3 \tag{CR1}$$

$$NO_2 + HO_2 \xrightarrow{M} HO_2NO_2 \tag{CR2}$$

The chemical reaction rate can be written as:

$$\frac{d[NO_2]}{dt} = -(k_1[OH] + k_2[HO_2])[NO_2]$$

$$\frac{d[NO_2]}{dt} = -k_{eff}[HO_x][NO_2]$$

where HO_x has been defined such that $[HO_x] = \frac{k_1[OH]+k_2[HO_2]}{k_1+k_2}$.

We assume that the concentration field at a fixed point can be expressed as the sum of spatially-averaged quantity and the instantaneous fluctuation, such that:

$$[NO_2] = \overline{[NO_2]} + [NO_2]'$$

$$[HO_x] = \overline{[HO_x]} + [HO_x]'$$

The chemical conversion rate of NO_x can therefore be written as:

$$\frac{d\overline{[NO_2]}}{dt} = -k_{eff} \times \overline{[HO_x][NO_2]}$$

$$= -k_{eff} \times \left(\overline{[HO_x]} \times \overline{[NO_2]} + \overline{[HO_x]' \times [NO_2]'}\right)$$

The first term on the right hand side leads to a net depletion. NO_2 is an emitted species. Therefore, the NO_2 fluctuation is positive in the core of the plume, while it is negative far away. HO_x, however, gets depleted to form HNO_3 and HO_2NO_2. Therefore, $[HO_x]' \leq 0$ in the inner plume and $[HO_x]' \geq 0$ outside of the core. Thus, the second term reduces NO_x conversion and is proportional to the correlation of the fluctuations. If both fluctuations are negatively correlated, the depletion is reduced compared the case where the fields are uniform.

This explains why, for the same emission quantity, a small plume with large spatial fluctuations leads to a lower conversion compared to a large plume with smaller gradients.

Appendix D: Validation of the contrail dynamics and microphysics

In this section, we compare the results of APCEMM's microphysical module to existing data from numerical simulations. Although observational data is sparse, direct comparison to in-situ measurements of both plume chemistry and ice would be a valuable future step.

We first compare the results of our simulation to Unterstrasser and Gierens (2010a) for different case studies. In all the following cases, the same meteorological background conditions (1-km deep layer) and emission characteristics as Unterstrasser and Gierens (2010a) are used. Using the same configuration, we then study the vertical distribution of the ice crystal number, surface and mass densities.

D1 Comparison

Figures D1 and D2 show the ice crystal concentration, ice mass concentration, extinction, and relative humidity profiles at three points in time according to the simulations from Unterstrasser and Gierens (2010a) and APCEMM respectively. We perform all comparisons using definitions from Unterstrasser and Gierens (2010a). The spatial distributions of ice crystal number and mass densities at t = 2,000 s are in qualitative agreement, with a maximum horizontal discrepancy less than 500 m, although the small scale discrepancies resolved by large eddy simulation are not reproduced by APCEMM. APCEMM also predicts a reduced vertical extent, likely because of a more uniform, smaller ice crystal size distribution. At later times, APCEMM fails to capture the greater horizontal extent of the contrail seen in the results from Unterstrasser and Gierens (2010a). We believe that this is due to the faster initial settling which occurs in the large eddy simulation. This discrepancy is visible on the ice water

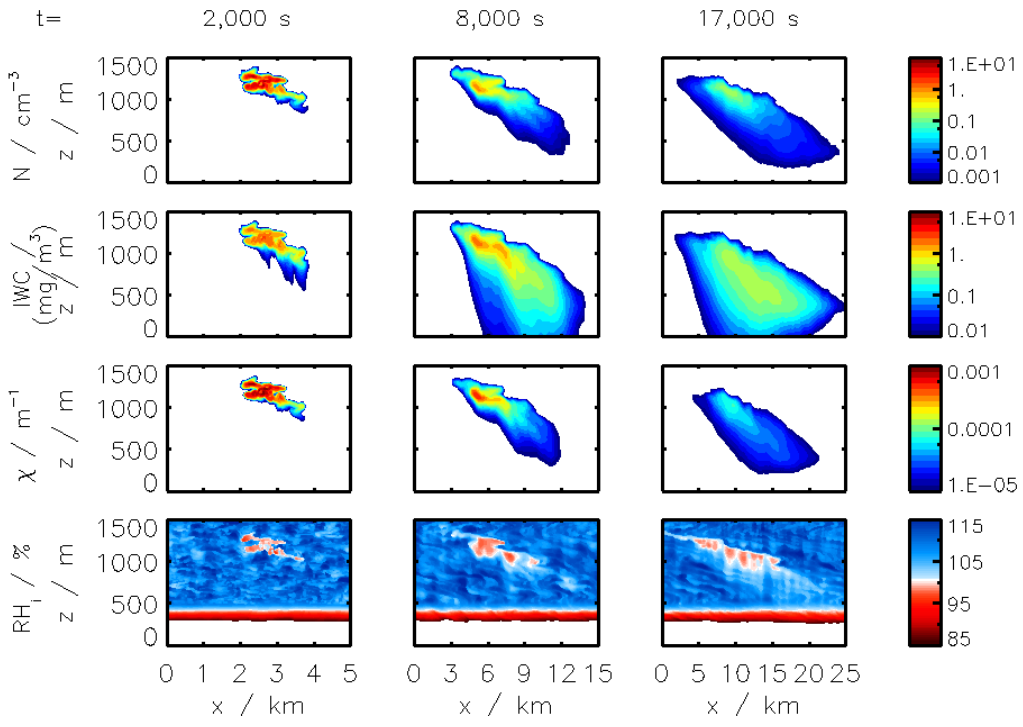

Figure D1. Results from the simulations of Unterstrasser and Gierens (2010a) showing snapshots of ice crystal number concentration, ice water content, extinction and relative humidity with respect to ice. Figure adapted from Unterstrasser and Gierens (2010a), courtesy of S. Unterstrasser.

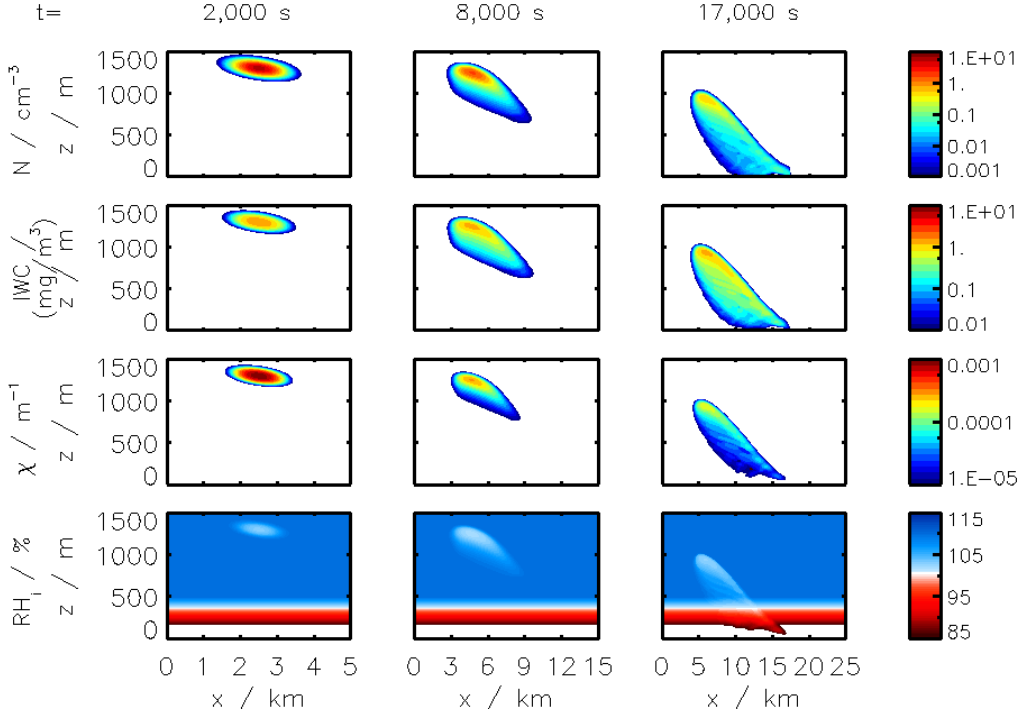

Figure D2. Ice crystal concentration N, ice mass concentration IWC, extinction χ and relative humidity RH_i for the same conditions as described in Unterstrasser and Gierens (2010a). The flight level is at a vertical distance of 1,300 m.

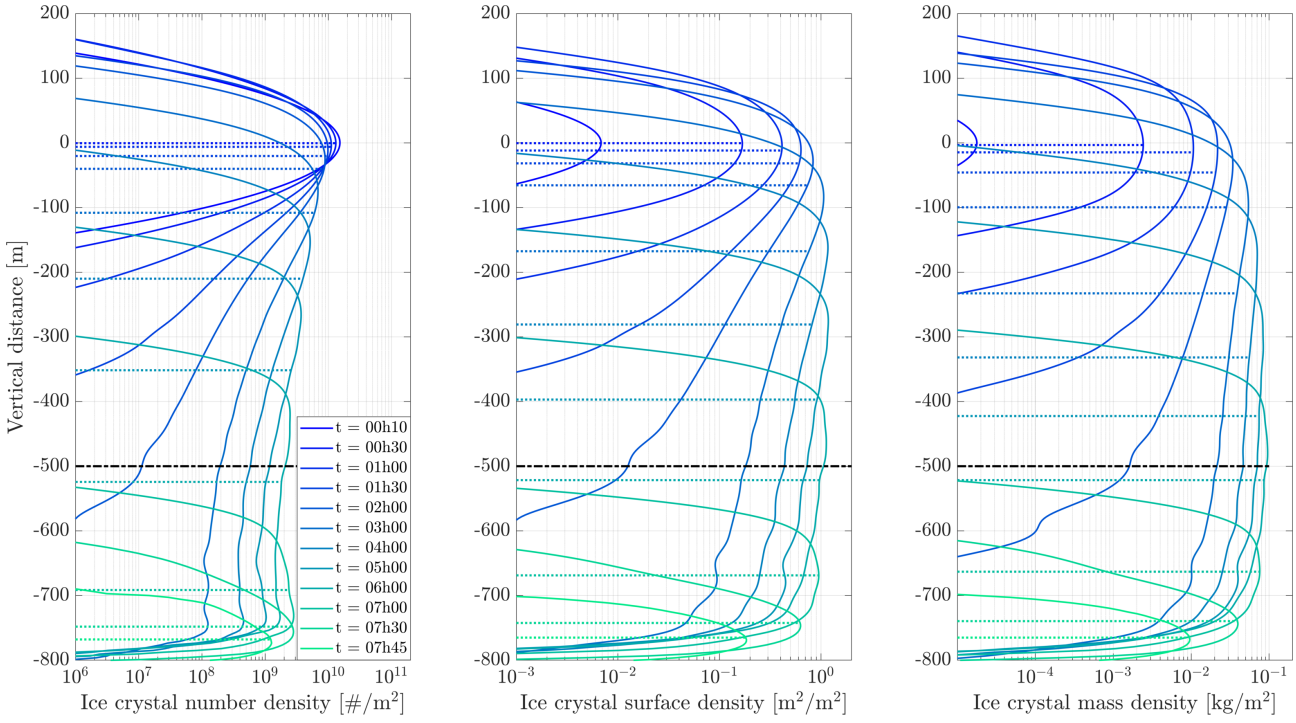

Figure D3. Time evolution of horizontally-integrated ice crystal number, surface and and mass densities. The color gradient refers to the contrail age. The supersaturation region extends from ±500 m around the flight altitude (represented as a dash-dotted black line). The median of each distributions are plotted as dotted lines.

content row in Figures D2 and D1 where APCEMM predicts a horizontal extent of 6 and 12 km at t = 8,000 s and t = 17,000 s respectively compared to 10 and 22 km according to the data from Unterstrasser and Gierens (2010a). In spite of this, the integrated contrail ice mass and number both differ by less than 10% at the three time instants.

D2 Discussion

The time evolution of the ice number density, mass density and extinction shows similar trends between APCEMM and the simulations from Unterstrasser and Gierens (2010a). Overall, APCEMM predicts a longer contrail lifetime with greater ice mass, particle number and extinction. This could be explained by the inherent turbulent motion causing fluctuations around supersaturation as described in Gierens and Bretl (2009) and Unterstrasser and Gierens (2010a), which is not modeled in APCEMM. Such local fluctuations in an overall supersaturated region would induce changes in the total ice mass and cause the local sublimation of ice crystals, which would tend to reduce the contrail lifetime.

D3 Contrail phases

This section aims to describe the different phases of the contrail as described by the simulations from APCEMM and Unterstrasser and Gierens (2010a).

The peak particle number concentration decreases over time from an initial value of ~10 #/cm^3. The fallstreak, particularly noticeable at t = 17,000 seconds in Figure D1 and Figure D2, represents a significant fraction of the total ice mass, especially considering that it is characterized by a low number of ice crystals (~20 times lower than the peak particle number). As described in Unterstrasser and Gierens (2010a), moist air is entrained at the periphery of the contrail leading to large spatial heterogeneities in the ice mass distribution. Given that the fallstreak is predominantly composed of large crystals, it can survive below the saturation depth until these crystals fully sublimate.

The extinction, as plotted on Figure D2, represents the lidar-detectable region of the contrail (with a detection threshold of $\chi_0 = 10^{-5}$ m^{-1}). As pointed out in Unterstrasser and Gierens (2010a), non-negligible regions of the contrail cannot be detected through lidar measurements, as large ice crystals have a low extinction parameter.

The relative humidity profiles in Figure D2 show that the core of the contrail is characterized with a uniform region, close to ice saturation. As the fallstreak sublimates under the saturation depth, it releases its water content at lower altitudes than the flight-level contributing to the dehydration of the upper-troposphere/lower-stratosphere.

Figure D3 displays the time evolution of horizontally-integrated ice crystal number, surface and mass densities assuming a 1-km deep saturation layer (extending from -500

to 500 m). In the first hour, the particle densities are approximately distributed symmetrically around the flight altitude as settling has not contributed significantly. The ice mass continually increases until 5 hours after emissions, leading to a vertical stretching of the contrail through gravitational settling of large particles. At that point, the ice mass density is concentrated at, or slightly below, the saturation depth (where the saturation reaches 100%) and starts to decrease until the contrail has fully sublimated at 7h45.

The colored dashed lines on Figure D3 show the median altitude of the ice crystal number, surface and mass density distributions respectively, at each time instant. Initially, all median values lie around the flight altitude. After ~3 hours, the median values start to "settle" at different speeds with the ice mass median altitude dropping the fastest, followed with the surface density and number density. This is due to the presence of a contrail core rich in small ice crystal particles (~1 µm) and a fallstreak composed of larger and fewer nuclei contributing to a large fraction of the ice mass.

Figure S7 of the Supplementary Information displays the same content as Figure D3 assuming a supersaturated region extending between ±200 m. The same conclusions as in Figure D3 can be drawn. After 6 hours, the contrail has fully sublimated and it appears from Figure S7 of the SI that the median altitudes converge towards the saturation depth.

Author contributions. T.M.F. implemented and ran the model, and wrote the manuscript. All authors were involved in study design, model validation and improvement, and manuscript review, editing, and finalization.

Competing interests. The authors declare no competing interests.

Acknowledgements. This work was supported by NASA grant number NNX14AT22A. We would like to thank S. Unterstrasser for providing data for comparison, as well as for the useful discussion regarding the simulation of the vortex sinking process.

References

Airbus: Global market forecast 2017-2036, https://www.airbus.com/aircraft/market/global-market-forecast.html, 2017.

Beard, K. V. and Ochs III, H. T.: Collisions between small precipitation drops. Part II: Formulas for coalescence, temporary coalescence, and satellites, Journal of the atmospheric sciences, 52, 3977–3996, 1995.

Boeing: Commercial Market Outlook 2018-2037, https://www.boeing.com/commercial/market/commercial-market-outlook, 2017.

Brasseur, G., Cox, R., Hauglustaine, D., Isaksen, I., Lelieveld, J., Lister, D., Sausen, R., Schumann, U., Wahner, A., and Wiesen, P.: European scientific assessment of the atmospheric effects of aircraft emissions, Atmospheric Environment, 32, 2329–2418, 1998.

Brasseur, G. P., Müller, J.-F., and Granier, C.: Atmospheric impact of NOx emissions by subsonic aircraft: A three-dimensional model study, Journal of Geophysical Research: Atmospheres, 101, 1423–1428, 1996.

Busen, R. and Schumann, U.: Visible contrail formation from fuels with different sulfur contents, Geophysical research letters, 22, 1357–1360, 1995.

Cariolle, D., Caro, D., Paoli, R., Hauglustaine, D., Cuenot, B., Cozic, A., and Paugam, R.: Parameterization of plume chemistry into large-scale atmospheric models: Application to aircraft NOx emissions, Journal of Geophysical Research: Atmospheres, 114, 2009.

Cziczo, D., DeMott, P., Brooks, S., Prenni, A., Thomson, D., Baumgardner, D., Wilson, J., Kreidenweis, S., and Murphy, D.: Observations of organic species and atmospheric ice formation, Geophysical research letters, 31, 2004.

Damian, V., Sandu, A., Damian, M., Potra, F., and Carmichael, G. R.: The kinetic preprocessor KPP-a software environment for solving chemical kinetics, Computers & Chemical Engineering, 26, 1567–1579, 2002.

DuBois, D. and Paynter, G. C.: " Fuel Flow Method2" for Estimating Aircraft Emissions, SAE Transactions, pp. 1–14, 2006.

Dürbeck, T. and Gerz, T.: Dispersion of aircraft exhausts in the free atmosphere, Journal of Geophysical Research: Atmospheres, 101, 26 007–26 015, 1996.

Eastham, S. D. and Barrett, S. R.: Aviation-attributable ozone as a driver for changes in mortality related to air quality and skin cancer, Atmospheric Environment, 144, 17–23, 2016.

Eastham, S. D., Weisenstein, D. K., and Barrett, S. R.: Development and evaluation of the unified tropospheric–stratospheric chemistry extension (UCX) for the global chemistry-transport model GEOS-Chem, Atmospheric Environment, 89, 52–63, 2014.

Ebert, E. E. and Curry, J. A.: A parameterization of ice cloud optical properties for climate models, Journal of Geophysical Research: Atmospheres, 97, 3831–3836, 1992.

Eyring, V., Stevenson, D. S., Lauer, A., Dentener, F. J., Butler, T., Collins, W. J., Ellingsen, K., Gauss, M., Hauglustaine, D. A., Isaksen, I. S., et al.: Multi-model simulations of the impact of international shipping on atmospheric chemistry and climate in 2000 and 2030, Atmospheric Chemistry and Physics, 7, 757–780, 2007.

Forstall, W. and Shapiro, A. H.: Momentum and mass transfer in coaxial gas jets, JOURNAL OF APPLIED MECHANICS-TRANSACTIONS OF THE ASME, 17, 399–408, 1950.

Gierens, K. and Bretl, S.: Analytical treatment of ice sublimation and test of sublimation parameterisations in twoÃĒÂÂmoment ice microphysics models, Atmospheric Chemistry and Physics, 9, 7481–7490, 2009.

Gierens, K., Schumann, U., Helten, M., Smit, H., and Marenco, A.: A distribution law for relative humidity in the upper troposphere and lower stratosphere derived from three years of MOZAIC measurements, in: Annales Geophysicae, vol. 17, pp. 1218–1226, Springer, 1999.

Goodman, J., Pueschel, R., Jensen, E., Verma, S., Ferry, G., Howard, S. D., Kinne, S., and Baumgardner, D.: Shape and size of contrails ice particles, Geophysical research letters, 25, 1327–1330, 1998.

Gottlieb, D. and Orszag, S. A.: Numerical analysis of spectral methods: theory and applications, vol. 26, Siam, 1977.

Gupta, K., Rehman, A., and Sarviya, R.: Bio-fuels for the gas turbine: A review, Renewable and Sustainable Energy Reviews, 14, 2946–2955, 2010.

Haag, W., Kärcher, B., Ström, J., Minikin, A., Lohmann, U., Ovarlez, J., and Stohl, A.: Freezing thresholds and cirrus cloud formation mechanisms inferred from in situ measurements of relative humidity, Atmospheric Chemistry and Physics, 3, 1791–1806, 2003.

Heymsfield, A. J., Lawson, R. P., and Sachse, G.: Growth of ice crystals in a precipitating contrail, Geophysical Research Letters, 25, 1335–1338, 1998.

Hidalgo, H.: The stratosphere perturbed by propulsion effluents, in: 11th Annual Meeting and Technical Display, p. 335, 1974.

Huszar, P., Teyssèdre, H., Michou, M., Voldoire, A., Olivié, D., Saint-Martin, D., Cariolle, D., Senesi, S., Melia, D. S. Y., Alias, A., et al.: Modeling the present and future impact of aviation on climate: an AOGCM approach with online coupled chemistry., Atmospheric Chemistry & Physics, 13, 2013.

Iwabuchi, H., Yang, P., Liou, K., and Minnis, P.: Physical and optical properties of persistent contrails: Climatology and interpretation, Journal of Geophysical Research: Atmospheres, 117, 2012.

Jacobson, M.: Numerical solution to drop coalescence/breakup with a volume-conserving, positive-definite, and unconditionally stable scheme, Journal of the Atmospheric Sciences, 68, 334–346, 2011.

Jacobson, M. Z.: Development and application of a new air pollution modeling system—II. Aerosol module structure and design, Atmospheric Environment, 31, 131–144, 1997.

Jacobson, M. Z.: Development of mixed-phase clouds from multiple aerosol size distributions and the effect of the clouds on aerosol removal, Journal of Geophysical Research: Atmospheres, 108, 2003.

Jacobson, M. Z.: Fundamentals of atmospheric modeling, Cambridge university press, 2005.

Jacobson, M. Z., Turco, R. P., Jensen, E. J., and Toon, O. B.: Modeling coagulation among particles of different composition and size, Atmospheric Environment, 28, 1327–1338, 1994.

Jaecker-Voirol, A. and Mirabel, P.: Heteromolecular nucleation in the sulfuric acid-water system, Atmospheric Environment (1967), 23, 2053–2057, 1989.

Jensen, E., Toon, O., Pueschel, R., Goodman, J., Sachse, G., Anderson, B., Chan, K., Baumgardner, D., and Miake-Lye, R.: Ice crystal nucleation and growth in contrails forming at low ambient temperatures, Geophysical research letters, 25, 1371–1374, 1998a.

Jensen, E. J., Ackerman, A. S., Stevens, D. E., Toon, O., Minnis, P., et al.: Spreading and growth of contrails in a sheared environment, Journal of Geophysical Research: Atmospheres, 103, 31 557–31 567, 1998b.

Jung, J. G., Pandis, S. N., and Adams, P. J.: Evaluation of nucleation theories in a sulfur-rich environment, Aerosol Science and Technology, 42, 495–504, 2008.

Kärcher, B.: A trajectory box model for aircraft exhaust plumes, Journal of Geophysical Research: Atmospheres, 100, 18 835–18 844, 1995.

Kärcher, B.: Physicochemistry of aircraft-generated liquid aerosols, soot, and ice particles-1. Model description, Journal of Geophysical Research-Atmospheres, 103, 17 111–17 128, 1998.

Kärcher, B.: Aviation-produced aerosols and contrails, Surveys in geophysics, 20, 113–167, 1999.

Kärcher, B.: Formation and radiative forcing of contrail cirrus, Nature communications, 9, 1824, 2018.

Kärcher, B. and Koop, T.: The role of organic aerosols in homogeneous ice formation, Atmospheric Chemistry and Physics, 5, 2005.

Kärcher, B. and Yu, F.: Role of aircraft soot emissions in contrail formation, Geophysical Research Letters, 36, 2009.

Kärcher, B., Hirschberg, M., and Fabian, P.: Small-scale chemical evolution of aircraft exhaust species at cruising altitudes, Journal of Geophysical Research: Atmospheres, 101, 15 169–15 190, 1996.

Kärcher, B., Busen, R., Petzold, A., Schröder, F., Schumann, U., and Jensen, E.: Physicochemistry of aircraft-generated liquid aerosols, soot, and ice particles: 2. Comparison with observations and sensitivity studies, Journal of Geophysical Research: Atmospheres, 103, 17 129–17 147, 1998.

Kärcher, B., Turco, R., Yu, F., Danilin, M., Weisenstein, D., Miake-Lye, R., and Busen, R.: A unified model for ultrafine aircraft particle emissions, Journal of Geophysical Research: Atmospheres, 105, 29 379–29 386, 2000.

Kärcher, B., Burkhardt, U., Unterstrasser, S., and Minnis, P.: Factors controlling contrail cirrus optical depth, Atmospheric Chemistry and Physics, 9, 6229–6254, 2009.

Kärcher, B., Burkhardt, U., Bier, A., Bock, L., and Ford, I.: The microphysical pathway to contrail formation, Journal of Geophysical Research: Atmospheres, 120, 7893–7927, 2015.

Kraabøl, A. G., Konopka, P., Stordal, F., and Schlager, H.: Modelling chemistry in aircraft plumes 1: comparison with observations and evaluation of a layered approach, Atmospheric environment, 34, 3939–3950, 2000.

Lee, J. J., Lukachko, S. P., Waitz, I. A., and Schafer, A.: Historical and future trends in aircraft performance, cost, and emissions, Annual Review of Energy and the Environment, 26, 167–200, 2001.

Lewellen, D., Meza, O., and Huebsch, W.: Persistent contrails and contrail cirrus. Part I: Large-eddy simulations from inception to demise, Journal of the Atmospheric Sciences, 71, 4399–4419, 2014.

Lukachko, S., Waitz, I., Miake-Lye, R., Brown, R., and Anderson, M.: Production of sulfate aerosol precursors in the turbine and exhaust nozzle of an aircraft engine, Journal of Geophysical Research: Atmospheres, 103, 16 159–16 174, 1998.

Mazraati, M.: World aviation fuel demand outlook, OPEC energy review, 34, 42–72, 2010.

Meijer, E., Velthoven, P., Thompson, A., Pfister, L., Schlager, H., Schulte, P., and Kelder, H.: Model calculations of the impact of NOx from air traffic, lightning, and surface emissions, compared with measurements, Journal of Geophysical Research: Atmospheres, 105, 3833–3850, 2000.

Meijer, E. W.: Modelling the impact of subsonic aviation on the composition of the atmosphere, Technische Universiteit Eindhoven, 2001.

Minnis, P., Young, D. F., Garber, D. P., Nguyen, L., Smith, W. L., and Palikonda, R.: Transformation of contrails into cirrus during SUCCESS, Geophysical Research Letters, 25, 1157–1160, 1998.

Murray, B. J., Wilson, T. W., Dobbie, S., Cui, Z., Al-Jumur, S. M., Möhler, O., Schnaiter, M., Wagner, R., Benz, S., Niemand, M., et al.: Heterogeneous nucleation of ice particles on glassy aerosols under cirrus conditions, Nature Geoscience, 3, 233–237, 2010.

Naiman, A., Lele, S., and Jacobson, M.: Large eddy simulations of contrail development: Sensitivity to initial and ambient conditions over first twenty minutes, Journal of Geophysical Research: Atmospheres, 116, 2011.

Napari, I., Noppel, M., Vehkamäki, H., and Kulmala, M.: Parametrization of ternary nucleation rates for H2SO4-NH3-H2O vapors, Journal of Geophysical Research: Atmospheres, 107, 2002.

Paoli, R. and Shariff, K.: Contrail modeling and simulation, Annual Review of Fluid Mechanics, 48, 2016.

Paoli, R., Vancassel, X., Garnier, F., and Mirabel, P.: Large-eddy simulation of a turbulent jet and a vortex sheet interaction: particle formation and evolution in the near field of an aircraft wake, Meteorologische Zeitschrift, 17, 131–144, 2008.

Paoli, R., Cariolle, D., and Sausen, R.: Review of effective emissions modeling and computation, Geosci. Model Dev., 4, 643–667, doi: 10.5194, 2011.

Penner, J. E.: Aviation and the global atmosphere: a special report of the Intergovernmental Panel on Climate Change, Cambridge University Press, 1999.

Petry, H., Hendricks, J., Möllhoff, M., Lippert, E., Meier, A., Ebel, A., and Sausen, R.: Chemical conversion of subsonic aircraft emissions in the dispersing plume: Calculation of effective emission indices, Journal of Geophysical Research: Atmospheres, 103, 5759–5772, 1998.

Petzold, A., Döpelheuer, A., Brock, C., and Schröder, F.: In situ observations and model calculations of black carbon emission by aircraft at cruise altitude, Journal of Geophysical Research: Atmospheres, 104, 22 171–22 181, 1999.

Picot, J., Paoli, R., Thouron, O., and Cariolle, D.: Large-eddy simulation of contrail evolution in the vortex phase and its interaction with atmospheric turbulence, Atmospheric Chemistry and Physics, 15, 7369–7389, 2015.

Pruppacher, H. R., Klett, J. D., and Wang, P. K.: Microphysics of clouds and precipitation, 1998.

Rojo, C., Vancassel, X., Mirabel, P., Ponche, J.-L., and Garnier, F.: Impact of alternative jet fuels on aircraft-induced aerosols, Fuel, 144, 335–341, 2015.

Schröder, F., Kärcher, B., Duroure, C., Ström, J., Petzold, A., Gayet, J.-F., Strauss, B., Wendling, P., and Borrmann, S.: On the transition of contrails into cirrus clouds, Journal of the atmospheric sciences, 75, 2018.

Schumann, U.: The impact of nitrogen oxides emissions from aircraft upon the atmosphere at flight altitudes—results from the AERONOX project, Atmospheric Environment, 31, 1723–1733, 1997.

Schumann, U.: A contrail cirrus prediction model, Geoscientific Model Development, 5, 543–580, 2012.

Schumann, U., Konopka, P., Baumann, R., Busen, R., Gerz, T., Schlager, H., Schulte, P., and Volkert, H.: Estimate of diffusion parameters of aircraft exhaust plumes near the tropopause from nitric oxide and turbulence measurements, Journal of Geophysical Research: Atmospheres, 100, 14 147–14 162, 1995.

Schumann, U., Schlager, H., Arnold, F., Baumann, R., Haschberger, P., and Klemm, O.: Dilution of aircraft exhaust plumes at cruise altitudes, Atmospheric Environment, 32, 3097–3103, 1998.

Schumann, U., Schlager, H., Arnold, F., Ovarlez, J., Kelder, H., Hov, Ø., Hayman, G., Isaksen, I., Staehelin, J., and Whitefield, P. D.: Pollution from aircraft emissions in the North Atlantic flight corridor: Overview on the POLINAT projects, Journal of Geophysical Research: Atmospheres, 105, 3605–3631, 2000.

Schumann, U., Arnold, F., Busen, R., Curtius, J., Kärcher, B., Kiendler, A., Petzold, A., Schlager, H., Schröder, F., and Wohlfrom, K.-H.: Influence of fuel sulfur on the composition of aircraft exhaust plumes: The experiments SULFUR 1–7, Journal of Geophysical Research: Atmospheres, 107, 2002.

Seidel, D. J., Free, M., and Wang, J.: Diurnal cycle of upper-air temperature estimated from radiosondes, Journal of Geophysical Research: Atmospheres, 110, 2005.

Sölch, I. and Kärcher, B.: A large-eddy model for cirrus clouds with explicit aerosol and ice microphysics and Lagrangian ice particle tracking, Quarterly Journal of the Royal Meteorological Society, 136, 2074–2093, 2010.

Song, C., Chen, G., Hanna, S., Crawford, J., and Davis, D.: Dispersion and chemical evolution of ship plumes in the marine boundary layer: Investigation of O3/NOy/HOx chemistry, Journal of Geophysical Research: Atmospheres, 108, 2003.

Speth, R. L., Rojo, C., Malina, R., and Barrett, S. R.: Black carbon emissions reductions from combustion of alternative jet fuels, Atmospheric Environment, 105, 37–42, 2015.

Stettler, M. E., Boies, A. M., Petzold, A., and Barrett, S. R.: Global civil aviation black carbon emissions, Environmental science & technology, 47, 10 397–10 404, 2013.

Tabazadeh, A., Jensen, E. J., and Toon, O. B.: A model description for cirrus cloud nucleation from homogeneous freezing of sulfate aerosols, Journal of Geophysical Research: Atmospheres, 102, 23 845–23 850, 1997.

Tang, M., Cox, R., and Kalberer, M.: Compilation and evaluation of gas phase diffusion coefficients of reactive trace gases in the atmosphere: volume 1. Inorganic compounds, Atmospheric Chemistry and Physics, 14, 9233–9247, 2014.

Thompson, A. M., Friedl, R. R., and Wesoky, H. L.: Atmospheric effects of aviation: First report of the Subsonic Assessment Project, 1996.

Toon, O. B. and Miake-Lye, R. C.: Subsonic aircraft: Contrail and cloud effects special study (SUCCESS), Geophysical Research Letters, 25, 1109–1112, 1998.

Tremmel, H., Schlager, H., Konopka, P., Schulte, P., Arnold, F., Klemm, M., and Droste-Franke, B.: Observations and model calculations of jet aircraft exhaust products at cruise altitude and inferred initial OH emissions, Journal of Geophysical Research: Atmospheres, 103, 10 803–10 816, 1998.

Tremmel, H. G. and Schumann, U.: Model simulations of fuel sulfur conversion efficiencies in an aircraft engine: Dependence on reaction rate constants and initial species mixing ratios, Aerospace Science and Technology, 3, 417–430, 1999.

Unterstrasser, S.: Properties of young contrails–a parametrisation based on large-eddy simulations, Atmospheric Chemistry and Physics, 16, 2059–2082, 2016.

Unterstrasser, S. and Gierens, K.: Numerical simulations of contrail-to-cirrus transition–Part 1: An extensive parametric study, Atmospheric Chemistry and Physics, 10, 2017–2036, 2010a.

Unterstrasser, S. and Gierens, K.: Numerical simulations of contrail-to-cirrus transition–Part 2: Impact of initial ice crystal number, radiation, stratification, secondary nucleation and layer depth, Atmospheric Chemistry and Physics, 10, 2037–2051, 2010b.

Unterstrasser, S., Gierens, K., and Spichtinger, P.: The evolution of contrail microphysics in the vortex phase, Meteorologische Zeitschrift, 17, 145–156, 2008.

Unterstrasser, S., Gierens, K., Sölch, I., and Wirth, M.: Numerical simulations of homogeneously nucleated natural cirrus and contrail-cirrus. Part 2: Interaction on local scale, Meteorol. Z, pp. 1–19, 2016.

Unterstrasser, S., Gierens, K., Sölch, I., and Lainer, M.: Numerical simulations of homogeneously nucleated natural cirrus and contrail-cirrus. Part 1: How different are they?, Meteorologische Zeitschrift, 26, 621–642, 2017.

Vehkamäki, H., Kulmala, M., Napari, I., Lehtinen, K. E., Timmreck, C., Noppel, M., and Laaksonen, A.: An improved parameterization for sulfuric acid–water nucleation rates for tropospheric and stratospheric conditions, Journal of Geophysical Research: Atmospheres, 107, 2002.

Vinken, G. C., Boersma, K. F., Jacob, D. J., and Meijer, E. W.: Accounting for non-linear chemistry of ship plumes in the GEOS-Chem global chemistry transport model, Atmospheric Chemistry and Physics, 11, 11 707–11 722, 2011.

Vohralik, P., Randeniya, L., Plumb, I., and Baughcum, S.: Effect of plume processes on aircraft impact, Journal of Geophysical Research: Atmospheres, 113, 2008.

Wong, H.-W. and Miake-Lye, R.: Parametric studies of contrail ice particle formation in jet regime using microphysical parcel modeling, Atmospheric Chemistry and Physics, 10, 3261–3272, 2010.

Yu, F., Turco, R. P., and Kärcher, B.: The possible role of organics in the formation and evolution of ultrafine aircraft particles, Journal of Geophysical Research: Atmospheres, 104, 4079–4087, 1999.